(2)

NAVAL POSTGRADUATE SCHOOL
Monterey, California

THESIS

SUBMESOSCALE STRUCTURE OF THE
CALIFORNIA CURRENT NEAR
SAN CLEMENTE ISLAND

by

Ching-Mao Tsai

June 1990

Co-Advisor Pe-Cheng Chu
Co-Advisor Curtis A. Collins

UNCLASSIFIED

SECURITY CLASSIFICATION OF THIS PAGE

REPORT DOCUMENTATION PAGE

Form Approved
OMB No 0704-0188

1a REPORT SECURITY CLASSIFICATION: Unclassified	1b RESTRICTIVE MARKINGS
2a SECURITY CLASSIFICATION AUTHORITY	3 DISTRIBUTION / AVAILABILITY OF REPORT: APPROVED FOR PUBLIC RELEASE; DISTRIBUTION IS UNLIMITED
2b DECLASSIFICATION / DOWNGRADING SCHEDULE	
4 PERFORMING ORGANIZATION REPORT NUMBER(S)	5 MONITORING ORGANIZATION REPORT NUMBER(S)
6a NAME OF PERFORMING ORGANIZATION: Naval Postgraduate School; 6b OFFICE SYMBOL (If applicable): CODE 68	7a NAME OF MONITORING ORGANIZATION: Naval Postgraduate School
6c ADDRESS (City, State, and ZIP Code): Monterey, CA 93943-5000	7b ADDRESS (City, State, and ZIP Code): Monterey, CA 93943-5000
8a NAME OF FUNDING / SPONSORING ORGANIZATION; 8b OFFICE SYMBOL (If applicable)	9 PROCUREMENT INSTRUMENT IDENTIFICATION NUMBER
8c ADDRESS (City, State, and ZIP Code)	10 SOURCE OF FUNDING NUMBERS: PROGRAM ELEMENT NO; PROJECT NO; TASK NO; WORK UNIT ACCESSION NO

11 TITLE (Include Security Classification)
SUBMESOSCALE STRUCTURE OF THE CALIFORNIA CURRENT NEAR SAN CLEMENTE ISLAND

12 PERSONAL AUTHOR(S)
CHING-MAO TSAI

13a TYPE OF REPORT	13b TIME COVERED	14 DATE OF REPORT (Year, Month, Day)	15 PAGE COUNT
Master's Thesis	FROM _____ TO _____	JUNE 1990	127

16 SUPPLEMENTARY NOTATION
The views expressed in this thesis are those of the author and do not reflect the official policy or position of the Department of Defense or the U.S. Government

17 COSATI CODES		
FIELD	GROUP	SUB-GROUP

18 SUBJECT TERMS (Continue on reverse if necessary and identify by block number)
coastal circulation, upper ocean current, San Clemente Island, nearshore eddies

19 ABSTRACT (Continue on reverse if necessary and identify by block number)

The purpose of the San Clemente Basin Experiment (SCBE) was to survey the upper ocean currents and temperature in a region southwest of San Clemente Island (SCI).

To accomplish this, two cruises were made in this area during which currents were measured by using a shipboard mounted Acoustic Doppler Current profiler(ADCP), and temperature was measured during the second cruise by deploying Expendable Bathythermographs (XBT). The first cruise took place during 17-21th July 1989 and the second one during 2-6 September 1989.

Data indicate a variety of features. Two different flow patterns were observed. Strong poleward alongshore flow (about 40 cm/s) occured 5-15 km west of SCI and small scale eddies were seen further offshore, i.e., farther than 15 km west of SCI. The alongshore flow intensified poleward, reaching 300 m depth. The small scale eddies have a length scale of about 10 km and are believed to be associated with larger scale horizontal shear due to the California current.

20 DISTRIBUTION / AVAILABILITY OF ABSTRACT	21 ABSTRACT SECURITY CLASSIFICATION
☒ UNCLASSIFIED UNLIMITED ☐ SAME AS RPT ☐ DTIC USERS	unclassified
22a NAME OF RESPONSIBLE INDIVIDUAL: Pe-Cheng Chu	22b TELEPHONE (Include Area Code): (408) 646-2768; 22c OFFICE SYMBOL: 68Cu

DD Form 1473, JUN 86 *Previous editions are obsolete*

S/N 0102-LF-014-6603

SECURITY CLASSIFICATION OF THIS PAGE

UNCLASSIFIED

Approved for public release; Distribution is unlimited

SUBMESOSCALE STRUCTURE OF THE
CALIFORNIA CURRENT NEAR
SAN CLEMENTE ISLAND

by

Ching-Mao Tsai
Commander, Taiwan, R.O.C. Navy
B.S., Chung-Cheng Institute of Technology,
Taiwan, R.O.C., 1976

Submitted in partial fulfillment of the
requirements for the degree of

MASTER OF SCIENCE IN PHYSICAL OCEANOGRAPHY

from the

NAVAL POSTGRADUATE SCHOOL

JUNE 1990

Author: Ching-Mao Tsai
Ching-Mao Tsai

Approved by: Pe-Cheng Chu
Pe-Cheng Chu, Thesis Co-Advisor

Curtis A. Collins
Curtis A. Collins, Thesis Co-Advisor

Curtis A. Collins
Curtis A. Collins, Chairman
Department of Oceanography Science

ABSTRACT

The purpose of the San Clemente Basin Experiment (SCBE) was to survey the upper ocean currents and temperature in a region southwest of San Clemente Island (SCI).

To accomplish this, two cruises were made in this area during which currents were measured by using a shipboard mounted Acoustic Doppler Current profile (ADCP), and temperature was measured during the second cruise by deploying Expendable Bathythermographs (XBT). The first cruise took place during 17-21 July 1989 and the second one during 2-6 September 1989.

Data indicate a variety of features. Two different flow patterns were observed. Strong poleward alongshore flow (about 40 cm/s) occured 5-15 km west of SCI and small scale eddies were seen further offshore, i.e., farther than 15 km west of SCI. The alongshore flow intensified poleward, reaching 300 m depth. The small scale eddies have a length scale of about 10 km and are believed to be associated with larger scale horizontal shear due to the California current.

TABLE OF CONTENTS

LIST OF TABLES

LIST OF FIGURES

ACKNOWLEDGEMENTS

Thanks are due for the help from many people in the oceanography department at NPS especially Dr. Stevens P. Tucker, Dr. Chung-Shang Wu, and Arlene A. Bird. For this research to to be completed, I thank my co-advisors Dr. Pe-Cheng Chu and Dr. Curtis A. Collins. Special thanks to oceanographer Paul F. Jessen. Paul supplied the initial data processing programs for the ADCP data as well as those programs for hydrographic and SAIL data processing and plotting. Paul also was most helpful in answering the mary questions and in offering his experiences during the data processing.

This research was supported by the Naval Facilities Engineering Command.

I. INTRODUCTION

Offshore of Southern California, islands, shallow banks, basins and troughs form a complex bathymetric region extending from the coast to 200 km offshore. The southern California coastline has a concave curvature from point Conception to the U.S. - Mexican border. This region is refered to as the California bight. The geographic configuration of the bight exerts an influence on the local circulation patterns and on the distributions of physical quantities. San Clemente Basin, located at 32° 50′ N, 118° 55′W in the California bight, is strongly effected by this bathymetric configuration as well as the offshore mesoscale eddy field (Simpson & Lynn, 1990).

Two surveys were conducted in San Clememte Basin by the *R/V Point Sur* to measure the ocean current and temperature structure. The first cruise took place during 17-21 July 1989, and the second during 2-6 September 1989. The ocean currents were measured by a shipboard Acoustic Doppler Current Profiler (ADCP) and the temperature was measured by eXpendable BathyThermographs (XBT). Presented in this research are velocity and temperature data collected from the ADCP and XBT's during these two cruises. XBTs were used only during the second cruise. In this research, we focus on the second cruise in which the ADCP/XBT data can be combined in some detail.

The objectives of this research are: (1) to determine the current and temperature structure; (2) to compute the dynamic flow; and (3)to investigate how current patterns are affected by topography.

This thesis consists of seven chapters. Chapter II discusses the data processing and calibration. Chapter III contains ship tracks for the study area off San Clemente Island, the locations where XBTs were launched, vertically averaged currents for different layers, and 20 current profiles. Chapter IV includes sections of onshore and alongshore currents, as well as sections of standard deviations of onshore and alongshore current components. Chapter V consists of eight temperature cross sections and the temperature gradient microstructure at 8°C, 9°C and 10°C. Chapter VI discusses the geostrophic velocity and dynamic height and compares these with ADCP data. Chapter VII summarizes the flow pattern in San Clemente Basin and discusses possible causes of these flow patterns. Two appendices are presented at the end of this thesis. Appendix A shows the 74 profiles of XBT during the second cruise 2-6 September, 1989. Appendix B shows the temperature and current structure along the cruise track from Moss Landing to San Clemente Island.

II. FIELD PROGRAM

The study area in the San Clemente Basin is located within four points [**a** (32° 52.8′ N 119° 09.2′ W), **b** (33° 06.3′ N 118° 54.2′ W), **c** (32° 35.2′ N 118° 46.7′ W), **d** (32° 48.8′ N 118° 31.8′ W)]. The range of water depth is 150-950 m at this area. Shallow water is located at the SE corner, 5-6 km offshore the island and deeper water is located near 32° 50′ N 118° 57′ W which is close to the center of the basin. The isobaths are roughly parallel to the west coast of the island and shoal while getting close to the island. The following section describes two cruises during July and September, 1989.

A. THE FIRST CRUISE (SCBE I)

The *R/V Point Sur* departed Moss Landing on the morning (1600 UT) of 17 July 1989. The course followed during the steam to the study area is shown in Figure B1 The track was designed to minimize course changes while allowing the ship to remain in water shallower than 400 m (the depth range of the ADCP). This allowed for current observations through the entire water column during the transit down the coast. Ship speed to the study area was approximately 10 knots. A description of water properties along the cruise track are presented in Appendix B.

The ship arrived at the northwest corner of the study area on 18 July at 1920 UT. Ship speed was reduced to approximately 5 knots to increase spatial resolution for the ADCP. The course followed in the study area consisted of 8 transects and a reciprocal course (Figure 1). Following completion of the grid, the ship increased speed to 10 knots and steamed back to Moss Landing. The ship arrived in Moss Landing at 2230 UT on 21 July, 1989.

B. THE SECOND CRUISE (SCBE II)

The ship departed Moss Landing on the morning of 2 September, 1989 at 1700 UT. The track followed to the study area was the same as the first cruise on 17 July 1989. XBTs were dropped every two hours starting at 2000 UT on the way to the study area. The ship arrived at the northwest corner of the study area on 3 September at 2240 UT. During the second cruise, ship's speed was increased to approximately 9 knots wnile in the study area thus allowing the grid to be completed twice.

The course followed during the first pass over the study area consisted of eight transects (Figure 2). The transects were made in a northwest to southeast direction. The eight transects were finished at 2330 UT on September 4.

The frequency of XBT drops was increased to one per hour in the study area. The station numbers and positions of XBTs dropped during the first pass of the grid are shown in Figure 2 where the triangle denotes the location of XBT sounding. XBT station numbers are from 15 to 42.

The second pass over the study area consisted of eight transects oriented perpendicular to those of the first pass. During this pass the ship speed was reduced to 7.5 knots allowing slightly better spatial resolution of ADCP data as compared to the first pass. The time needed to complete each transect was increased to about 4 hours. Position and station number of XBT deployment during the second pass of the grid are shown in Figure 3 where the solid circles denote the location of XBT sounding and XBT station number from 42 to 74. The stations M1-M9, E1-E6, D1-D5 are chosen for the sample stations which describe the water property in the next chapter. Transect eight of the second grid was completed at 0640 UT on 6 September.

Following the completion of two passes, the ship increased speed to 10 knots and steamed for Santa Barbara, arriving at about 2000 UT on September 6.

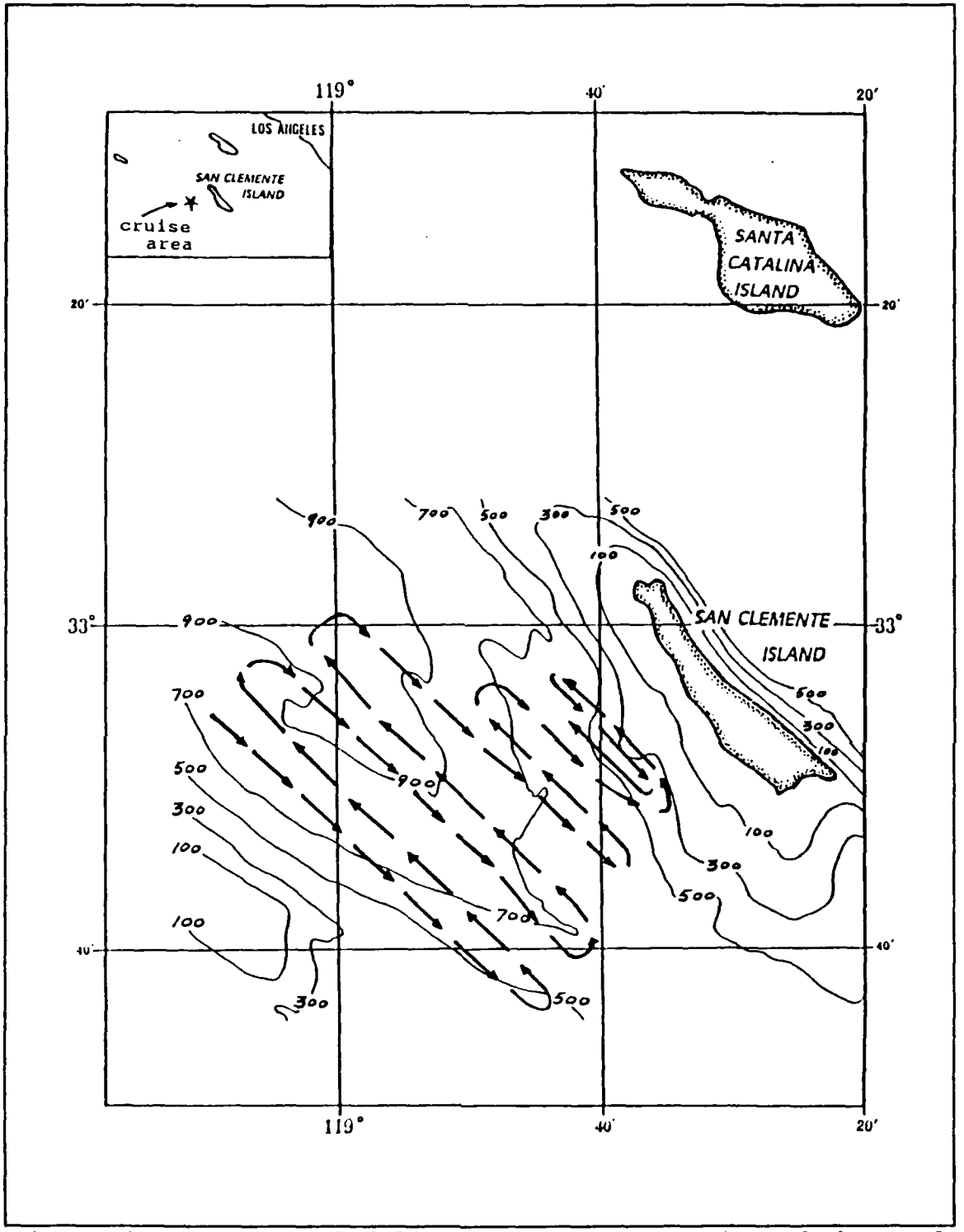

Figure 1. Cruise track followed during occupation of the study area off San Clemente Island during the first cruise SCBE-I, 17-21 July, 1989.

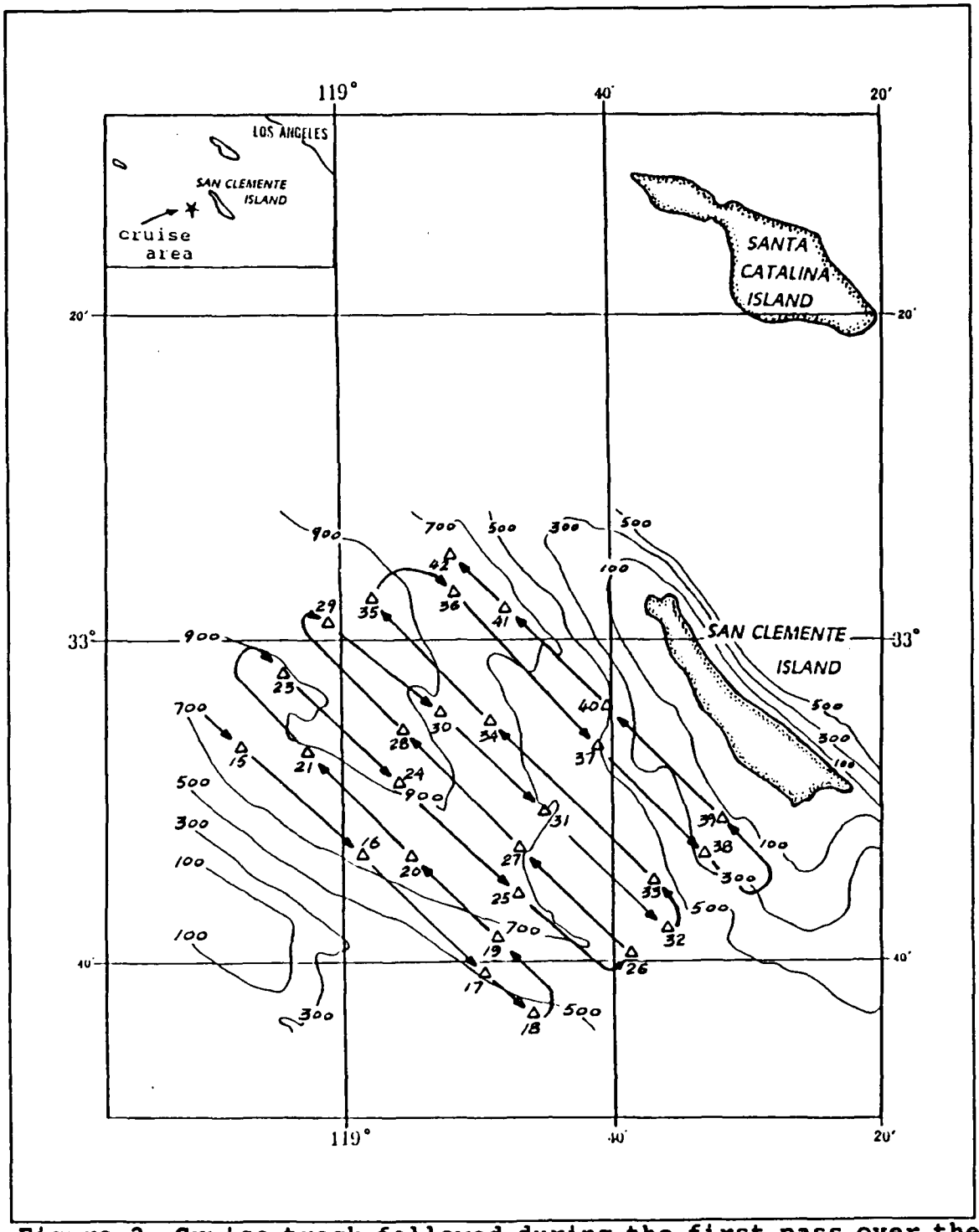

Figure 2. Cruise track followed during the first pass over the study area off San Clemente Island during the second cruise SCBE-II, 2-6 September, 1989. The Δ denotes location of XBT soundings.

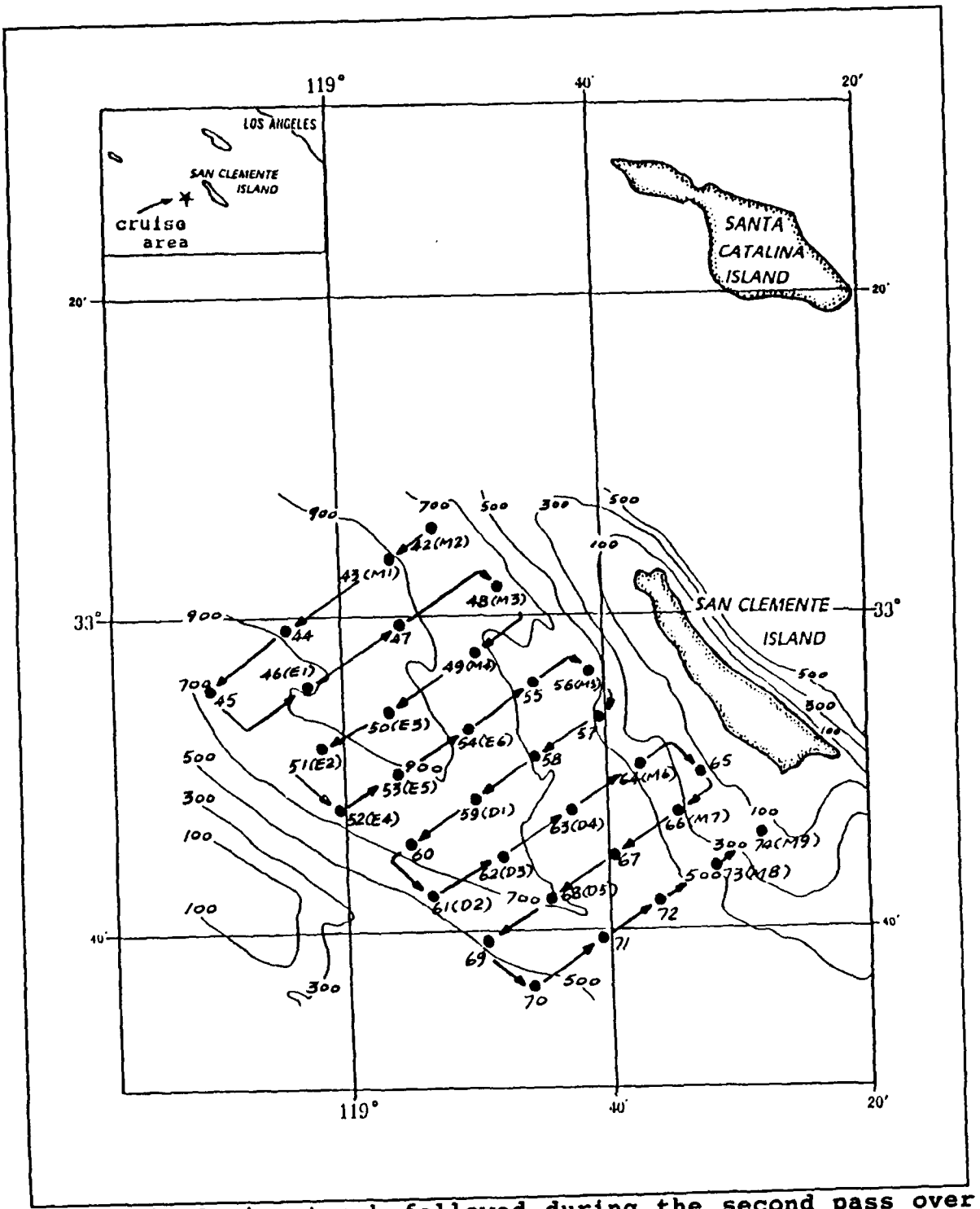

Figure 3. Cruise track followed during the second pass over the study area off San Clemente Island during the cruise SCBE-II, 2-6 September, 1989. The ♦ denotes location of XBT sounding.

III. ADCP DATA PROCESSING

A. RAW DATA

The ADCP data was processed by Paul Jessen of the NPS Oceanography Department. The first step is the correction of navigation data. "Bad" navigation data are replaced with values linearly interpolated from the preceding and following "good" data. From the corrected navigation data, the ship velocity is calculated. The second step in processing the data is the initial determination of the depth (bin number) to which the data of each ensemble remains reliable. If the percent of good returns drops below 60%, all deeper data are dropped.

After the first and second steps a reference layer five bins wide (62-78 m) was chosen. The choice of a reference layer depth is some what arbitrary, but appears to have little affect on the final calculated water velocities. Subtracting the ships velocity from the average velocity within the chosen reference layer yields an absolute reference layer velocity for each ensemble. The series of absolute reference velocity was filtered with a low pass Hanning window filter. The cutoff frequency of this filter is in the range of 0.03-0.05 cycles per minute.

The Sippican T-4 XBT's provided temperature profiles down to 450 m. The processing and storage of XBT data were done with a HP computer system and software developed by the Department of Oceanography, Naval Postgraduate School. MK-9 XBT/XSV system as a deck unit for signal acquisition. The temperature profiles can be plotted from the printer on ship. The manufacturer specifications of ADCP and XBT are listed in Table I.

TABLE I. ADCP AND XBT MANUFACTURER SPECIFICATIONS

Instrument	Range	Accuracy	Resolution
ADCP	0-450 m	± 2-3 cm/s	0.1 cm/s
XBT	-2.2°C 35.6°C	±0.15°C	0.01°C

B. CALIBRATION

The ADCP measured currents are relative to the ADCP, which can be oriented arbitrarily and moved relative to the earth. It is necessary to correct the data for ADCP attitude and motion. There are two kinds of motion that require correction: rotation (pitch, roll and heading) and translation (ship velocity).

Properly averaging the relative velocity measurements, the vectors must first be transformed from the ships coordinate system (x', y', z') to geographic coordinates with origin at the ships transducer and coordinate axes x, y and z pointing east, north and up respectively. The transformation between

geographic and ship's coordinates is done by a series of three rotations. Any arbitrary vector whose representaion in ship coordinates is A' will have a representation in geographic coordinates given by $A = R_\theta R_\rho R_\phi A'$ where θ is the ship's heading measured from y axis (North) to x axis (ship's bow), ρ the roll angle positive from port side elevated, and ϕ the pitch angle positive for bow elevated.

$$R_\theta = \begin{vmatrix} \sin\theta & -\cos\theta & 0 \\ \cos\theta & \sin\theta & 0 \\ 0 & 0 & 1 \end{vmatrix} \qquad (1)$$

$$R_\rho = \begin{vmatrix} 1 & 0 & 0 \\ 0 & -\cos\rho & -\sin\rho \\ 0 & \sin\rho & \cos\rho \end{vmatrix} \qquad (2)$$

$$R_\phi = \begin{vmatrix} \cos\phi & 0 & -\sin\phi \\ 0 & 1 & 0 \\ \sin\phi & 0 & \cos\phi \end{vmatrix} \qquad (3)$$

If the relative velocity vector measured in ship coordinates is V', the time average relative velocity in geographic coordinates will be $\overline{V} = \overline{R_\theta R_\rho R_\phi V'}$. . Because the transformation between the two systems is time dependent, the data must be transformed to geographic coordinates before averaging to obtain correct averages. Since the transformation

is performed using measured values of θ, ρ, and ϕ, the errors in measuring this angle will affect inferred average velocity.

1. Pitch and Roll

The effect of pitch and roll of the ship on measured profiles of the relative vector requires consideration of two effects: (1) the components of V' must be rotated to level coordinates; (2) the location of the measurements of Z' must be transformed. The relationship between V(z) and V'(z') is

$$V(z) = R_\theta \, [V'(z') - E] \qquad (4)$$

The full error vector E is the velocity over estimate if the profile is not corrected for pitch and roll.

The long term average of ship vertical velocity has a substantial bias of order 3-4 cm/s when pitch and roll compensation is not performed. The long term bias in the horizontal velocities is less than 1 cm/sec (Kosro, SIO Ref., 1985). These indicate that for a well-riding vessel, the averages of acoustic profiles can be calculated with minimal error in horizontal velocity estimates by treating the data as though they were measured in a level plane ignoring corrections for pitch and roll.

2. Heading

The ship's heading, the angle between North and the ship's bow, is the third reference angle which must be determined before the relative velocity profile can be rotated to geographic coordinates. The measurements of heading

introduce the largest uncertainty into current velocity estimates. A small measurement error in θ can lead to large error in the inferred geographic components of relative velocity, and therefore to large spurious current. If the measured heading is $\tilde{\theta} = \theta - \delta\theta$, where $\delta\theta$ is the measurement error, then the geographic components of relative velocity will be in error by

$$\tilde{U}(z) - U(z) = U(z)\,(\cos\delta\theta - 1) + V(z)\sin\delta\theta \qquad \textbf{(5a)}$$

$$\tilde{V}(z) - V(z) = U(z)\sin\delta\theta + V(z)\,(\cos\delta\theta - 1) \qquad \textbf{(5b)}$$

The heading error is dominated by rotation of the large foreward component of velocity into the athwartship component. The error currents will be polarized in the athwartship direction and will increase with the speed of ship, errors $\delta\theta$ of this order of magnitude cannot be ruled out.

To provide a heading measurement, the gyrocompass must sense its orientation relative to three directions. The fore/aft axis of the ship, the direction of gravitational acceleration and the axis of the Earth provide these reference directions. An error in the direction of anyone of these will yield an error in the measured heading.

Some characteristics of measurement error present in gyrocompasses are as follows:

1. The misalignment angle which is the constant angle between the gyrocompass foreward direction and the foreward direction defined by the acoustic beams.

2. The latitude error and velocity error which are usually corrected in the course of normal ship operations.

3. The acceleration error which takes the form of damped oscillations in the heading at 84 minute period.

4. The quadrantal error, the wave-induced rolling error, depends on the method of the gyrocompass construction.

There are many ways to measure rotation and translation. The use of one method depends on a variety of factors. Rotation (heading) can be measured by either a gyrocompass or a flux-gate compass. Rotation (pitch and roll) can be detected by either a vertical gyro or pendulums. Finally, translation can be measued by electronic navigation (LORAN-C, GPS, microwave, etc.), bottom tracking, or by assuming a 'layer of no motion' (reference layer).

A scheme for ADCP calibration which may take advantage of bottom tracking by the ADCP if water depths are not too large, is illustrated as follows (Joyce, 1989). Let (u',v') represent the east and north velocity components as measured in the (x',y') coordinate system and (u,v) the east and north components in the true (x,y) coordinates system. Velocity in the two coordinate systems is related by

$$\begin{pmatrix} u' \\ v' \end{pmatrix} = \begin{pmatrix} \cos\alpha & \sin\alpha \\ -\sin\alpha & \cos\alpha \end{pmatrix} \begin{pmatrix} u \\ v \end{pmatrix} \qquad (6)$$

Thus the water velocities in the true (x,y) coordinate system are:

$$u_w = u_s + (1 + \beta)\,(u_d\cos\alpha - v_a\sin\alpha) \qquad (7a)$$

$$v_w = v_s + (1+\beta)\,(u_a\sin\alpha + v_a\cos\alpha) \qquad (7b)$$

Where (U_w, v_w) is the water velocity, (u_s, v_s) is the ship velocity, and (u_d, v_d) is the Doppler velocity, β is the scale factor, and α is the heading angle between true north and measured north direction. The water velocity (u_w, v_w) is further decomposed into offshore (U) and alongshore (V) components by using a similar rotation formula:

$$\begin{pmatrix} U \\ V \end{pmatrix} = \begin{pmatrix} u_w \\ v_w \end{pmatrix} \begin{pmatrix} \cos\gamma & \sin\gamma \\ -\sin\gamma & \cos\gamma \end{pmatrix} \qquad (8)$$

where γ is 313°. This coordinate system is shown in figure 9.

C. OTHER DATA

In addition to ADCP and XBT data, meteorological and surface oceanographic data were collected by a Serial ASCII Interface Loop (SAIL) system. This system monitors, averages, and stores: ship position, speed and heading, relative wind speed and direction, air temperature, dew point temperature, sea surface salinity, sea surface temperature, visible and infrared solar insolation, and sea surface skin temperature. These data were averaged over 30 second intervals and recorded on an HP9826 computer.

IV. CURRENT STRUCTURE

Two flow patterns can be discerned from these surveys, a strong alongshore poleward current (centered at 5-15 km from San Clemente Island) and some small-scale eddies (one occured about 10 km from the island during 18-21 July, 1989, and the others further than 30 km from San Clemente Island during the second cruise during 4-6 September, 1989). Comparing the data from these cruises, eddy variability was complicated.

In general, current characteristics were:

1. The poleward alongshore currents occuring in the upper 50 meter were stronger than the cross-shelf currents. The jet speed of the poleward currents was around 35-50 cm/sec.

2. Eddies were shown variable from time to time and place to place, with length scale 10 km and velocity about 15-30 cm/sec.

In figure 2, ADCP data was missing from station 35 to station 37. In figure 5h and 6h, some data was dropped due to bad return signals around 400 m depth.

A. HORIZONTAL DISTRIBUTION

Figures 4a-4h show the vertically averaged current in the following layers : 12-28 m, 42-58 m, 92-108 m, 142-158 m, 192-208 m, 242-258 m, 292-308 m and 392-408 m. These were made during the first cruise (17-21 July, 1989). The following characterizes the flow pattern:

1. The strongest current occured near the surface at 32° 36'N-32° 50'N, 118° 35'W-118° 45'W. Maximum velocity is about 50 cm/sec and current direction is parallel to the island from SE to NW.

2. A cyclonic eddy occurred at 32° 51'N 118° 40'W with a velocity of approximately 30 cm/s at 6 km from the eddy center. The length scale of this eddy is about 10 km and it extended to a depth of 50 meters.

3. Except the areas mentioned in (1) and (2) above, currents in the rest of this study area did not have a systematic pattern. Maximum velocity near the surface reduced from 50 cm/s to approximately 20 cm/s at a depth of 400 m.

Figure 5 shows the vertically averaged current in the following layers: 12-28 m, 42-58 m, 92-108 m, 142-158 m, 192-208 m, 242-258 m, 292-308 m and 392-408 m during 4-6 September, 1989. The ship's course was from SE to NW and vice versa. These were made during the first pass over San Clemente Basin on cruise SCBE II. Results are:

1. The poleward flow center is located 11 km offshore. Strongest currents are in the 12-58 m layers with flow speeds of over 50 cm/s and are located at 32° 50' N, 118° 46'.

2. There are two eddies observed 30 km from San Clemente Island. The first eddy is centered at 32° 50' N, 118° 59' W and the second eddy is centered at 32° 45' N, 118° 50' W. The length-scale of these two eddies is approximately 10 km.

Figure 6 shows the vertically averaged current in the following layers: 12-28 m, 42-58 m, 92-108 m, 142-158 m, 192-208 m, 242-258 m, 292-308 m and 392-408 m. These were obtained during the second pass over San Clemente Basin on cruise SCBE II during 4-6 September, 1989. The ship's course was from NE to SW and return. The results are:

1. The poleward flow velocity, approximately 30 cm/s, was weaker than first pass after over 30 hours.

2. The northern region of study area shows a strong offshore current of about 30 cm/s from surface to a depth of 250 m. The maximum velocity of 45 cm/s was found at 32° 45′ N, 118° 42′ W.

3. The eddies were weakened after 30 hours. There were no apparent eddies found during the second pass.

The circulation measured during the second pass, figure 6a to 6h, was much different from the circulation measured during the first pass, figure 5a to figure 5h, especially in the poleward flow area. Nevertheless, the strong poleward currents were observed during these two measurements.

B. VERTICAL PROFILES

Twenty current (u,v) profiles were plotted (figure 7a - 7t). Each profile consists of U and V components from the sea surface to a depth of 400 m over the San Clemente Basin, where U and V are onshore and alongshore velocity respectively.

The location of these data is shown in figure 3 where stations M1, M2.....M9 were in the poleward flow area, stations E1, E2.....E6 represent the region of the first eddy area, and stations D1, D2.....D5 represent the second eddy area. Table II shows the U,V component for 20 stations which change with depth. The results shown from these vertical profiles are:

1. Figure 7a shows strong alongshore flow at station M2 of over 50 cm/s at the surface with the velocity decreasing rapidly at about 30 m depth. Stations M3,

M4, M5, M6, M8 in figure 7a, 7b show a strong alongshore flow pattern.

2. Profiles at E2 and E3 in figure 7c near the center of the first eddy showed a weak flow from the surface to a depth of 400 m.

The mean flow pattern in the study area is shown in figure 8. The strong poleward flow velocity (15 cm/s) from the surface to a depth of 30 m decreased gradually with an increase of depth to a velocity of approximately 5 cm/s at a depth of 400 m. The mean offshore flow velocity of 5 cm/s in the upper layer decreased to 1 cm/s at a depth of 250 m.

TABLE II. VELOCITY DATA AT 20 STATIONS

Site	Station No.	Latitude	Longitude	Bottom depth (m)	Instrument depth (m)	Onshore Current (cm/s)	Alongshore Current (cm/s)
E1	46	32° 52.4'N	119° 2.1'W	1600	0	9.7	-12.6
					50	-2.1	4.1
					100	-6.9	0.3
					200	-4.5	2.2
					300	-4.1	8.0
					400	-6.0	3.7
E2	51	32° 50.5'N	119° 0.8'W	1625	0	10.4	-11.4
					50	-6.1	-6.5
					100	-2.2	-7.8
					200	-4.2	-6.1
					300	.05	-1.2
					400		
E3	50	32° 52.9'N	118° 55.9'W	1675	0	-3.7	-14.2
					50	1.0	-7.8

Site	Station No.	Latitude	Longitude	Bottom depth (m)	Instrument depth (m)	Onshore Current (cm/s)	Alongshore Current (cm
					100	-6.6	-0.2
					200	-4.7	-8.1
					300	-0.4	-2.4
					400	-0.9	-3.1
E4	52	32° 46.7'N	118° 59.6 W	1400	0	-3.6	-20.2
					50	11.2	8.3
					100	7.5	8.4
					200	12.0	10.9
					300	6.3	7.8
					400	12.5	5.9
E5	53	32° 48.9'N	118° 55.1'W	1550	0	-18.7	9.4
					50	-4.7	17.3
					100	-5.4	23.4
					200	-10.3	24.7
					300	-8.8	16.7
					400	-6.1	22.4
E6	54	32° 51.8'N	118° 49.7'W	1575	0	25	18.9
					50	-19.4	5.6
					100	-11.7	13.9
					200	-8.5	7.5
					300	-4.7	11.2
					400	-7.7	10.2
D1	59	32° 47.2'N	118° 49.1'W	1225	0	17.6	31.1
					50	-18.5	-0.7
					100	-10.7	-4.5
					200	-8.5	-2.1
					300	-11.0	-4.4
					400		

Site	Station No.	Latitude	Longitude	Bottom depth (m)	Instrument depth (m)	Onshore Current (cm/s)	Alongshore Current (cm/s)
D2	61	32° 41.1'N	118° 52.5'W	1020	0	17.6	31.1
					50	-2.0	19.6
					100	8.9	16.6
					200	11.6	7.0
					300	2.6	9.9
					400	2.9	6.4
D3	62	32° 43.5'N	118° 47.2'W	1550	0	-7.1	18.6
					50	-14.5	26.4
					100	-10.3	19.2
					200	-8.9	17.5
					300	-3.5	16.8
					400	-3.2	14
D4	63	32° 43.5'N	118° 41.9'W	1200	0	-24	23.1
					50	-23.8	40.8
					100	-20.1	27.4
					200	-17.0	17.5
					300	-24.0	16.4
					400	-20.4	16.3
D5	68	32° 40.8'N	118° 43.4'W	1260	0	6.63	-11.8
					50	5.4	-5.5
					100	5.73	-6.3
					200	1.2	-9.0
					300	5.4	-3.7
					400		
M1	43	33° 2.8'N	118° 56.1'W	1700	0	-12.8	-12.7
					50	-10.0	-17.6
					100	-0.4	-17.1
					200	2.5	-14.5

Site	Station No.	Latitude	Longitude	Bottom depth (m)	Instrument depth (m)	Onshore Current (cm/s)	Alongshore Current (cm/s)
					300	-1.7	-9.5
					400	4.5	-16.9
M2	42	33° 4.9'N	118° 52.'W	1600	0	-35.4	2.7
					50	-37.2	5.6
					100	-39.1	1.7
					200	-38.8	5.0
					300	-32.5	5.9
					400	-19.6	4.4
M3	48	33° 1.4'N	118° 47.4'W	11360	0	-32.6	-1.4
					50	-23.4	7.6
					100	-14.1	9.2
					200	-10.0	12.6
					300	-4.0	7.9
					400	-13.6	7.4
M4	49	32° 56.9'N	118° 49.2'W	1350	0	-31.1	-5.0
					50	-16.3	-18.8
					100	-18.5	-10.2
					200	-8.3	-3.5
					300	-8.4	-12.0
					400		
M5	56	32° 55.5'N	118° 40.1'W	1000	0	-30.3	6.4
					50	-33.0	7.2
					100	-18.7	0.5
					200	-5.7	6.5
					300	-12.3	3.6
					400	-14.3	6.1
M6	64	32° 49.3'N	118° 36.5'W	850	0	-22.2	27.7
					50	-26.2	38

Site	Station No.	Latitude	Longitude	Bottom depth (m)	Instrument depth (m)	Onshore Current (cm/s)	Alongshore Current (cm/s)
					100	-21.3	18.3
					200	-23.0	18.1
					300	-16.6	18.9
					400	-16.0	18.8
M7	66	32° 46.3'N	118° 33.6'W	550	0	-0.2	-1.1
					20	-23.7	-3.4
					100	-2.9	28.3
					200	-6.3	-5.1
					300	-4.7	-2.0
					400	-3.0	-0.3
M8	73	32° 42.8'N	118° 30.7'W	680	0	-27.8	-11.7
					50	-5.8	-2.9
					128	-18.6	-10.8
					200	-9.4	-7.5
					300	-10.2	-13
					400	-3.9	-5.7
M9	74	32° 44.8'N	118° 27.0'W	240	0	-10.2	12.5
					50	15.7	19.6
					132	-13.2	17.5
					200	-3.5	19.2

C. CROSS SECTIONS

1. Onshore and Alongshore Currents

Figure 9 shows the coordinate system and the primary cruise track along which most shipboard current measurements were made during the second pass over the study area from 4-6 September, 1989 during SCBE-II. The coordinate origin is at

32° 47′ N, 118°. 26′ W, and the Y-axis has been rotated 313°., i.e., from a north to a northwest direction. The study area is located in the minus X direction. Primary lines were separated approximately 7-8 km from 0 km to 54 km from southeast to northwest.

Figure 10a-10h shows the section of onshore and alongshore currents from the 54 km to the 0 km line.

(1) The figure indicates strong poleward current on the surface at an offshore distance approximately 5-10 km with weak flow offshore 20-30 km. Equatorward current increased farther offshore beginning at a distance of 35 km. Each primary line from north to south displays strong mean current flow of approximately 20 cm/s, located offshore 10 km, from the surface to 400 m depth.

(2) Onshore currents are variable. The 15 km line in Fig. 10f shows a strong onshore current of 15-30 cm/s. The 31 km and 23 km line also show a somewhat strong onshore current, but the 54 km and 39 km line show offshore flow.

(3) A jet appeared in Fig. 10e to 10h with a speed of around 35-45 cm/s. The core of the jet appears to accelerate and move onshore from South to North.

(4) Cyclonic eddy structure can be found from a transition zone on the 31 km primary line (figure 10d). The 39 km line (figure 10c) contains opposing alongshore flows and the 31 km line onshore current. The 39 km line has offshore flow.

2. Standard Deviation of the Currents

The standard deviation of fluctuations are a measure of the variability of the current velocity. Fluctuations in U and V about their mean values (Fig. 11a - Fig. 11h) are at least as large as the mean velocity. Far from shore, the fluctuations in U and V are weaker. As the coast is approched the fluctuations in V are stronger.

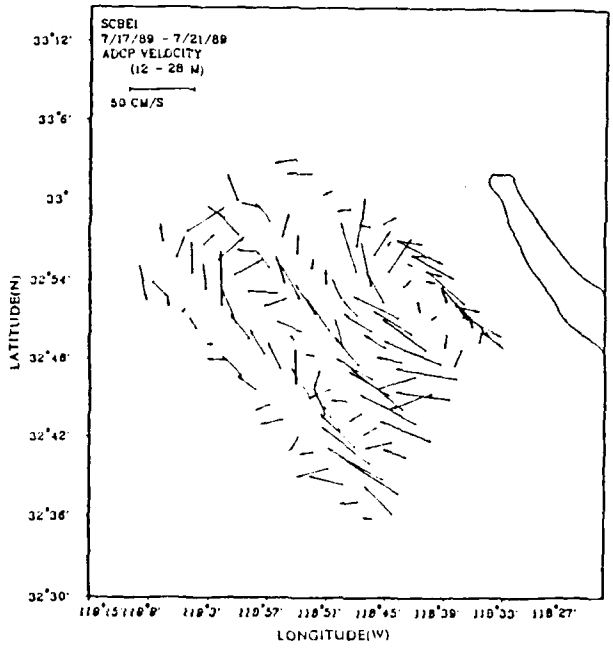

Figure 4a. Vertically averaged currents (12-28 m) measured during the cruise SCBE-I (1920 UT, 18 July - 1411 UT, 20 July).

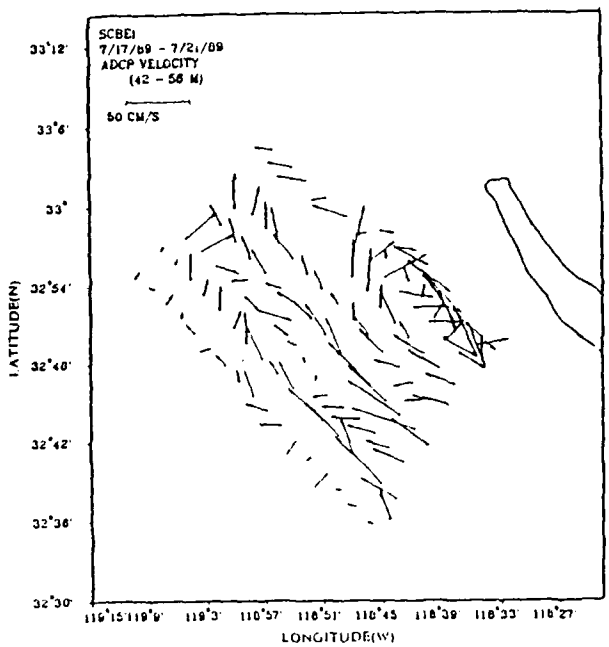

Figure 4b. Vertically averaged currents (42-58 m) measured during the cruise SCBE-I (1920 UT, 18 July - 1411 UT, 20 July).

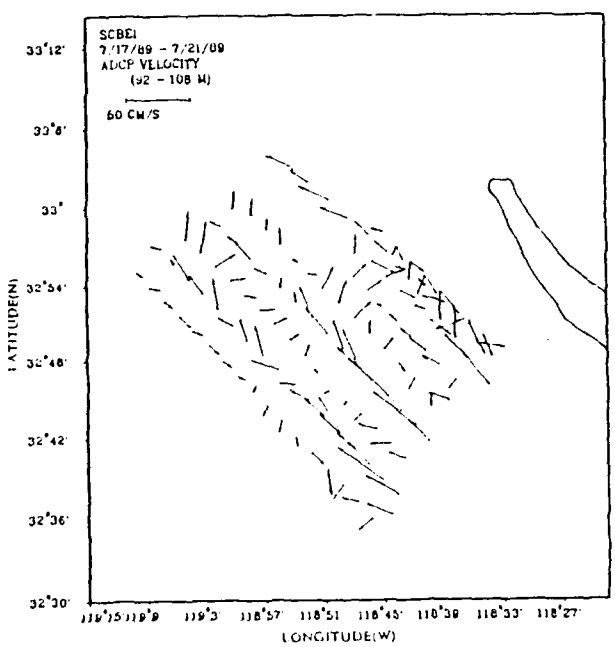

Figure 4c. Vertically averaged currents (92-108 m) measured during the cruise SCBE-I (1920 UT, 18 July - 1411 UT, 20 July).

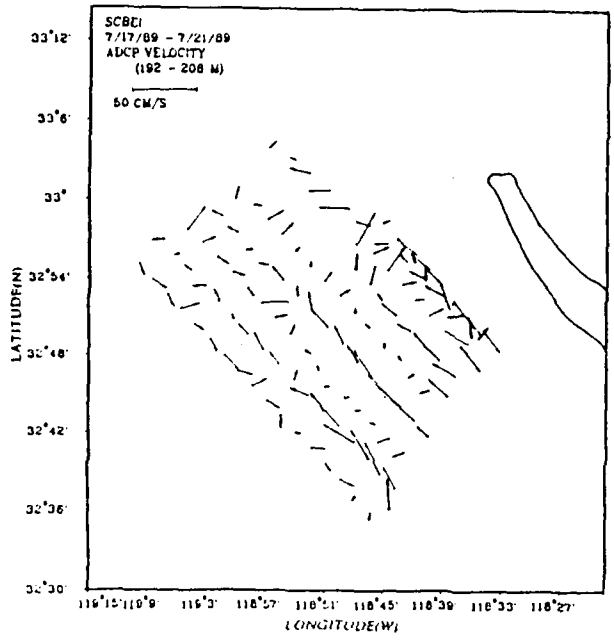

Figure 4d. Vertically averaged currents (192-208 m) measured during the cruise SCBE-I (1920 UT, 18 July - 1411 UT, 20 July).

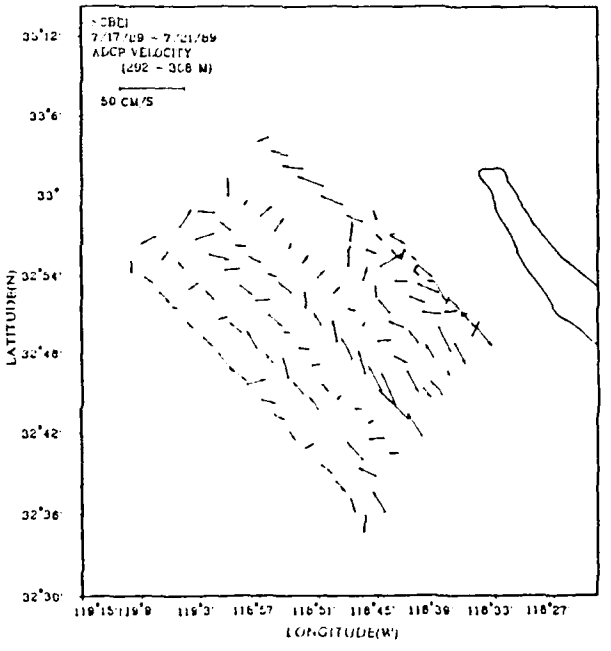

Figure 4e. Vertically averaged currents (292-308 m) measured during the cruise SCBE-I (1920 UT, 18 July - 1411 UT, 20 July).

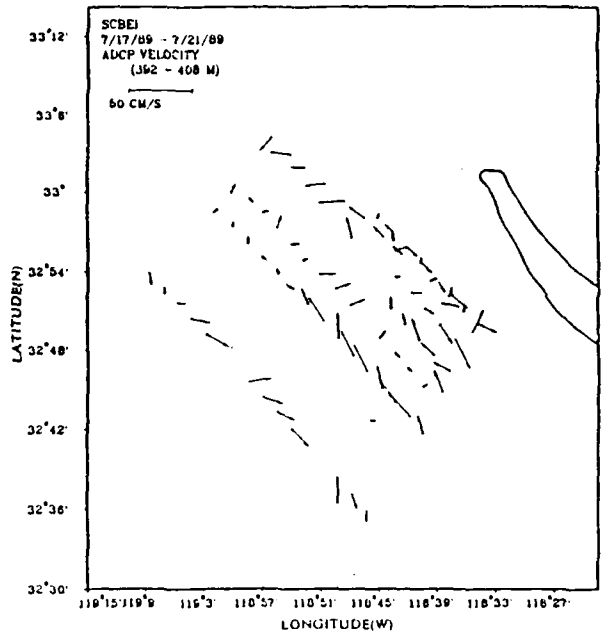

Figure 4f. Vertically averaged currents (392-408 m) measured during the cruise SCBE-I (1920 UT, 18 July - 1411 UT, 20 July).

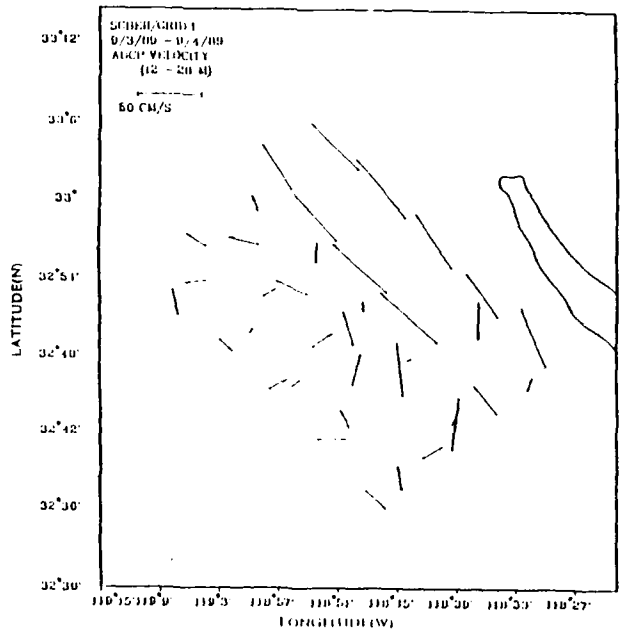

Figure 5a. Vertically averaged currents (12-28 m) measured during the cruise SCBE-II (2240 UT, 3 September - 2330 UT, 4 September)

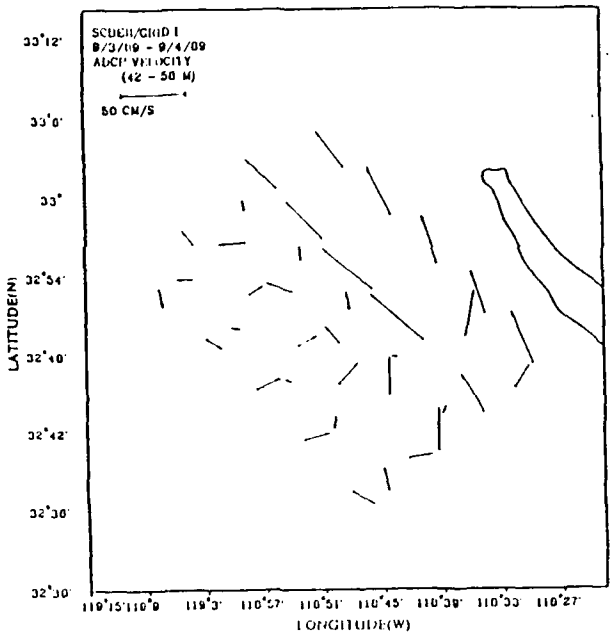

Figure 5b. Vertically averaged currents (42-58 m) measured during the cruise SCBE-II (2240 UT, 3 September - 2330 UT, 4 September)

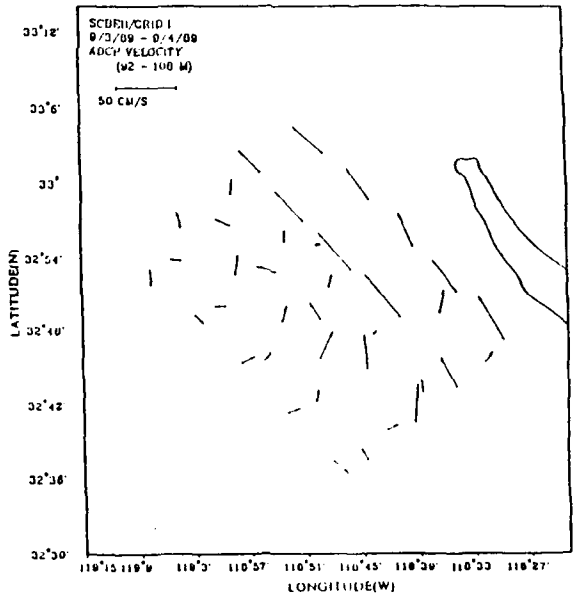

Figure 5c. Vertically averaged currents (92-108 m) measured during the cruise SCBE-II (2240 UT, 3 September, - 2330 UT, 4 September)

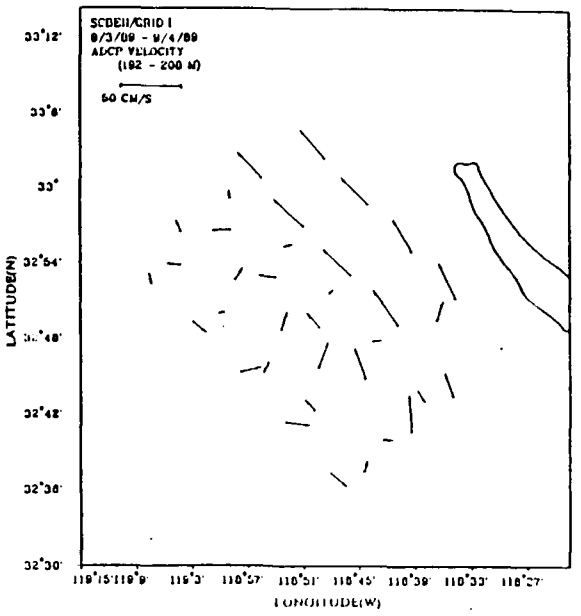

Figure 5d. Vertically averaged currents (192-208 m) measured during the cruise SCBE-II (2240 UT, 3 September - 2330 UT, 4 September)

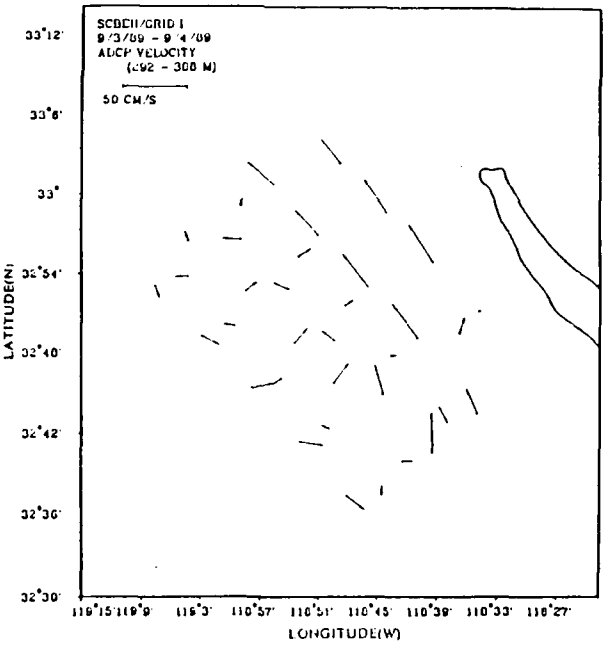

Figure 5e. Vertically averaged currents (292-308 m) measured during the cruise SCBE-II (2240 UT, 3 September, - 2330 UT, 4 September)

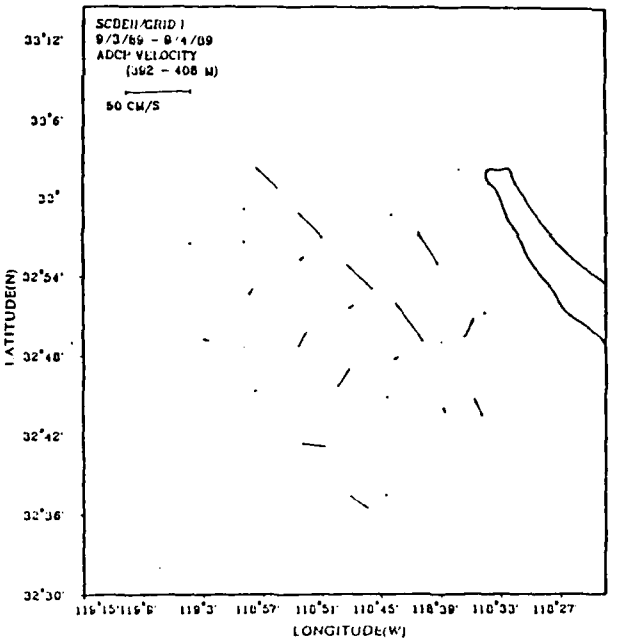

Figure 5f. Vertically averaged currents (392-408 m) measured during the cruise SCBE-II (2240 UT, 3 September - 2230 UT, 4 September)

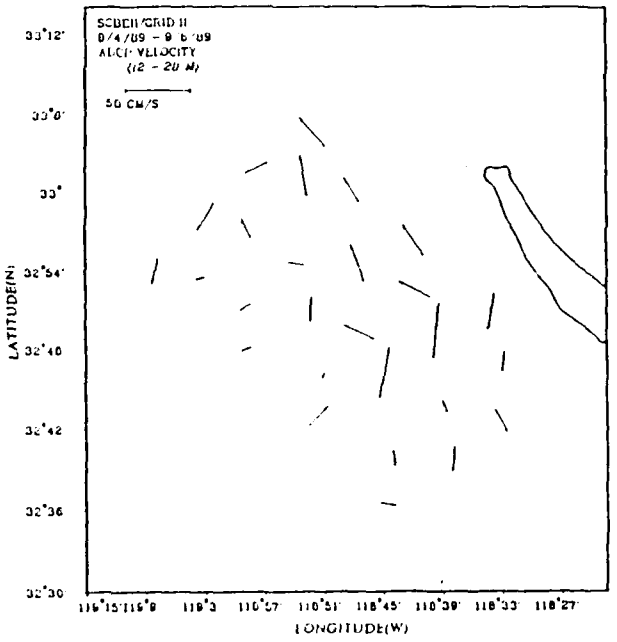

Figure 6a. Vertically averaged currents (12-28 m) measured during the cruise SCBE-II (2240 UT, 4 September - 0640 UT, 6 September)

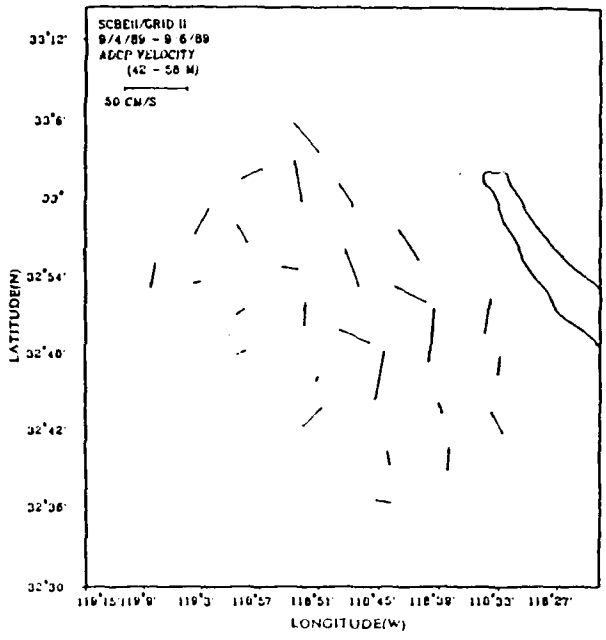

Figure 6b. Vertically averaged currents (42-58 m) measured during the cruise SCBE-II (2240 UT, 4 September - 0640 UT, 6 September)

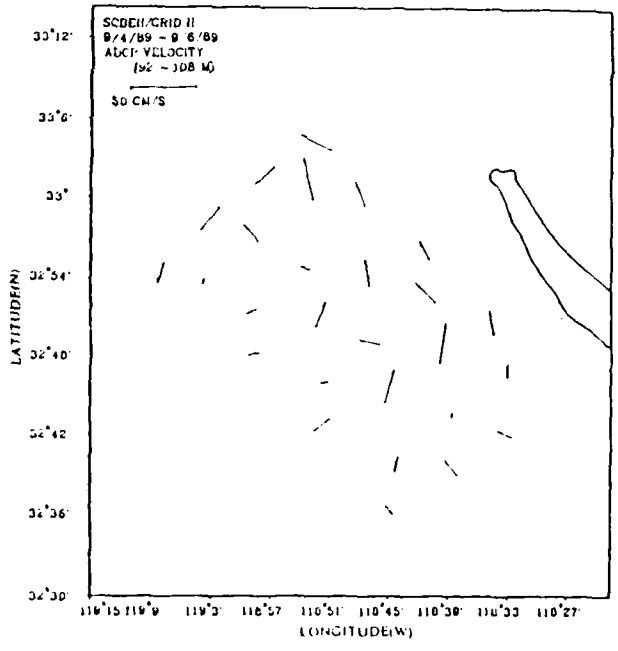

Figure 6c. Vertically averaged currents (92-108 m) measured during the cruise SCBE-II (2240 UT, 4 September - 0640 UT, 6 September)

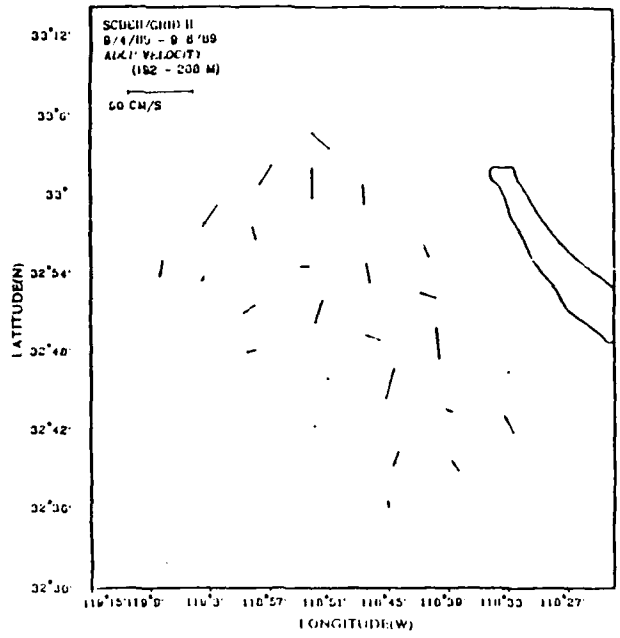

Figure 6d. Vertically averaged currents (192-208 m) measured during the cruise SCBE-II (2240 UT, 4 September - 0640 UT, 6 September)

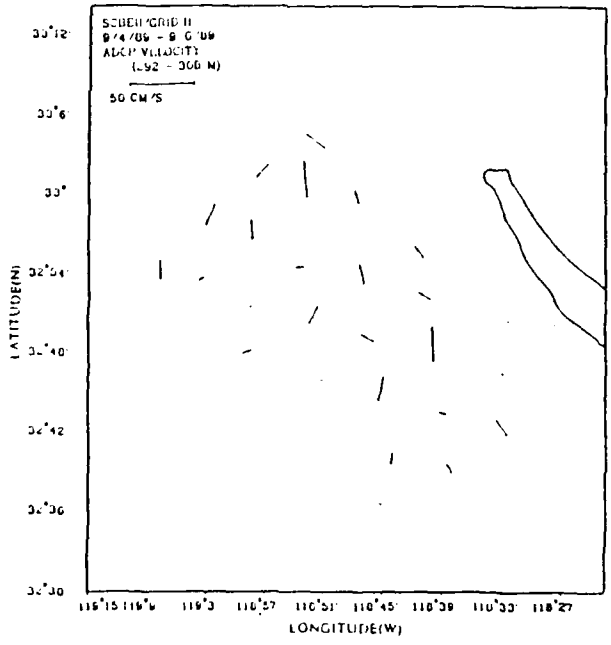

Figure 6e. Vertically averaged currents (292-308 m) measured during the cruise SCBE-II (2240 UT, 4 September - 0640 UT, 6 September)

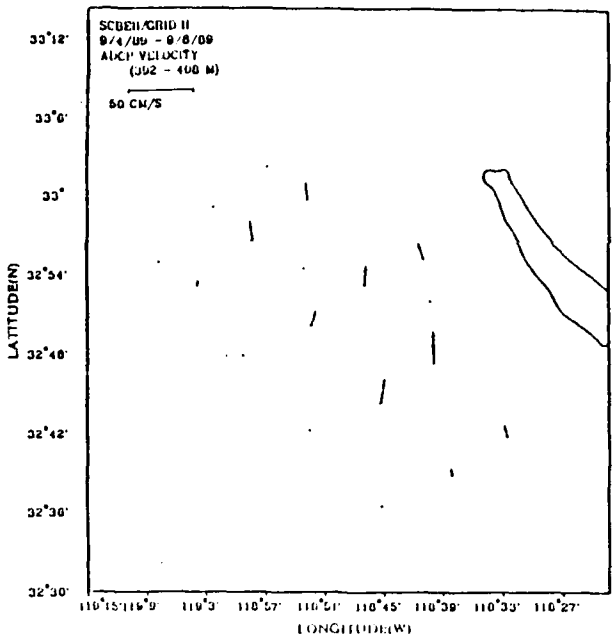

Figure 6f. Vertically averaged currents (392-408 m) measured during the cruise SCBE-II (2240 UT, 4 September - 0640 UT, 6 September)

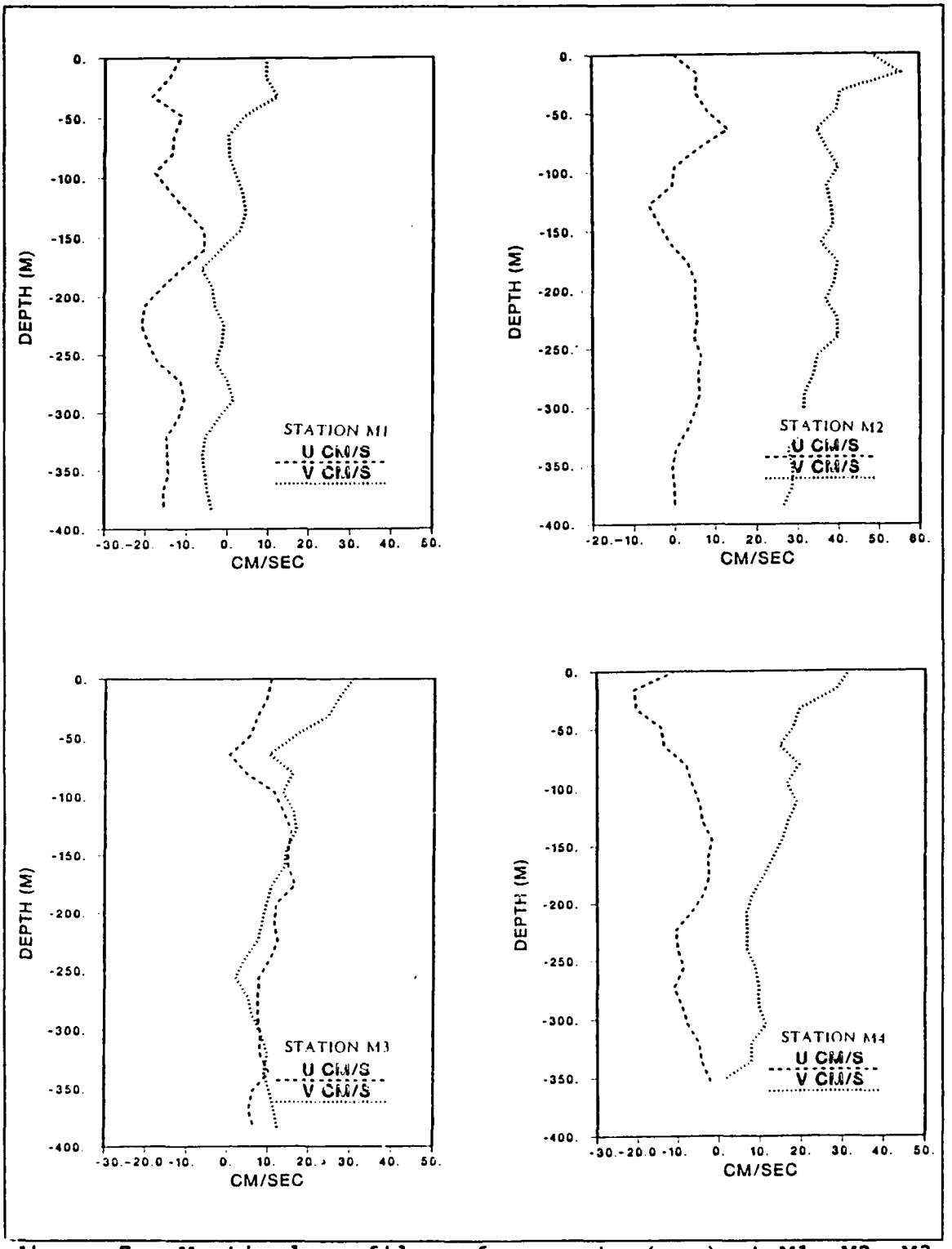

Figure 7a. Vertical profiles of currents (u,v) at M1, M2, M3, M4 in figure 3

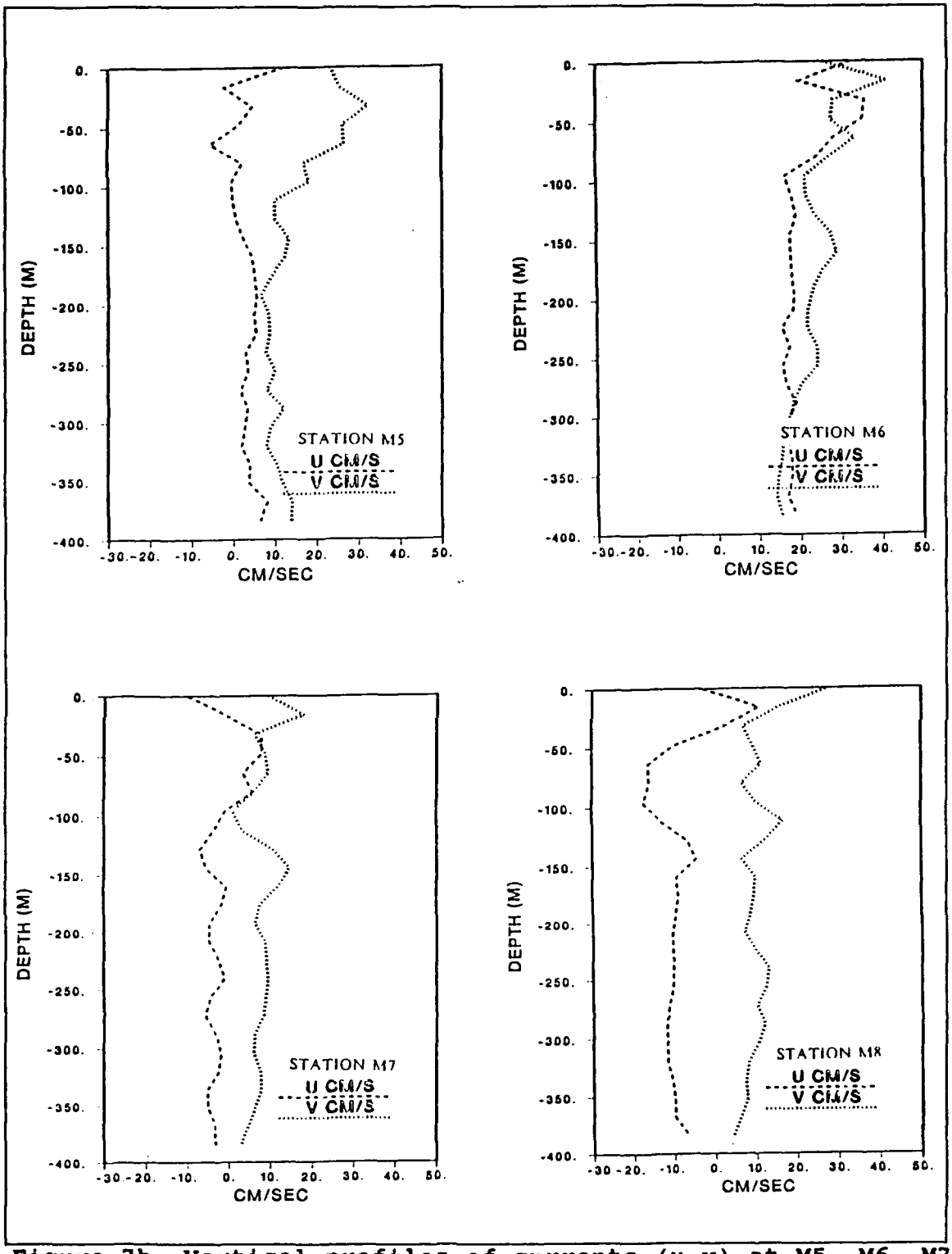

Figure 7b. Vertical profiles of currents (u,v) at M5, M6, M7, M8 in figure 3

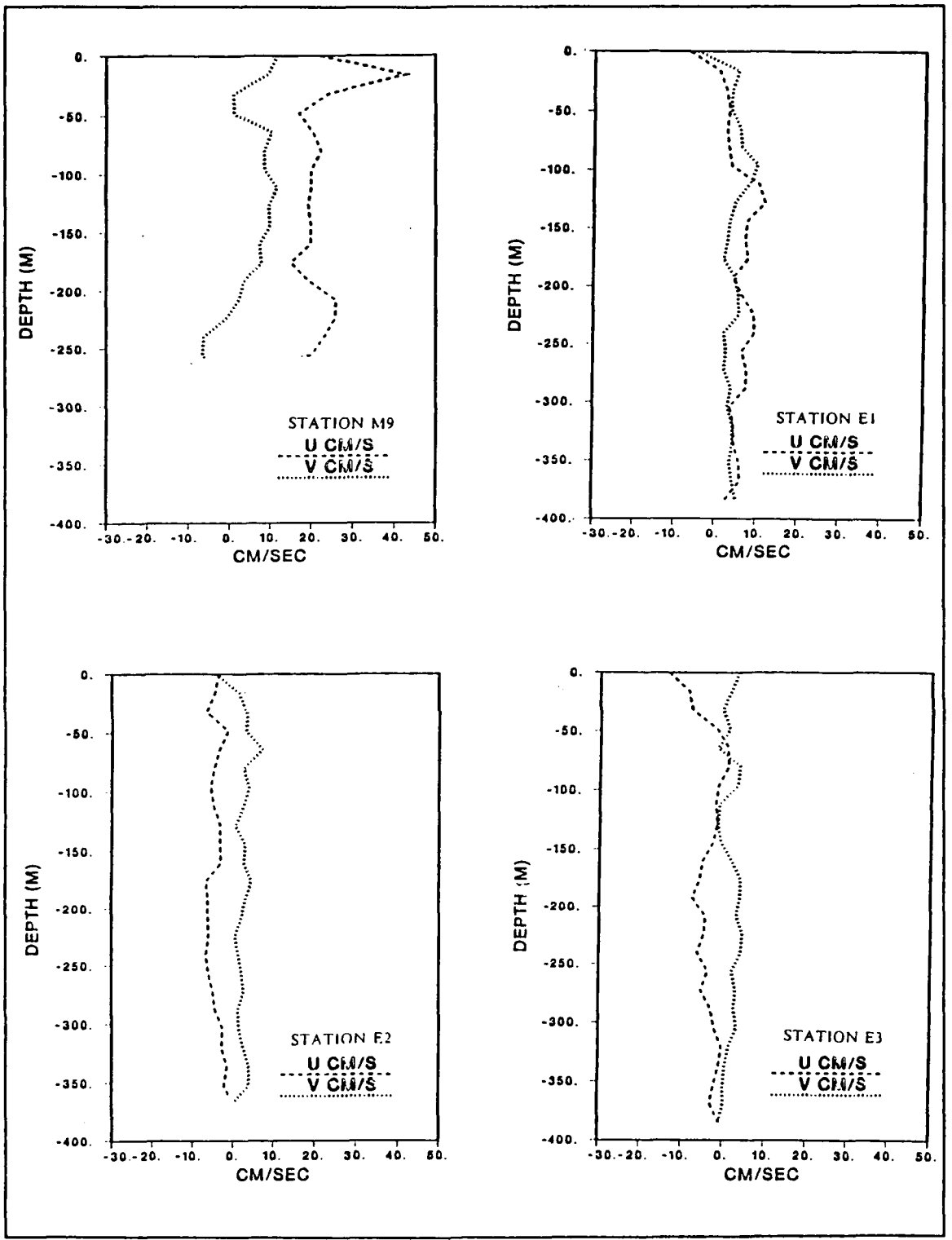

Figure 7c. Vertical profiles of currents (u,v) at M9, E1, E2, E3 in figure 3

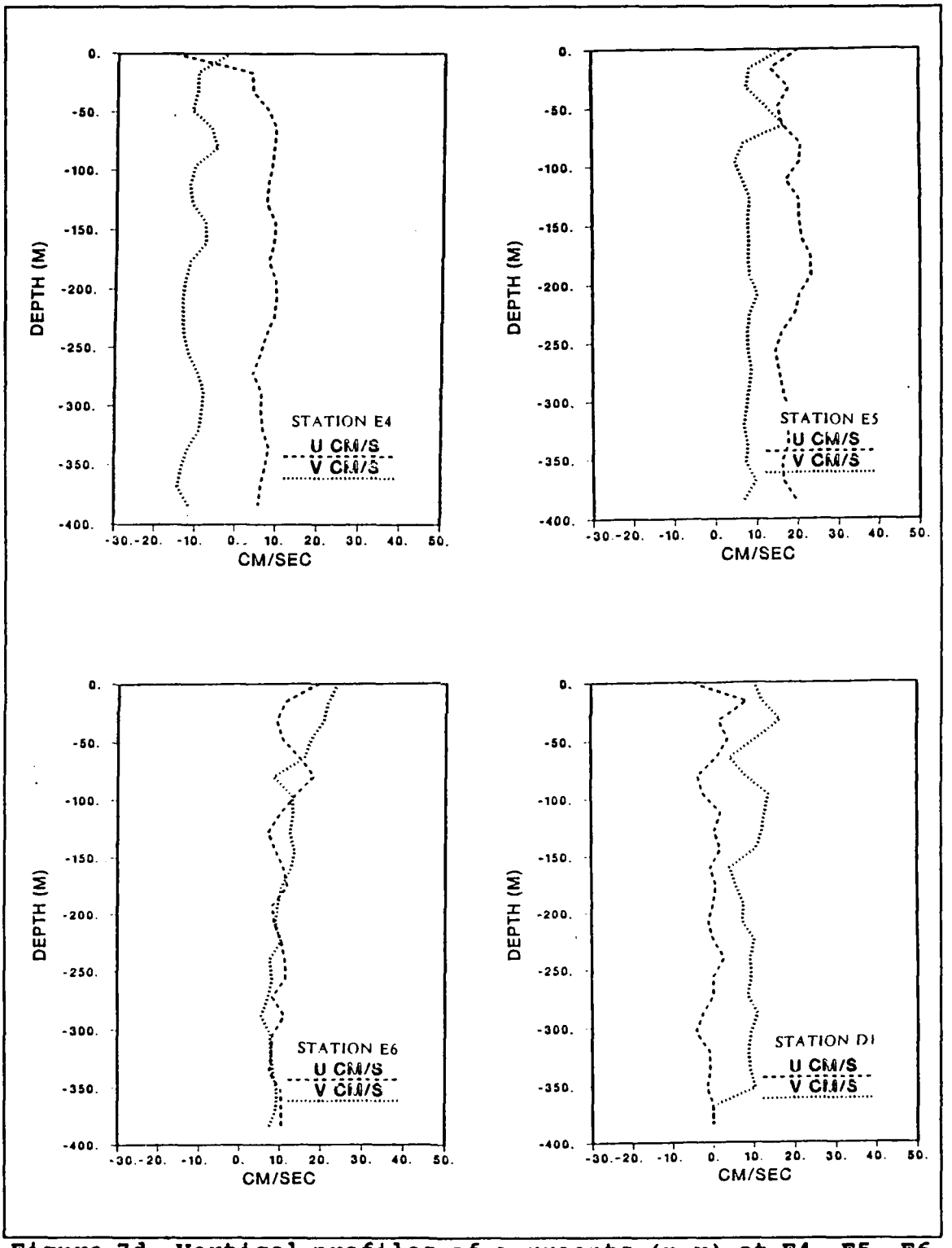

Figure 7d. Vertical profiles of curreents (u,v) at E4, E5, E6, D1 in figure 3.

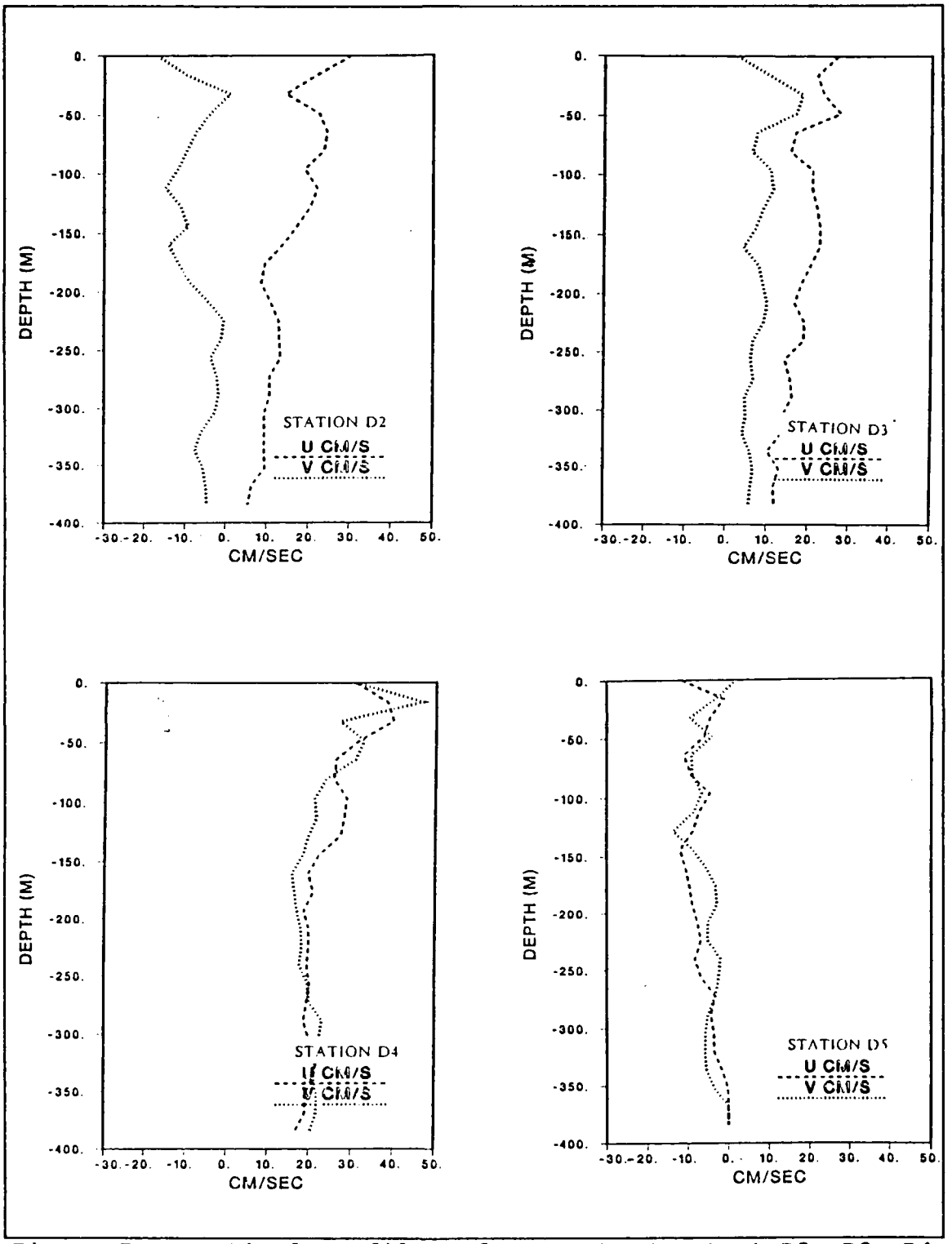

Figure 7e. Vertical profiles of currents (u,v) at D2, D3, D4, D5 in figure 3

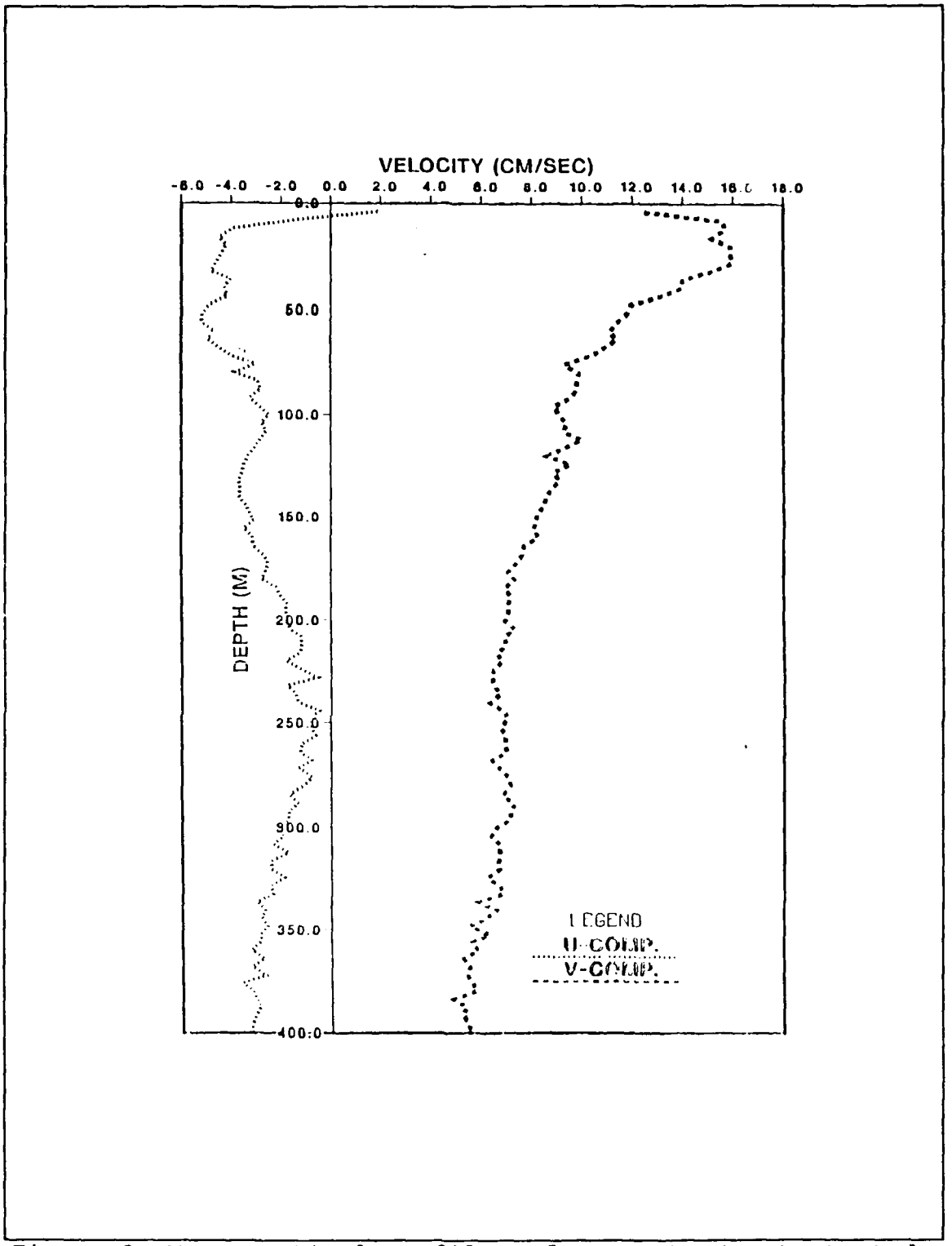

Figure 8. Mean vertical profiles of currents (u,v) at study area given in figure 2 and figure 3

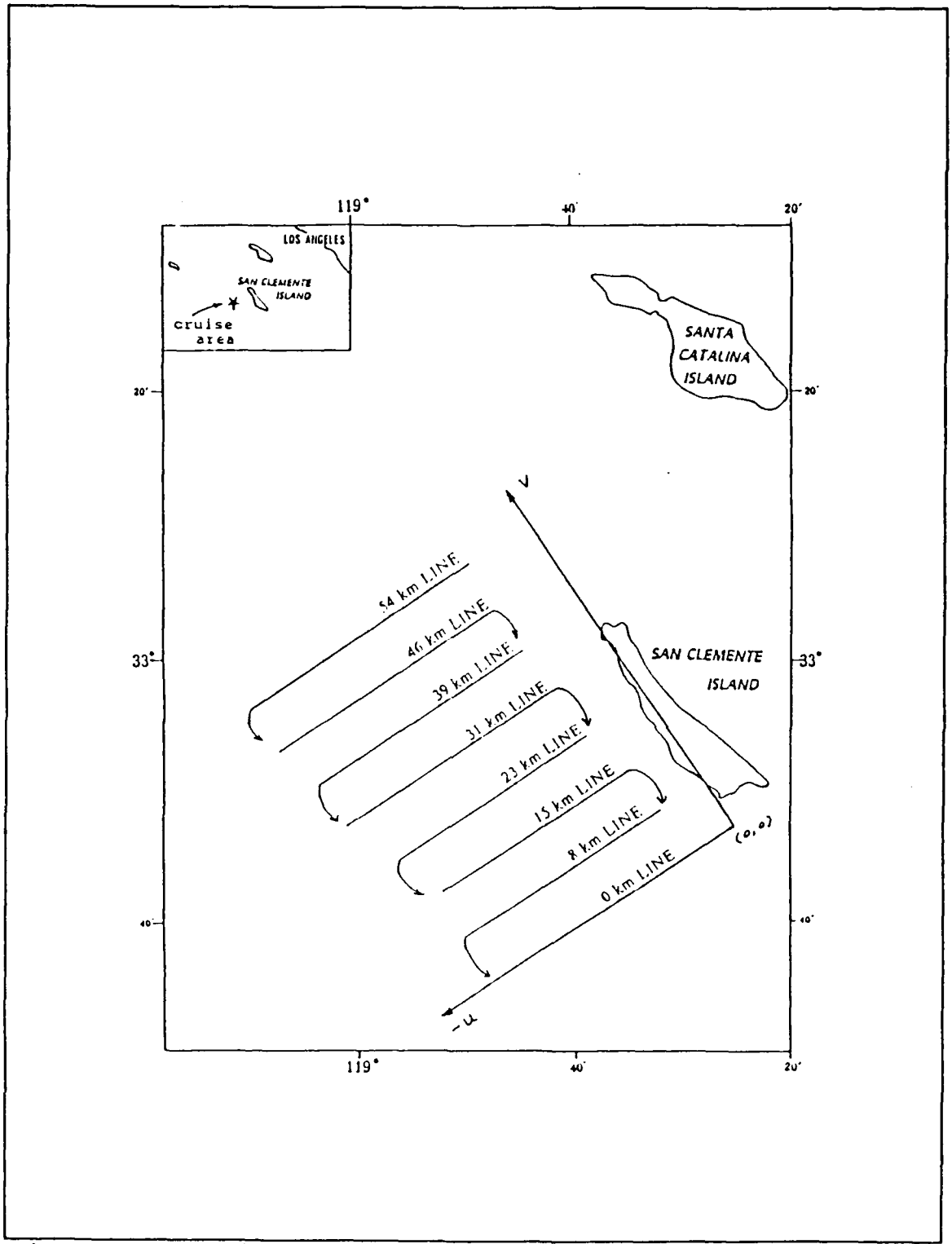

Figure 9. Coordinate system and primary cruise lines along which most shipboard current measurements were made

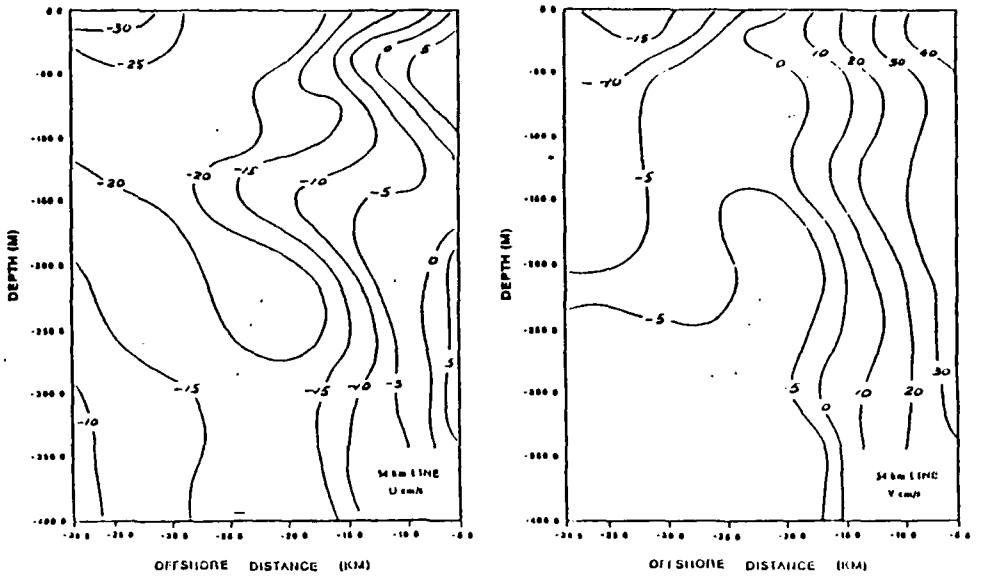

Figure 10a. Vertical cross-section of onshore and alongshore current components at the 54 km line in figure 9.

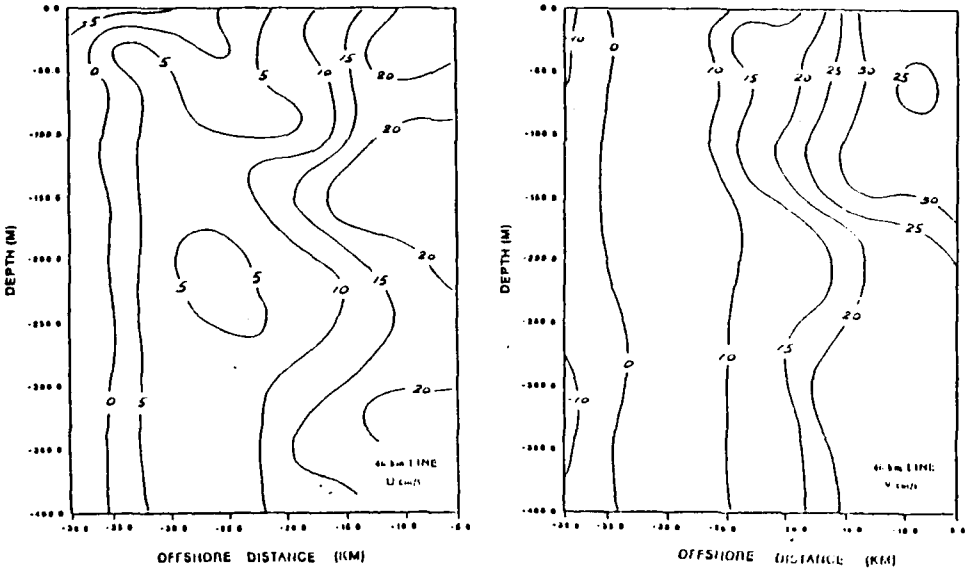

Figure 10b. Vertical cross-section of onshore and alongshore current components at the 46 km line in figure 9

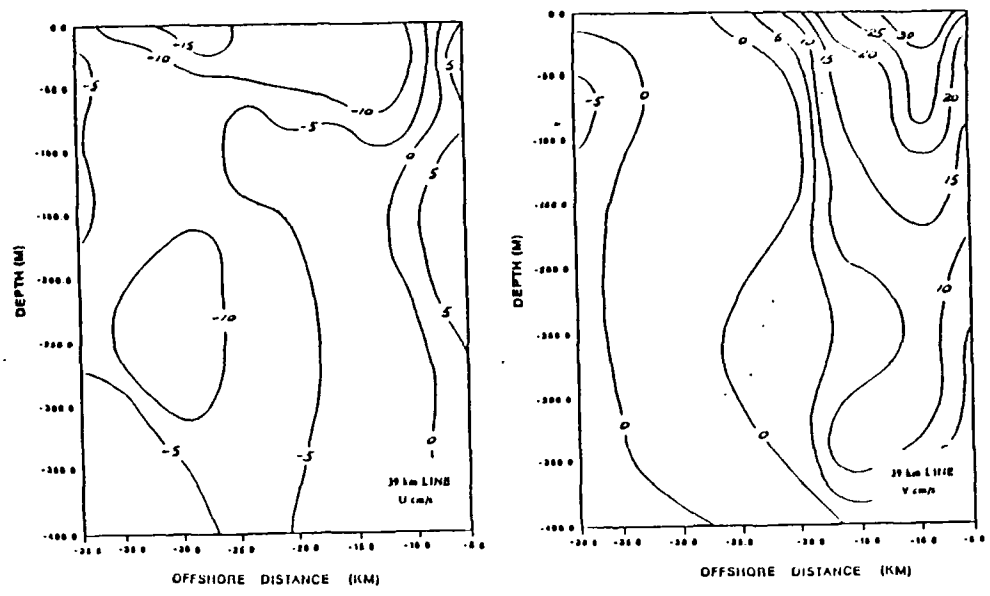

Figure 10c. Vertical cross-section of onshore and alongshore current components at the 39 km line in figure 9

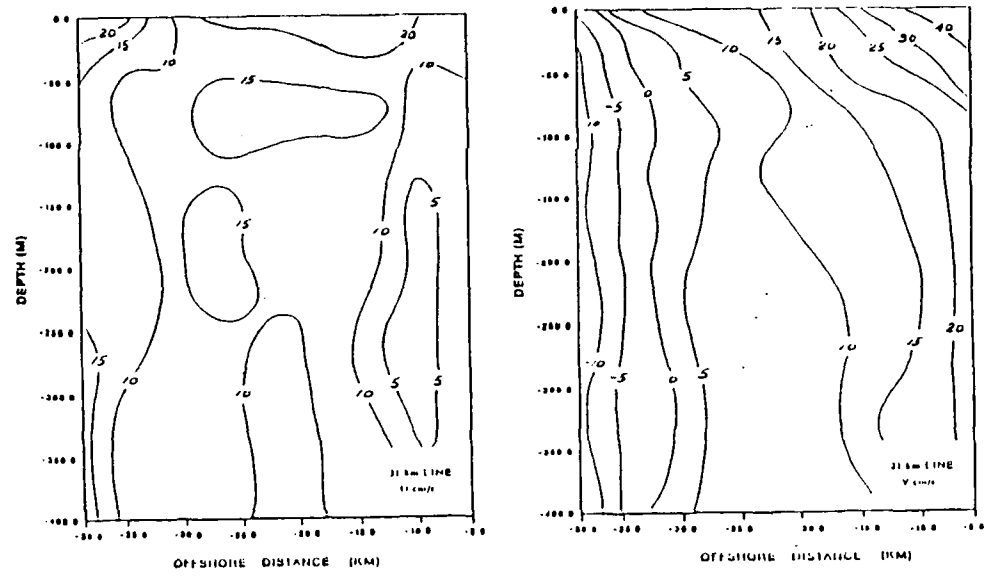

Figure 10d. Vertical cross-section of onshore and alongshore current components at the 31 km line in figure 9

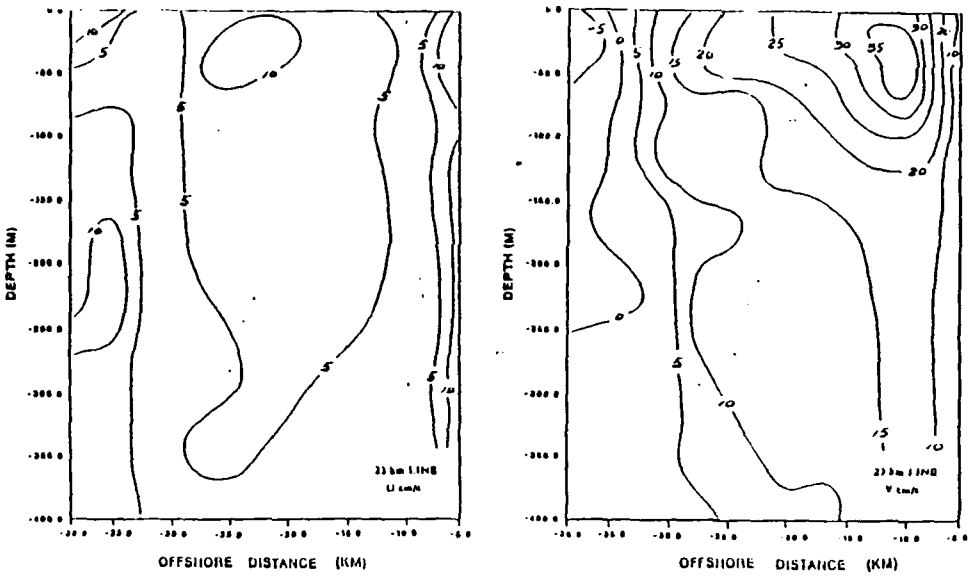

Figure 10e. Vertical cross-section of onshore and alongshore current components at the 23 km line in figure 9

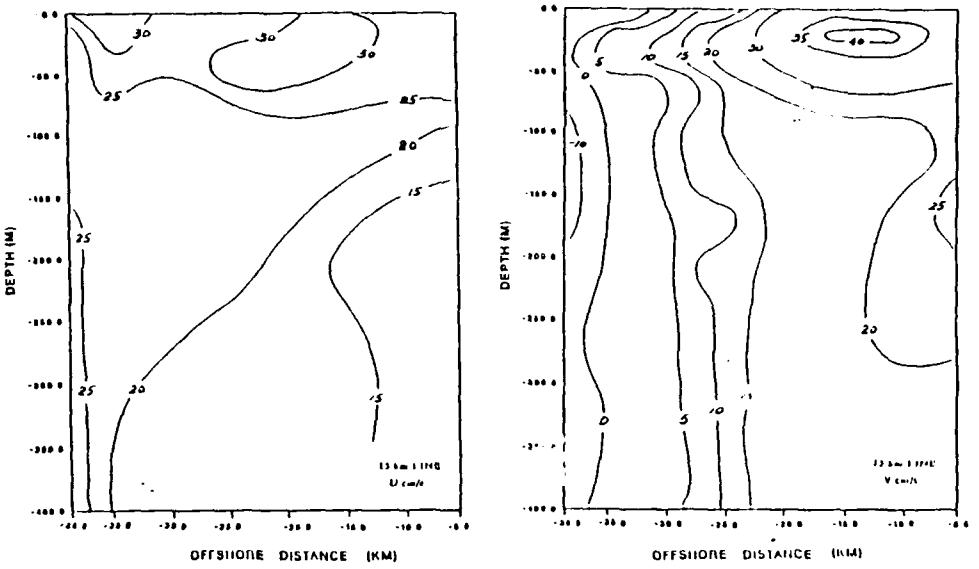

Figure 10f. Vertical cross-section of onshore and alongshore current components at the 15 km line in figure 94

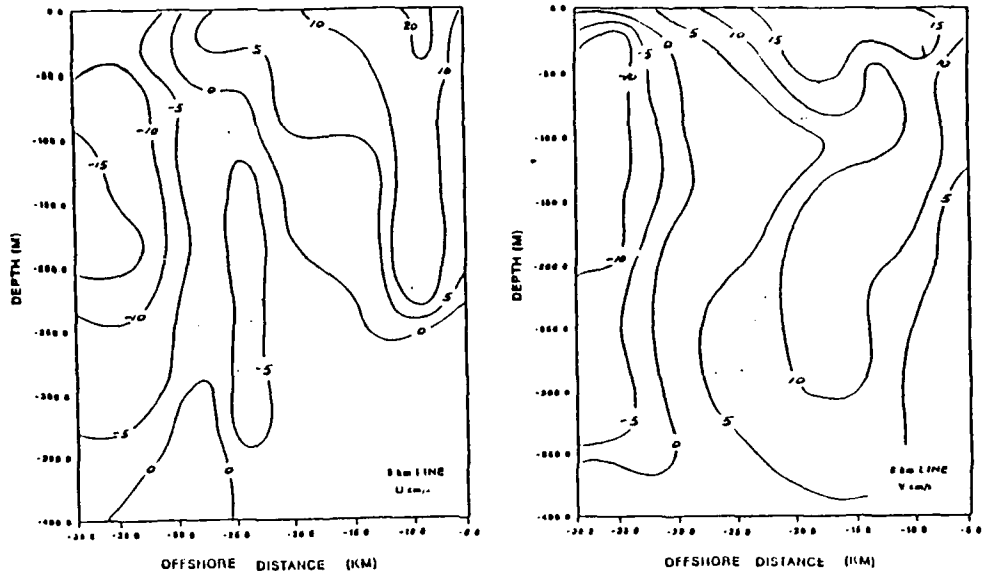

Figure 10g. Vertical cross-section of onshore and alongshore current components at the 8 km line in figure 9

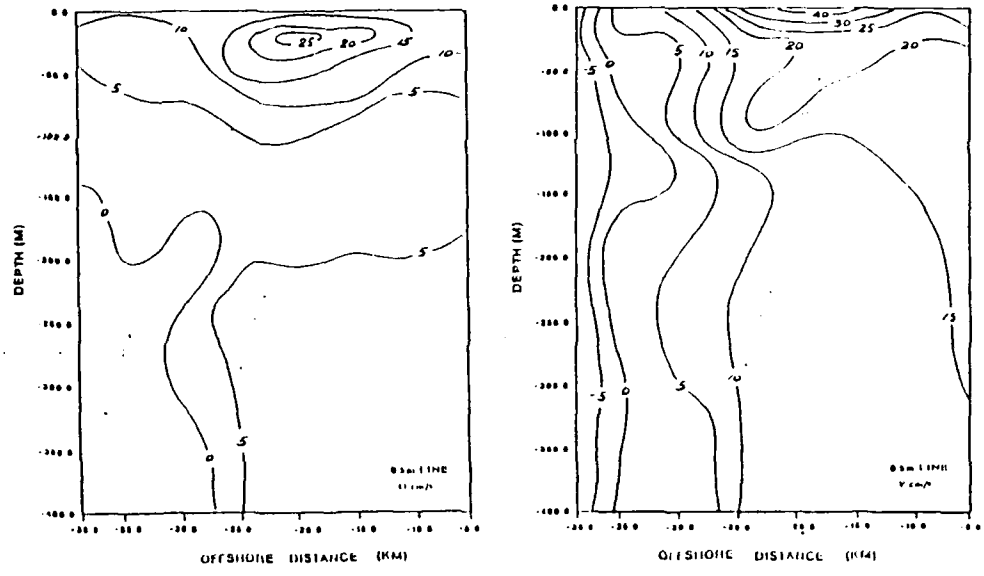

Figure 10h. Vertical cross-section of onshore and alongshore current components at the 0 km line in figure 9

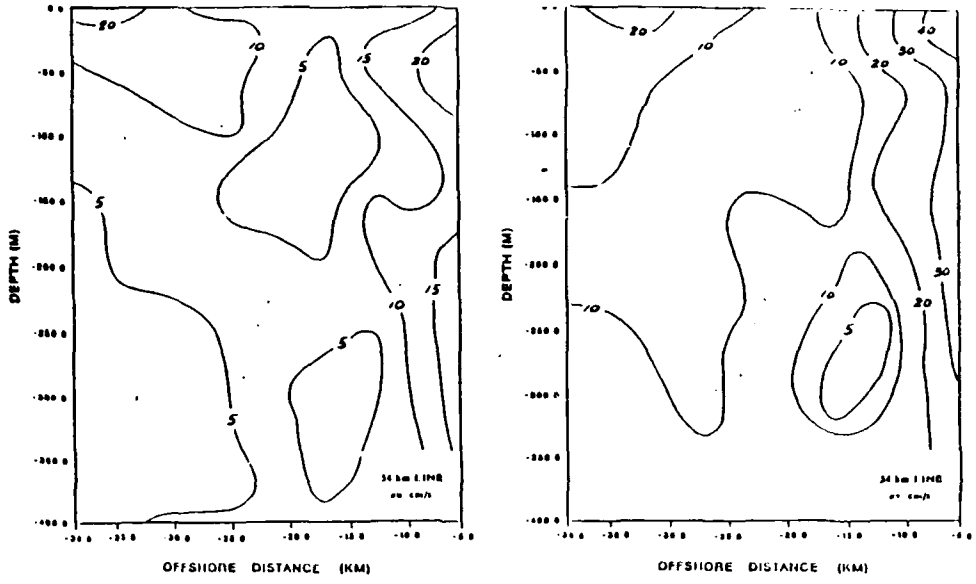

Figure 11a. Vertical cross-section of standard deviation of onshore and alongshore current components at the 54 km line in figure 9

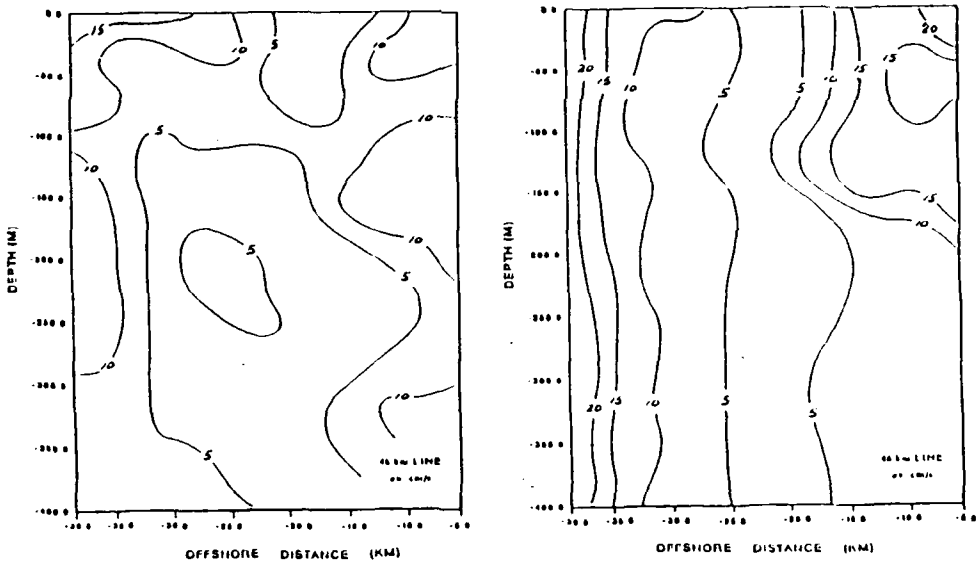

Figure 11b. Vertical cross-section of standard deviation of onshore and alongshore current components at the 46 km line in figure 9

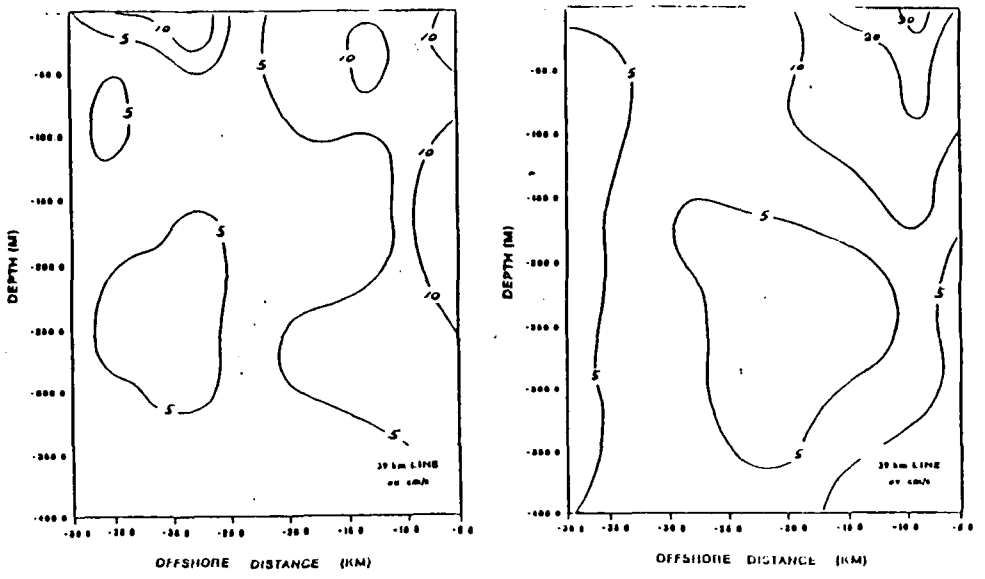

Figure 11c. Vertical cross-section of standard deviation of onshore and alongshore current components at the 39 km line in figure 9

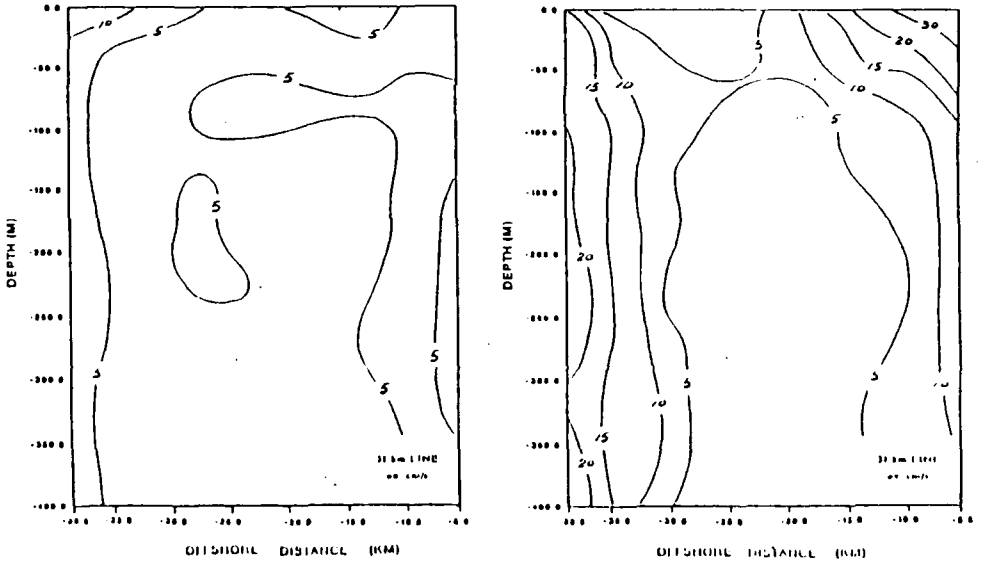

Figure 11d. Vertical cross-section of standard deviation of onshore and alongshore current components at the 31 km line in figure 9

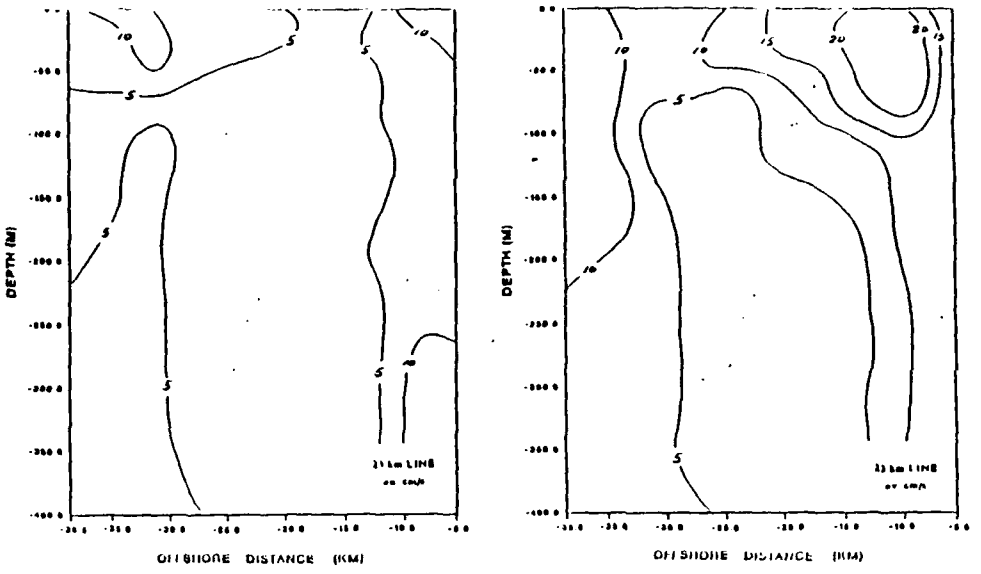

Figure 11e. Vertical cross-section of standard deviation of onshore and alongshore current components at the 23 km line in figure 9.

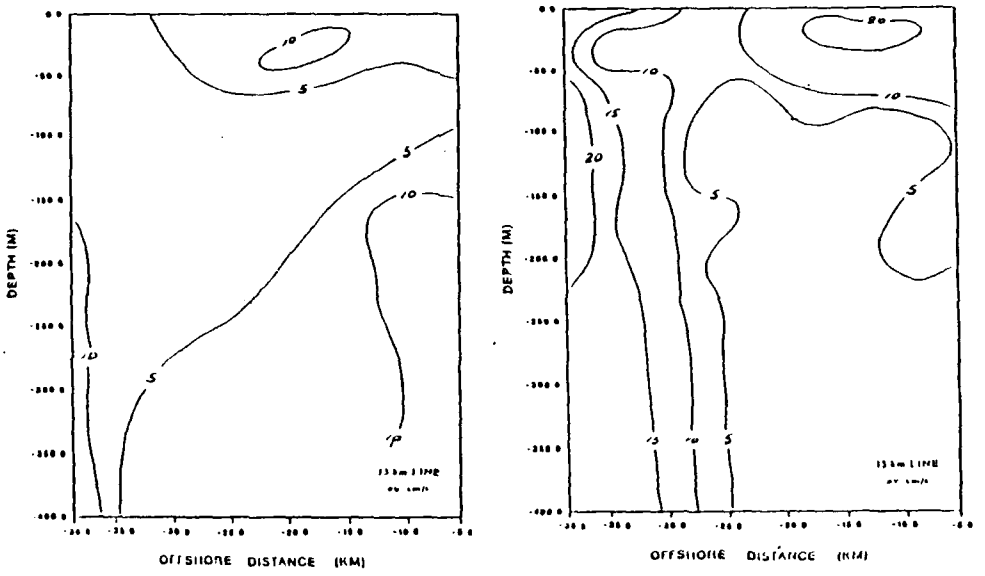

Figure 11f. Vertical cross-section of standard deviation of onshore and alongshore current components at the 15 km line in figure 9.

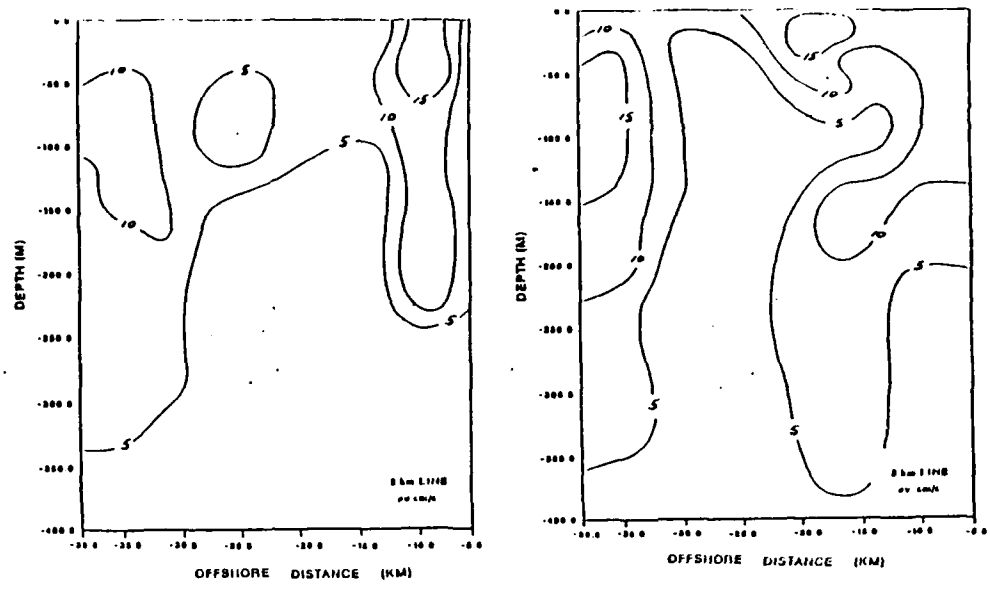

Figure 11g. Vertical cross-section of standard deviation of onshore and alongshore current components at the 8 km line in figure 9

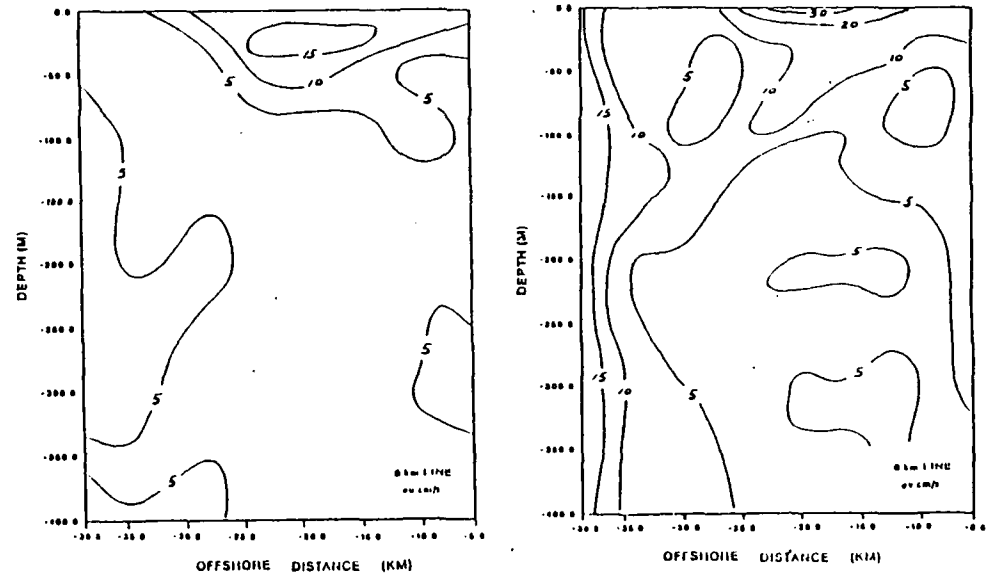

Figure 11h. Vertical cross-section of standard deviation of onshore and alongshore current components at the 0 km line in figure 8.

V. THERMAL STRUCTURE

Temperature data were collected using XBT probes during the SCBE II (4-6 September 1989). 74 XBTs were launched; about 14 XBTs were employed during the steam from Moss Landing to the study area (temperature structure was discussed and shown in appendix B and in figure B-3), and about 60 XBTs were dropped in the study area. 28 XBTs were dropped during the first pass over the study area heading parallel to the shore line and 32 XBTs were dropped during the second pass heading in an across shore direction.

Temperature data reveals the following features:

1. The thickness of the upper mixed layer was very shallow (< 10m) and varied slightly during the SCBE II second pass.

2. The temperature changed from 19°C on the surface to 11° between 50 m and 400 m was usually between 11°C and 6°C.

The mean temperature profile in figure 12 shows:

1. The maximum mean temperature was approximately 19° C on the surface and the minimum mean temperature was approximately 7° C at 400 m depth.

2. There was a very shallow mixed layer (less than 10 m).

3. The thermocline extended from 15 m to 50 m depth and the temperature gradient across the thermocline was about 9°C.

4. Below the thermocline, temperature decreased slowly with depth; the lapse rate in the layer below the thermocline was around 0.8° C/100 m.

Figure 12 also shows the mean temperature decreased almost linearly with increasing depth beneath 50 m. If density were solely dependent upon temperature, the mean vertical density structure deeper than 50 m would be better approximated by a constant buoyancy frequency than by a multilayered structure.

A. HORIZONTAL DISTRIBUTION

Regarding the horizontal distribution of temperature, figures 13a-13c describe the depths of the 8°, 9°, 10°C isotherms in the study area.

In figure 13a the depth of the 8° C isotherm ranged from 200 m in the NW corner to 300 m offshore (5-15 km from the island) suggesting a strong offshore temperature gradient 10-30 km to the west of SCI. Warm water was distributed near the shore at 150-300 m depth. The 9°C and 10°C isotherms also showed an offshore temperature gradient; the gradient became larger when closer to SCI. 9°C isotherm depth varied from 160 m in the NW corner to 180 m in the SE corner and the 10 °C isotherm depth ranged from 100 m to 60 m. Upwelling may have decreased the temperature in the upper column. The data also reveal high temperature near the SE corner, which is 6 km from and roughly parallel to the island below 100 m depth.

B. VERTICAL PROFILES

Figures A1-A7 show temperature profiles from station 15-42 on SCBE II during the first pass over the study area. In Fig

A8-A15, temperature profiles are shown from station 43-74 on SCBE II during the second pass over the study area. By comparing XBT drops between the first and second passes, 6 pairs of XBT stations were found at almost the same place (stations 18-70, 25-62, 32-72, 37-57, 39-65, 41-48), as shown in figure 15.

The lower three diagrams in figure 15 give a comparison of temperature profiles at three stations (37-57, 39-65, 41-48) located in the mean flow area. The vertical profiles of temperature varied less than 1°C for passes 10-24 hours apart. In the eddy area in the upper three diagrams in figure 15 (stations 18-70 and 25-62), mixed layer temperatures dropped 0.5° C in the 24-48 hours between passes. There was little temperature change below the mixed layer in the eddy region.

Several temperature inversions are observed at 50-100 m depth (station 38 in figure A6, station 64 and 66 in figure A13, station 73 in figure A15). These four stations were located approximately 15 km offshore near the south of San Clemente Island around the mean flow area. A similar inversion also can be found at 150-300 m (station 36 in figure A-6, station 52 and 53 in figure A-10). Two of these stations were located around the eddy area. The source and movement of waters implied by these inversions had not been previously investigated.

Table 3 shows the location of 20 stations that were choosen for geostrophic flow investigation in the next chapter. The

criteria for this selection were that the stations are located in or near the mean flow area (poleward flow area near the island), including stations M1 to M9; or the eddy area, which includes stations E1-E6 and D1-D5.

C. CROSS SECTIONS

Vertical temperature cross-sections from the 54 km primary line to the 0 km line are shown on Fig. 14a-14h. These plots reveal a strong vertical stratification of temperature over the study area. From the surface to 30 m depth the temperature changes from 19° C to 10° C. In figure 14a-14h the 8°C contour varied from 200m-300m depth.

In figure 14h, the 0 km line cross section shows that the 9°C contour varied from 170 m-220 m depth at 13km- 23 km offshore and the 8°C contour varied from 260 m-300 m depth at 6 km-30 km offshore, suggesting that the maximum downwelling (or convergent flow) occured at this layer.

TABLE III. TEMPERATURE DATA AT 20 STATIONS

Site	Station No.	Latitude	Longitude	Bottom depth (m)	Instrument depth (m)	Temperature (°C)
E1	46	32° 52.4'N	119° 2.1'W	1600	14	19
					80	10
					91	9
					268	8
					391	7
E2	51	32° 50.5'N	119° 0.8'W	1625	14	18

Site	Station No.	Latitude	Longitude	Bottom depth (m)	Instrument depth (m)	Temperature (°C)
					391	7
E2	51	32° 50.5'N	119° 0.8'W	1625	14	18
					58	[illegible]
					93	9
					243	8
					355	7
E3	50	32° 52.9'N	118° 55.9'W	1675	20	18
					81	10
					160	9
					271	8
					405	7
E4	52	32° 46.7'N	118° 59.6 W	1400	21	18
					57	10
					109	9
					255	8
					369	7
E5	53	32° 48.9'N	118° 55.1'W	1550	19	18
					71	10
					136	9
					258	8
					389	7
E6	54	32° 51.8'N	118° 49.7'W	1575	21	18
					84	10
					154	9
					246	8
D1	59	32° 47.2'N	118° 49.1'W	1225	12	18
					73	10
					129	9

Site	Station No.	Latitude	Longitude	Bottom depth (m)	Instrument depth (m)	Temperature (^{O}C)
					264	8
					372	7
D2	61	32^{O} 41.1'N	118^{O} 52.5'W	1020	30	18
					85	10
					173	9
					293	8
					404	7
D3	62	32^{O} 43.5'N	118^{O} 47.2'W	1550	19	18
					86	10
					141	9
					260	8
					376	7
D4	63	32^{O} 43.5'N	118^{O} 41.9'W	1200	17	18
					86	10
					152	9
					283	8
					419	7
D5	68	32^{O} 40.8'N	118^{O} 43.4'W	1260	15	18
					65	10
					161	9
					250	8
					301	7
M1	43	33^{O} 2.8'N	118^{O} 56.'W	1700	12	19
					76	10
					184	9
					242	8
					418	7
M2	42	33^{O} 4.9'N	118^{O} 52. W	1600	17	19

Site	Station No.	Latitude	Longitude	Bottom depth (m)	Instrument depth (m)	Temperature (^{O}C)
					82	10
					148	9
					234	8
					328	7
M3	48	33^{O} 1.4'N	118^{O} 47.4'W	11360	15	19
					81	10
					160	9
					301	8
					392	7
M4	49	32^{O} 56.9'N	118^{O} 49.2'W	1350	15	19
					87	10
					159	9
					265	8
					377	7
M5	56	32^{O} 55.5'N	118^{O} 40.1'W	1000	15	19
					106	10
					167	9
					323	8
					452	7
M6	64	32^{O} 49.3'N	118^{O} 36.5'W	850	16	19
					90	10
					174	9
					275	8
					445	7
M7	66	32^{O} 46.3'N	118^{O} 33.6'W	550	13	19
					93	10
					182	9
					310	8

Site	Station No.	Latitude	Longitude	Bottom depth (m)	Instrument depth (m)	Temperature (°C)
					450	7
M8	73	32° 42.8'N	118° 30.7'W	680	21	19
					97	10
					159	9
					274	8
					421	7
M9	74	32° 44.8'N	118° 27.0'W	240	24	18
					94	10
					167	9
					238	0

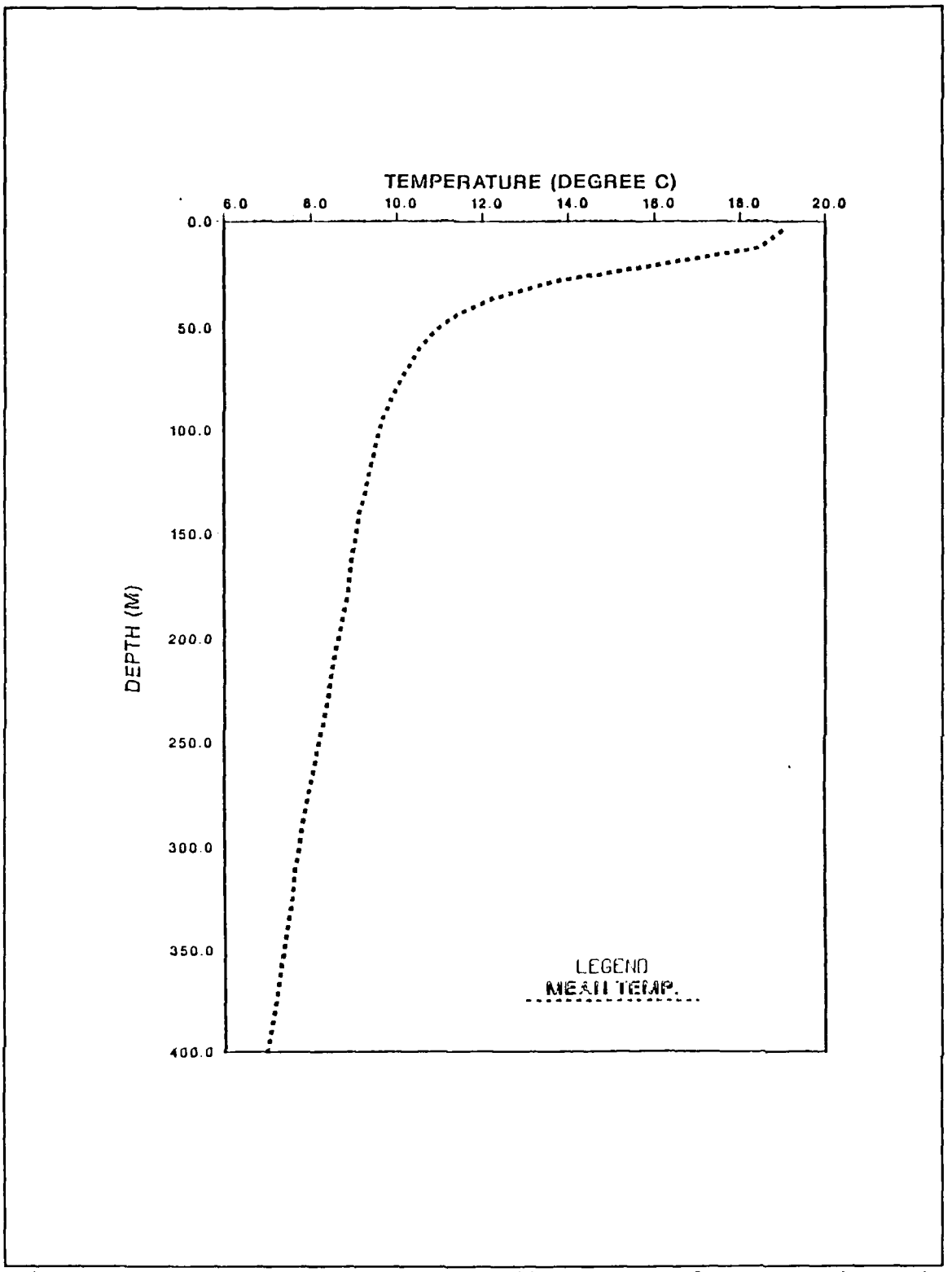

Figure 12. Mean temperature profile at study area given in figure 2 and figure 3

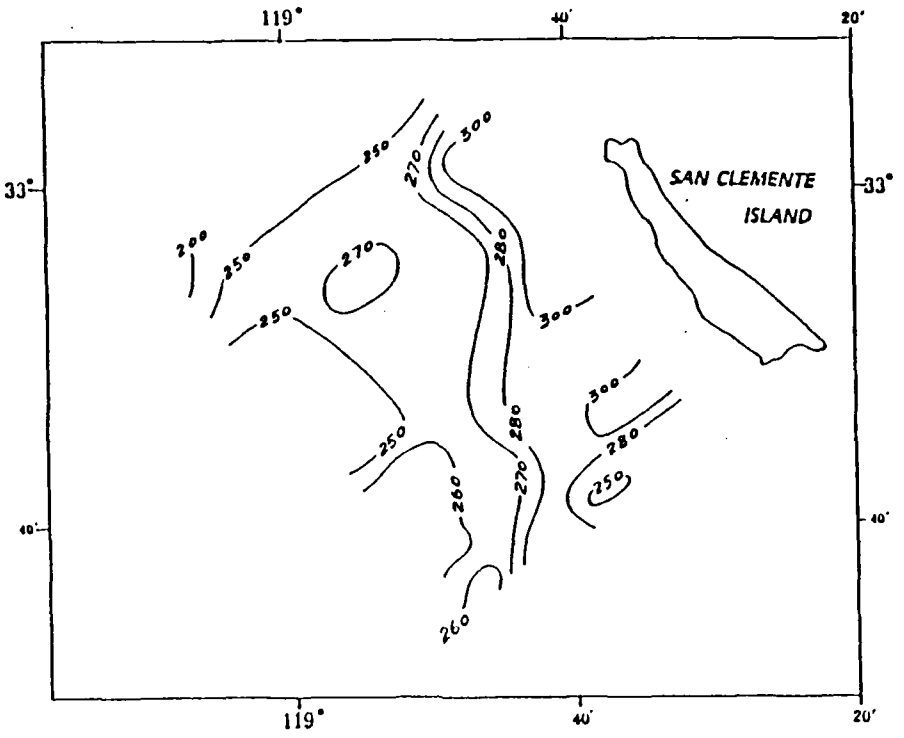

Figure 13a. The depth of 8°C isotherm in the study area

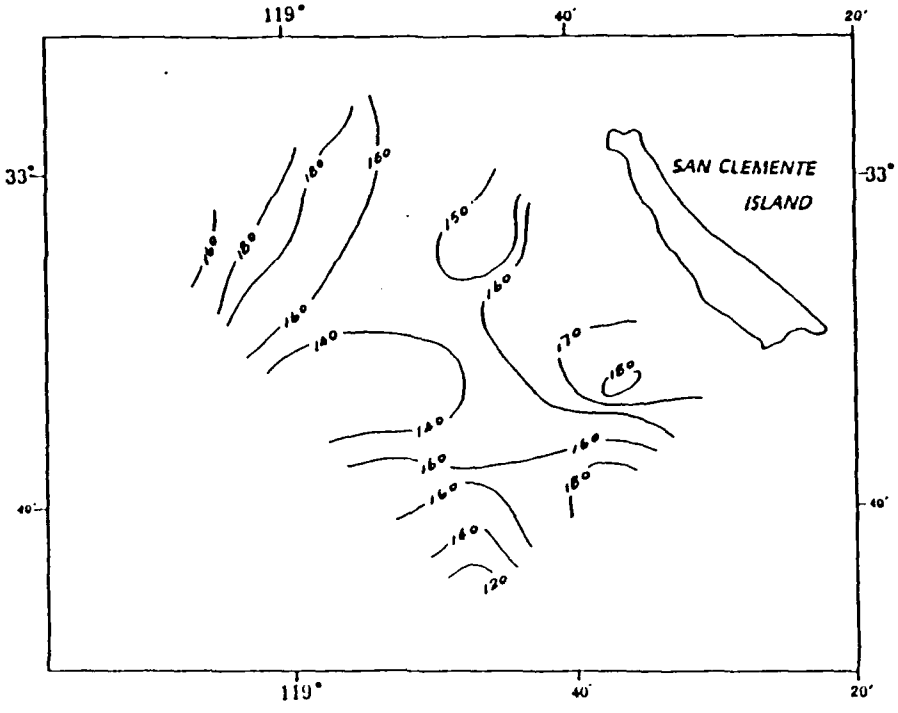

Figure 13b. The depth of 9°C isotherm in the study area

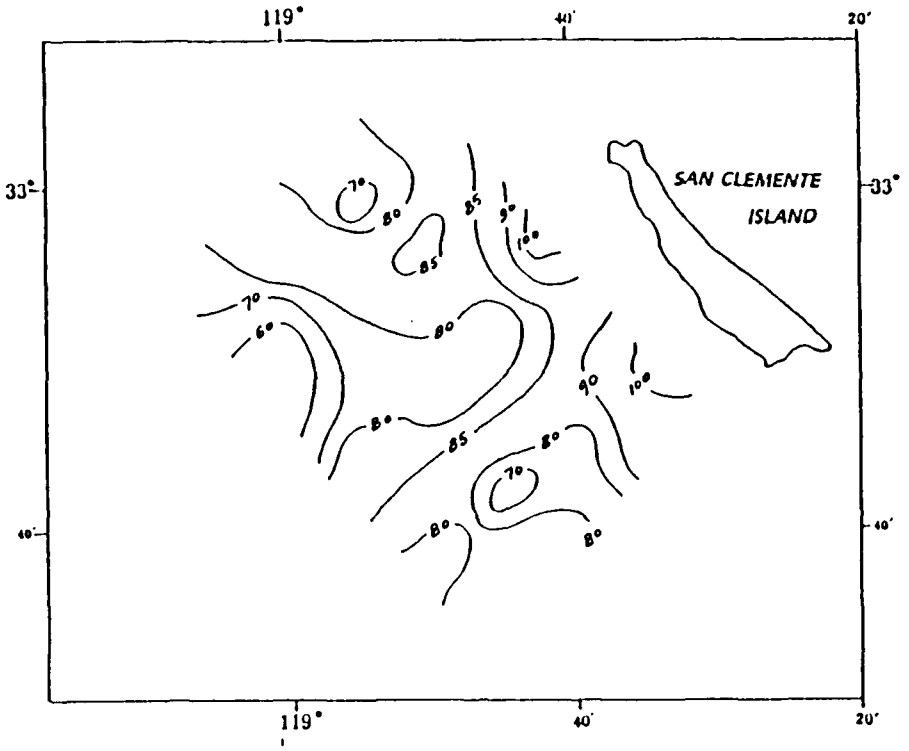

Figure 13c. The depth of 10°C isotherm at study area

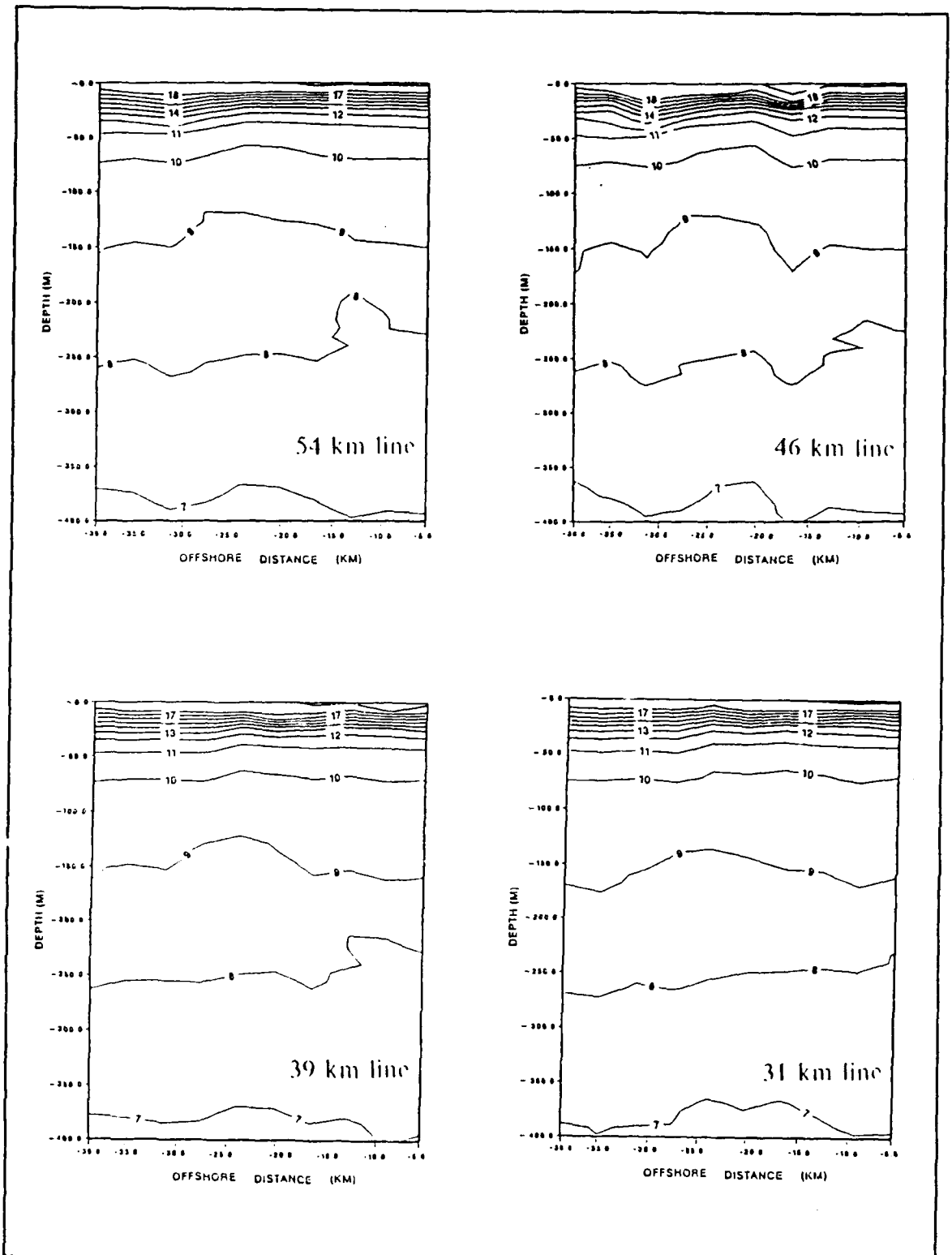

Figure 14a. Vertical cross-section of temperature at the 54 km, 46 km, 39 km and 31 km line in figure 9

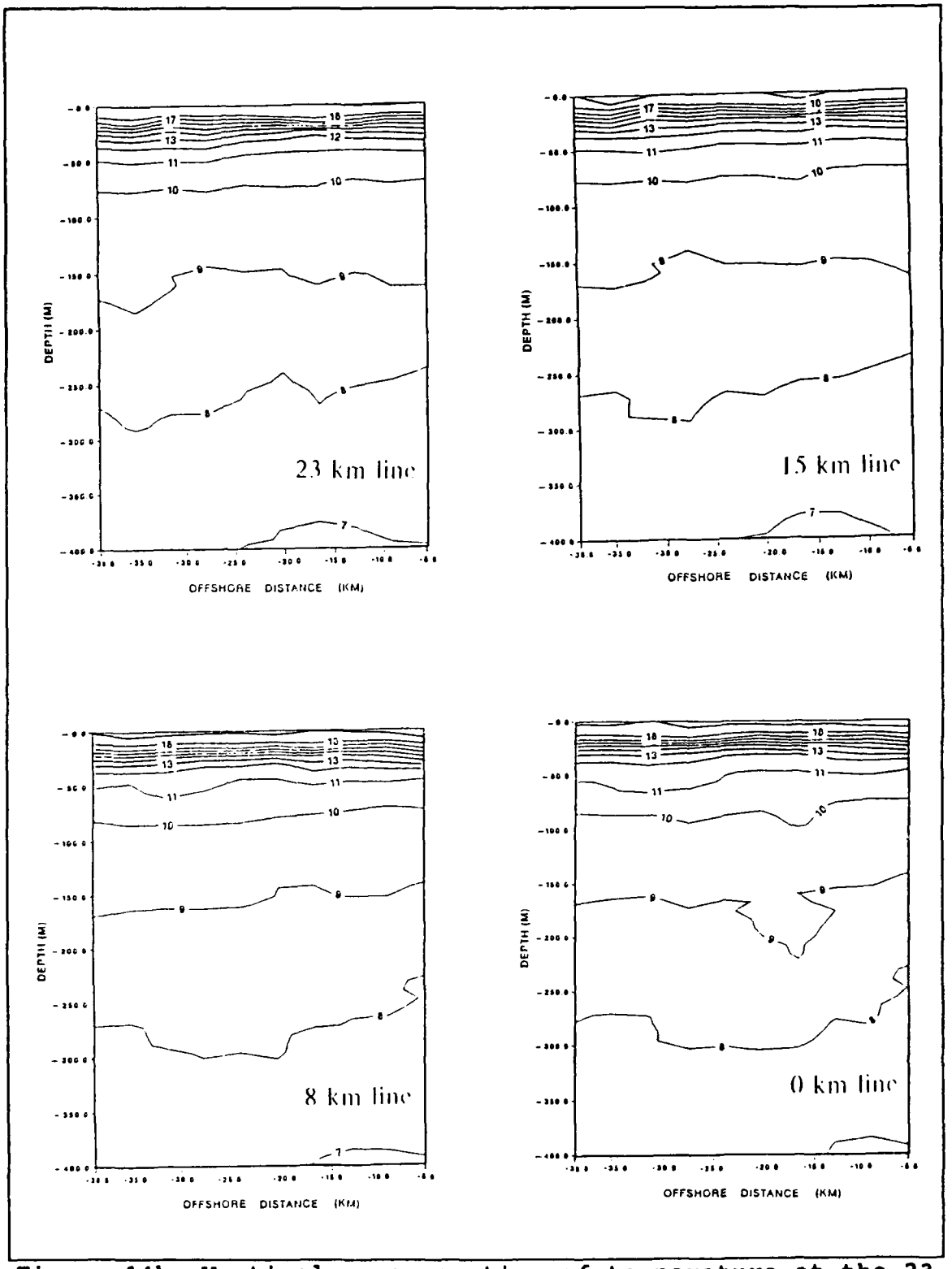

Figure 14b. Vertical cross-section of temperature at the 23 km, 15 km, 8 km and 0 km line in figure 9

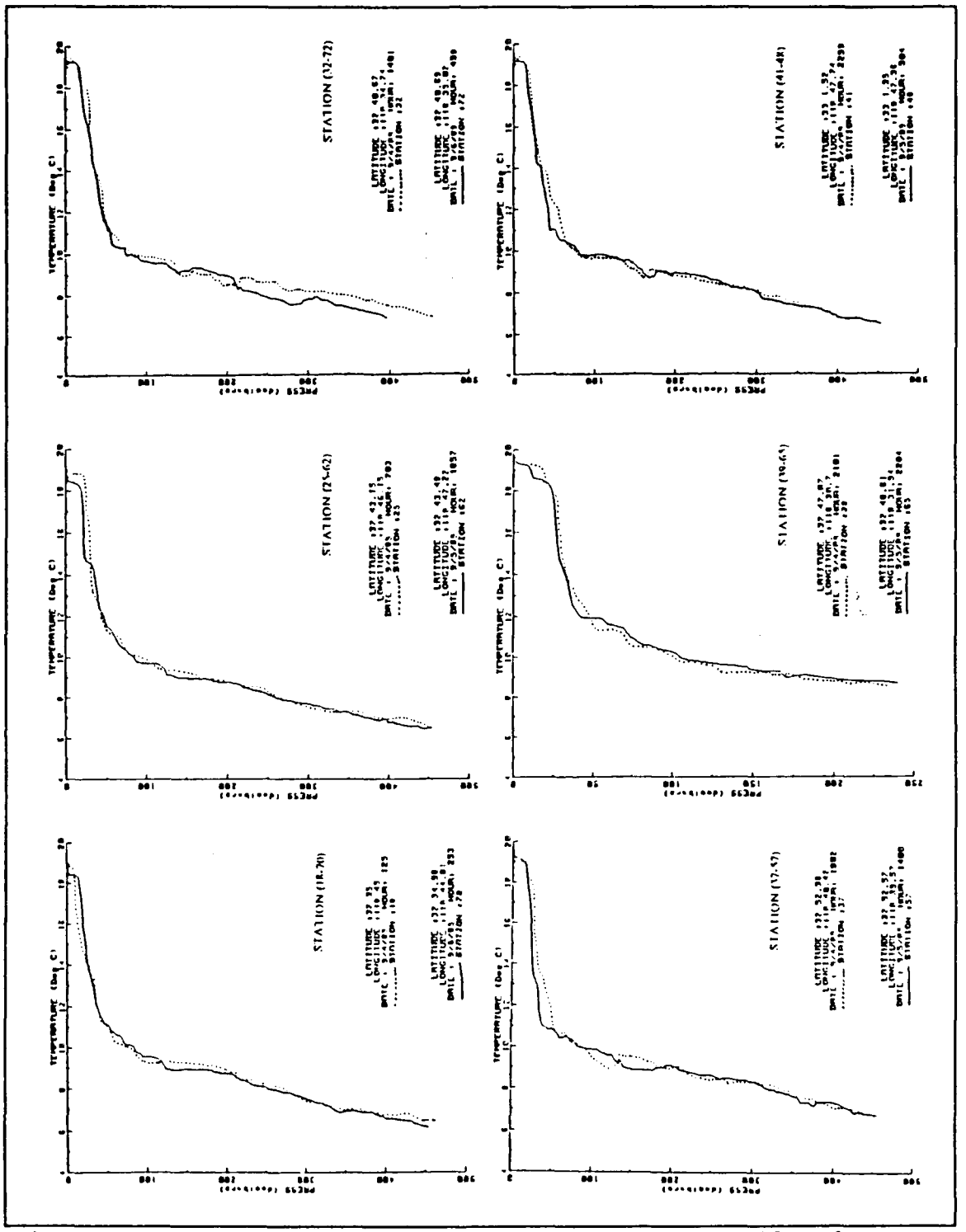

Figuree 15. Six comparisons of temperature profiles between first and second pass over the study area for station (18-70), (25-62), (32-72), (37-57), (39-65), (41-48)

VI. GEOSTROPHIC FLOW

In the upper water, where density is determined chiefly by Temperature, a temperature section will allow the estimate of flow direction. Steeper isotherms indicate stronger currents. In upper layers at the northern hemisphere, light water is on the right side of the geostrophic flow, while heavy water is on the left side of the geostrophic flow.

This chapter describes the geostrophic velocity and dynamic height and includes calculation of values. Because of the limitation of cruise time, only XBT's were deployed. No salinity data below sea surface were collected during the San Clemente Basin Experiment cruises. Geostrophic velocity and dynamic height data were created by T-S relations from CALCOFI cruise reports in 1988 and 1972.

Most comparisons between geostrophic velocity cross sections and ADCP velocity cross sections show strong agreement in flow pattern and velocity measurements. Some geostrophic sections show greater equatorward velocity at 25-38 km offshore in the upper 100 m depth than the ADCP measurements.

Dynamic height (geostophic flow) correlates well with vertical averaged horizontal currents at the strong alongshore

current area. Poor agreement exists between dynamic height and ADCP horizontal current at 15 km away from the island.

This implied three points:

1. The pressure gradient caused by density is important around the strong poleward mean flow area 5-15 km offshore.
2. T-S relations are acceptable for salinity and density calculation in this case.
3. Flow patterns farther than 15 km offshoe are more complicated and variable.

A. DATA CALCULATION

1. T-S Relation

Hydrographic observations reported by Huyer(1984) suggested that temperature and salinity contributions to density were correlated. Salinity data was created by a T-S relation cited from CALCOFI cruise 8810, station 90.45, on Oct. 10th, 1988. This station is located at 32° 55.1'N 118° 56.2'W, north of San Clemente Island, 20 km away from the center of study area. Table 4 lists the T-S data from CALCOFI cruise report at the same station in 1972 and 1988. T-S curves from 1972 and 1988 are consistent (figure not shown).

2. Density

Hydrostatic pressure is determined by the density structure of the ocean, and we can calculate this from measurements of temperature, salinity, and depth. The density

TABLE IV. T AND S DATA LOCATED AT 32° 55.1'N 118° 56.2'W FROM CALCOFI CRUISE REPORT IN 1972 AND 1988

CALCOFI Cruise 7202 Sept. 2, 1972			CALCOFI Cruise 8810 Oct. 16, 1988		
Z(M)	t (°C)	S (p.p.t.)	Z(M)	T (°C)	S (p.p.t.)
0	12.16	33.39	0	18.75	33.64
10	12.14	33.39	10	16.62	33.51
20	12.14	33.40	20	15.92	33.58
30	12.13	33.40	30	14.19	33.49
50	11.29	33.46	50	11.36	33.59
75	10.24	33.62	75	10.55	33.70
100	9.29	33.63	100	9.71	33.84
125	9.06	33.86	125	9.40	33.92
150	8.93	33.92	150	9.03	33.99
200	8.50	34.11	200	8.46	34.09
250	7.91	34.18	239	8.0	34.14
300	7.54	34.22	300	7.52	34.23
400	6.96	34.29	400	6.76	34.30
500	6.37	34.33	500	6.09	33.34

(ρ, kg/m^3) of sea water is a function of salinity (s), temperature (t, °C) and pressure (p, decibars) given by (EOS 80)

$$\rho(s,t,p) = \rho(s,t,0)/[1 - p/k(s,t,p)] \qquad (9)$$

In this equation k(s,t,p) stands for the secant bulk modulus. Temperature varied from 19°C on the surface to 6°C at 400 m depth. Pressure varied from 0 db on the surface to 400 db at the 400 m depth. The specific volume (α) is the reciprocal of density, with units m^3/Kg. The specific volume anomaly (δ) is

$$\delta = \alpha_{s,t,p} - \alpha_{35,0,p} \qquad (10)$$

Where $\delta_{s,t,p}$ is the specific volume *in situ*, $\alpha_{35,0,p}$ is the specific volume of an arbitrary standard sea water of salinity 35‰ temperature 0°C at pressure P.

EOS 80 was used in calculating the specific volume anomaly from pressure, temperature and salinity.

3. Geostrophic velocity

Some velocity characteristics can be deduced from a simple examination of vertical profiles of density and dynamic height which is related to the density distribution. "Thermal wind" can be written as:

$$\frac{\partial(\rho f v)}{\partial z} = -g\frac{\partial \rho}{\partial x} \qquad (11a)$$

$$\frac{\partial(\rho f u)}{\partial z} = g\frac{\partial \rho}{\partial y} \qquad (11b)$$

Where (u,v) = geostrophic flow,

f = Coriolis parameter,

ρ = water density,

g = gravitational acceleration.

To use the geostrophic equation, a line of stations was selected and the current calculated between each pair of stations and a vertical section of the horizontal current was plotted.

B. GEOSTROPHIC VELOCITY VS ADCP VELOCITY

Eight geostrophic velocity cross sections were calculated and plotted (four sections used in comparison with ADCP velocity are showed in figures 16a-16d). Each cross section consists of V and U component from the sea surface to 400 m depth along the primary lines of 54 km, 46 km, 39 km, 31 km, 23 km, 15 km, 8 km and 0 km, as shown in figure 10. Each geostrophic section shows the station number on the top of the x-axis. The geostrophic velocity is contoured in cm/s such that positive numbers represent poleward flow and negative numbers represent equatorward flow.

Figure 16a-16d show the comparison between the geostrophic section and ADCP the section at the 54 km line, the 46 km line, the 23 km line and the 15 km line. XBT data in stations 42, 43, 44 and 45 was used in the calculation of the 54 km line geostrophic section. The flow characteristics derived from geostrophy and ADCP section (figure 16a) show excellent agreement. The transition zone (zero velocity) was located between 15 and 20 km offshore. In the upper 80 m of the ocean, the geostrophic section shows about 20 cm/s smaller in poleward velocity at 5-10 km offshore than the ADCP section, but about 20 cm/s more equatorward velocity than in ADCP section.

XBT data in stations 46, 47 and 48 were used in the calculation of the 46 km line geostrophic section. The flow patterns of geostrophic velocity and ADCP section (figure 16b)

are in close agreement. The transition zone was located between 20 and 35 km offshore. Between 5-10 km offshore, the geostrophic section showed a poleward velocity of approximately 25 cm/s in the upper 50 m of water. This poleward velocity was similar to that seen in the ADCP section, although slightly stronger.

XBT data in stations 57, 58, 59 and 60 were used in the calculation of the 23 km line geostrophic section. The flow characteristics of the geostrophic velocity and the ADCP section (figure 16c) closely agree. The transition zone was located between 30 and 35 km offshore. The geostrophic section shows the same poleward velocity at about 35 cm/s offshore 10-12 km on upper 20-70 m depth as does the ADCP section. Equatorward velocities of about 10-15 cm/s at 35 km offshore are similar to the ADCP section. One equatorward jet with 10 cm/s in geostrophic section is located offshore at 30-38 km between 200-400 m depth which was not found on the ADCP section.

XBT data for stations 61, 62, 63 and 64 were used in the calculation of the 15 km line geostrophic section. The flow patterns of the geostrophic velocity and ADCP sections (figure 16d) are in close agreement. The transition zone was located between 32 and 36 km offshore. The geostrophic section shows less poleward velocity, about 20 cm/s at 5-15 km offshore between 10- 30 km depth, than does the ADCP section. Greater equatorward velocity is seen by the geostrophic section, at

35-387 km offshore between 80-180 m depth, than by the ADCP section.

Generally speaking, strong poleward currents near the island on the upper 50 m show good agreement between the geostrophic and the ADCP flows. The flow pattern and characteristics also show good agreement.

Some geostrophic sections show stronger velocity than that of ADCP sections at 20 km - 38 km offshore. Visual comparison of geostrophic velocity profiles to ADCP profiles (in V component only) generally shows poor agreement between the magnitudes and the offshore distance. There are two reasons why there is a poor agreement between geostrophic velocity and ADCP velocity:

1. Geostrophic velocity is calculated from data gathered from two stations widely separated both in space and time.

2. The pressure gradient is assumed to be linear between those two stations.

Each geostrophic section shows zero velocity at 400 m depth where the ADCP velocity may exceed 20 cm/s on some sections. That is because XBT data only reached 450 m or less. The depth of 400 m was chosen as the level of no motion for the geostrophic flow calculation. In the mean flow area, strong poleward current flow existed from the surface down to 400 m depth.

C. DYNAMIC HEIGHT VS ADCP HORIZONTAL VELOCITY

In this section, the dynamic height field, which was calculated from XBTs at different layers, is presented and compared with the ADCP data. The comparison between horizontal geostrophic and ADCP current circulation is shown in figures 17a-17d at the depth of 50 m, 100 m, 200 m and 300 m (relative to 400 db, level of no motion).

Dynamic height is contoured in dyn m. The contours from dynamic height show the pressure gradient. Flow directions followed the stream lines and current intensified where the distance between the streamline were narrow and vice versa. The lower values of the pressure were located on the left hand side of the streamlines and the higher values were located on the right hand side. A specific lower value corresponds to a cyclonic eddy and a higher value corresponds to an anticyclonic eddy. The range of dynamic height from 0.70 (dyn m) to 0.44 (dyn m) at above 400 m depth is relative to 400 db at this study area during 2-6 September, 1989.

The large coherent features between the dynamic height field and ADCP currents were:

1. The strong poleward flow near the island, centered at 10 km offshore, from the SE corner of the study area to the NE.

2. Most of the onshore flowing water at southern part of the study area appeared to turn about and join the poleward flow close to the island.

3. Other than the two points mentioned above, most of the velocity vectors were not well correlated with the dynamic height field. The velocity vectors were

uncorrelated when the velocity magnitude fell below the noise level of the ADCP measurement, which is taken to be 5 cm/s. (Jessen, personal communication)

An example of this is figure 17a where the dynamic height field showed several cyclonic and anticyclonic circulations 15 km offshore, but the ADCP data did not quite agree with it. Excellent agreement of flow patterns were present in the poleward flow near the island.

Figure 17b showed good agreement between dynamic height flow and ADCP horizontal velocity. This included:

1. Strong poleward flow near the island.
2. The strong onshore current which appeared to turn and join the poleward flow.
3. A small 10 km eddy centered at 32^{O} 42' N, 118^{O} 54' W, which was present in both ADCP velocity and dynamic height flow measurements.

An anticyclonic eddy centered at 32^{O} 53' N, 119^{O} 01'W, found in the dynamic height field, did not show the flow pattern corresponding to ADCP flow. Figures 17c and 17d flow features were similar to 17a's as mentioned before. From the mesoscale Southern California current system, the currents in the study area are supposed to flow poleward in the whole area. The geostrophic dynamic fields revealed the various flow paths at this study area which implied that the topography around the island was important to the California current system. The pattern of geostrophic circulation provides evidence that dynamic instabilities develop.

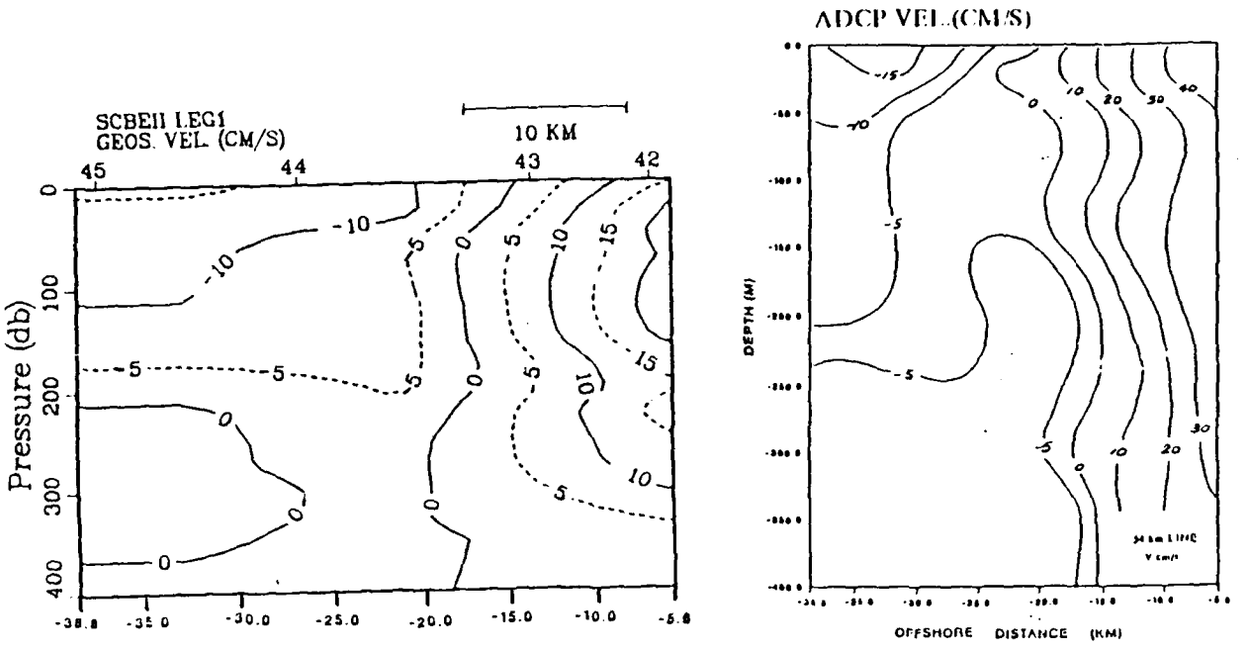

Figure 16a. Vertical structure between geostrophic section and ADCP secion at 54 km primary line in figure 9

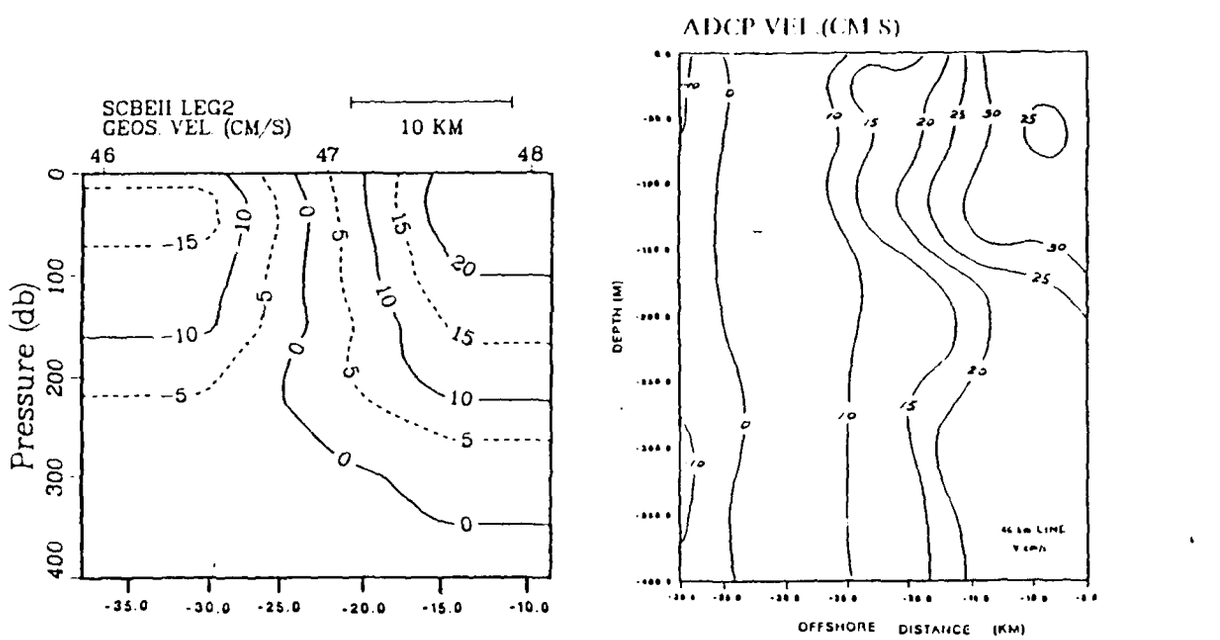

Figure 16b. Vertical structure between geostrophic section and ADCP section at 46 km primary line in figure 9

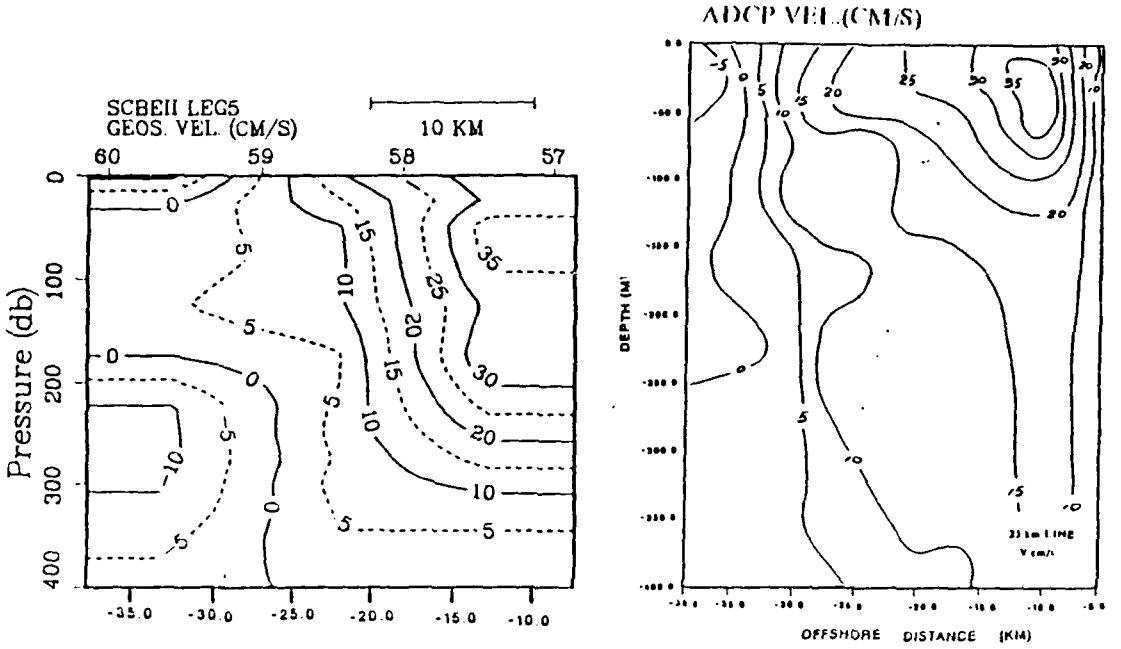

Figure 16c. Vertical structure between geostrophic section and ADCP secion at 23 km primary line in figure 9

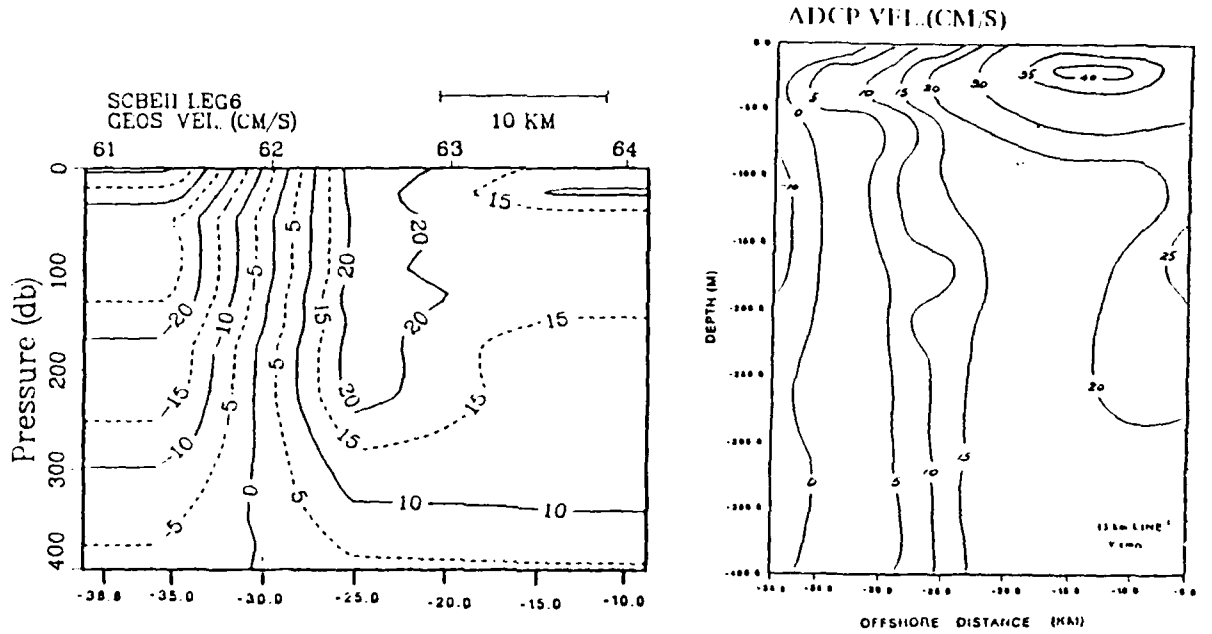

Figure 16d. Vertical structure between geostrophic section and ADCP section at 15 km primary line in figure 9

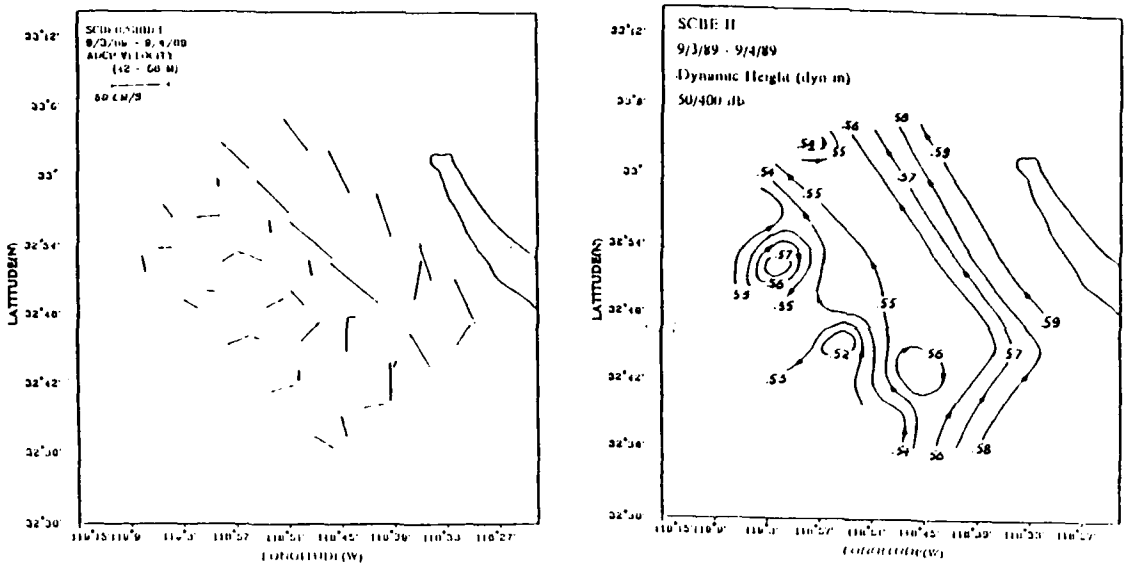

Figure 17a. Dynamic height (relative to 400 dB) vs ADCP velocity at 50 dB measured during the cruise SCBE-II, 3-4 September 1989

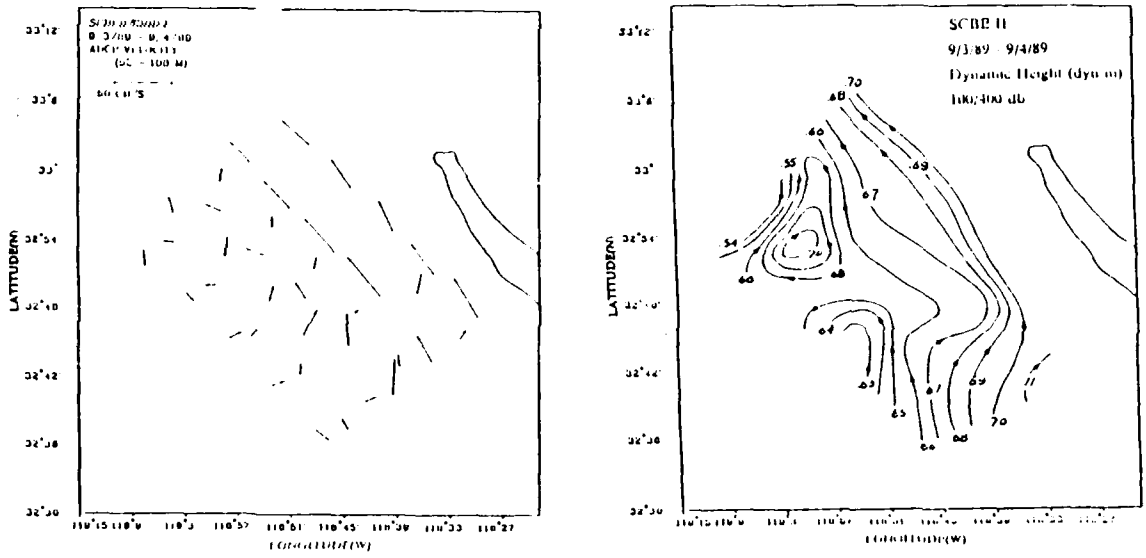

Figure 17b. Dynamic height (relative to 400 dB) vs ADCP velocity at 100 dB measured during the cruise SCBE-II, 3-4 September, 1989

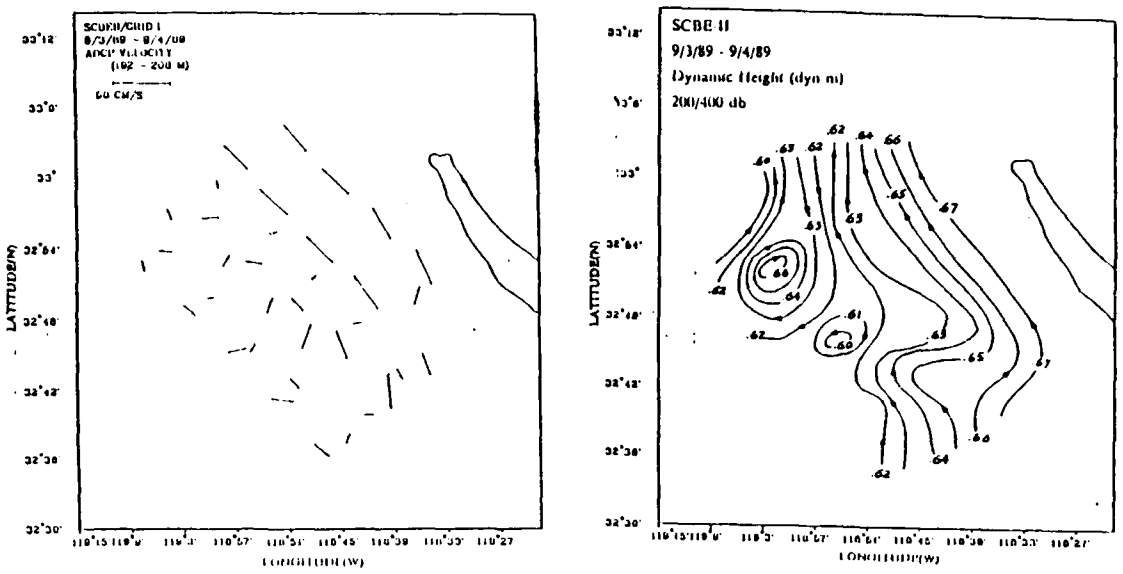

Figure 17c. Dynamic height (relative to 400 dB) vs ADCP velocity at 200 dB measured during the cruise SCBE-II, 3-4 September, 1989

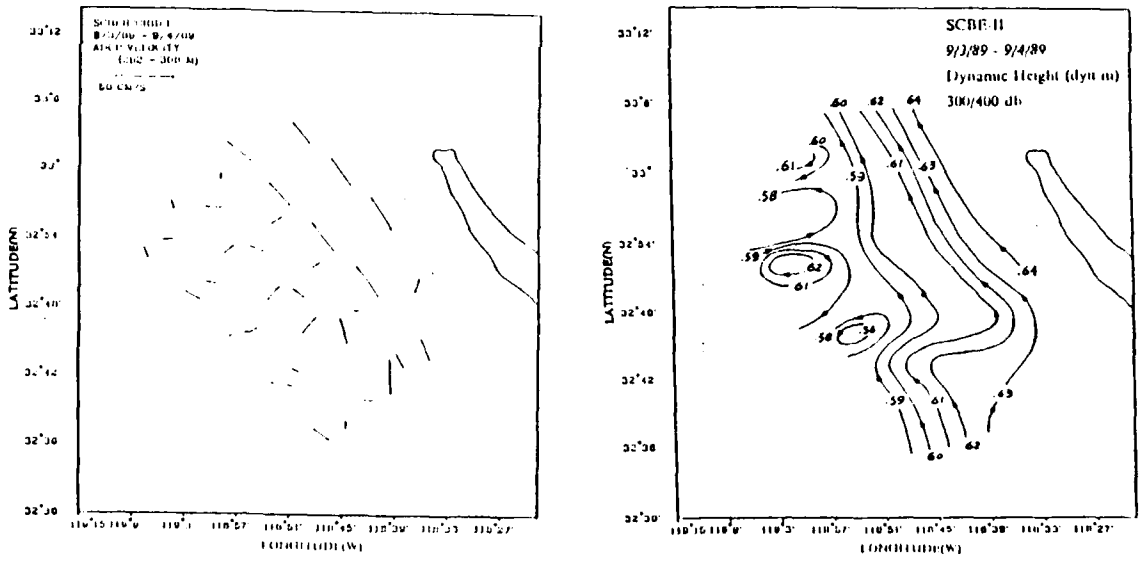

Figure 17d. Dynamic height (relative to 400 dB) vs ADCP velocity at 300 dB measured during the cruise SCBE-II, 3-4 September, 1989

VII. CONCLUSIONS

The San Clemente Basin Experiment provided information on mesoscale structure by combining the ADCP velocity and XBT temperature surveys near San Clemente Island.

Data from this research show the topographic effects on the coastal currents near San Clemente Island as well as the variabilities of the Southern California Current system in this basin zone.

A. CURRENT STRUCTURE

(1) Two different flow patterns were observed: strong alongshore poleward (northwestly) currents (centered 10 km west of SCI) and small-scale eddies (located more than 15 km west of SCI). (2) Two small-scale cyclonic eddies were observed during the second cruise. They were located at (119° 5'W, 32° 55'N) and (118° 53'W, 32° 47'N). The length-scale of these two eddies were approximately 10 km. In general, eddies occuring in this area varied with time and space.

(3) The appearance of the eddies beween the northwestward coastal current and the California Current offshore is believed to be due to the horizontal shear.

(4) The alongshore poleward currents intensified in the poleward direction. They were only observed between 5-15 km offshore, and were oriented roughly parallel to the bottom

contour with maximum velocities of about 40-50 cm/s. This intensification could extend to 300 m depth. (5) The onshore current at 32° 38′- 42′ N, 118° 35′- 40′ W turned around and joined the poleward flow, following the 300-500 m contour. This also suggests the influence of the topography.

(6) The coincidence of the strong alongshore poleward currents with the baroclinic zone and the disappearance of these two systems 35 km farther from the SCI suggests a large topographical impact on the oceanic currents and thermal structure in the San Clemente Island region.

B. THERMAL STRUCTURE

The thermal structure in this area showed the following charecteristics.

(1) Horizontal temperature distributions were nearly uniform in the upper 50 m, but below 100 m depth the temperature decreased with increasing distance from shore.

(2) The XBT data show that the mixed layer depth was very shallow (<10 m) during the second cruise; however, up to a 30 m mixed layer depth could be seen in other cruises.

(3) The temperature difference between the surface and 20 m was about 0.5-1.0°C implying that the wind effect is important. The shipboard wind speed varied between 3.7 - 8.5 m/s, and the wind direction ranged from 94° to 128° between 4-6 September, 1989. The mean wind direction was 110°.

(4) The 8° C isotherm thickness indicate a strong baroclinic zone (i.e. a strong cross-shore temperature gradient), which was nearly parallel to and 10-30 km to the west of SCI. The wind was quite steady during the second pass, and the strong cross-shore temperature gradient was consistent with the upwelling favorable wind. We would expect upwelling from the center of basin; in fact, cold water did appear in the NW corner of the study area.

C. GEOSTROPHIC FLOW

Most comparisons between geostrophic flow and measured ADCP velocity clearly show an agreement in flow pattern and velocity at the strong alongshore current area, implying that the pressure gradient caused by density is an important element in the strong poleward mean flow area 5-15 km offshore.

APPENDIX A. TEMPERATURE PROFILES AT STUDY AREA

Twenty-eight XBTs, (figure 3) were employed from 2300 UT 3 September to 2302 UT 4 September 1989(SCBE-II), during the first pass over the study area. The temperature profiles can be found in this Appendix (figure A1 to A7).

Thirty-two XBTs (figure 5) were employed from 2359 UT 5 September to 0639 UT 6 September 1989(SCBE-II), during the second pass over the study area. The temperature profiles can also be found in this Appendix (figure A8 to A16).

A detailed description of the thermal structure can be found in chapter V.

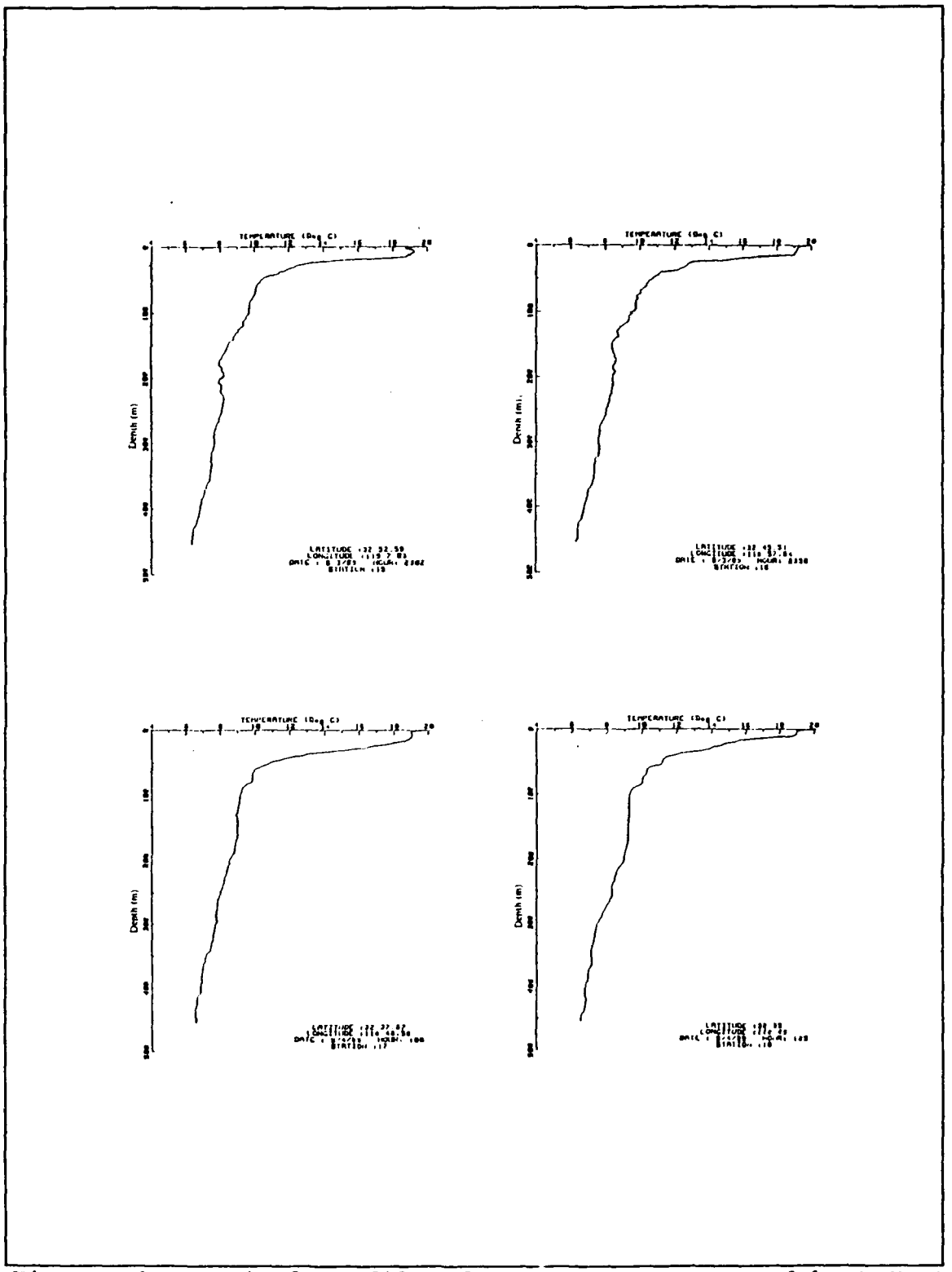

Figure A1. Vertical profile of temperature measured by XBT at station No. 15, No. 16, No. 17, No. 18 in figure 2

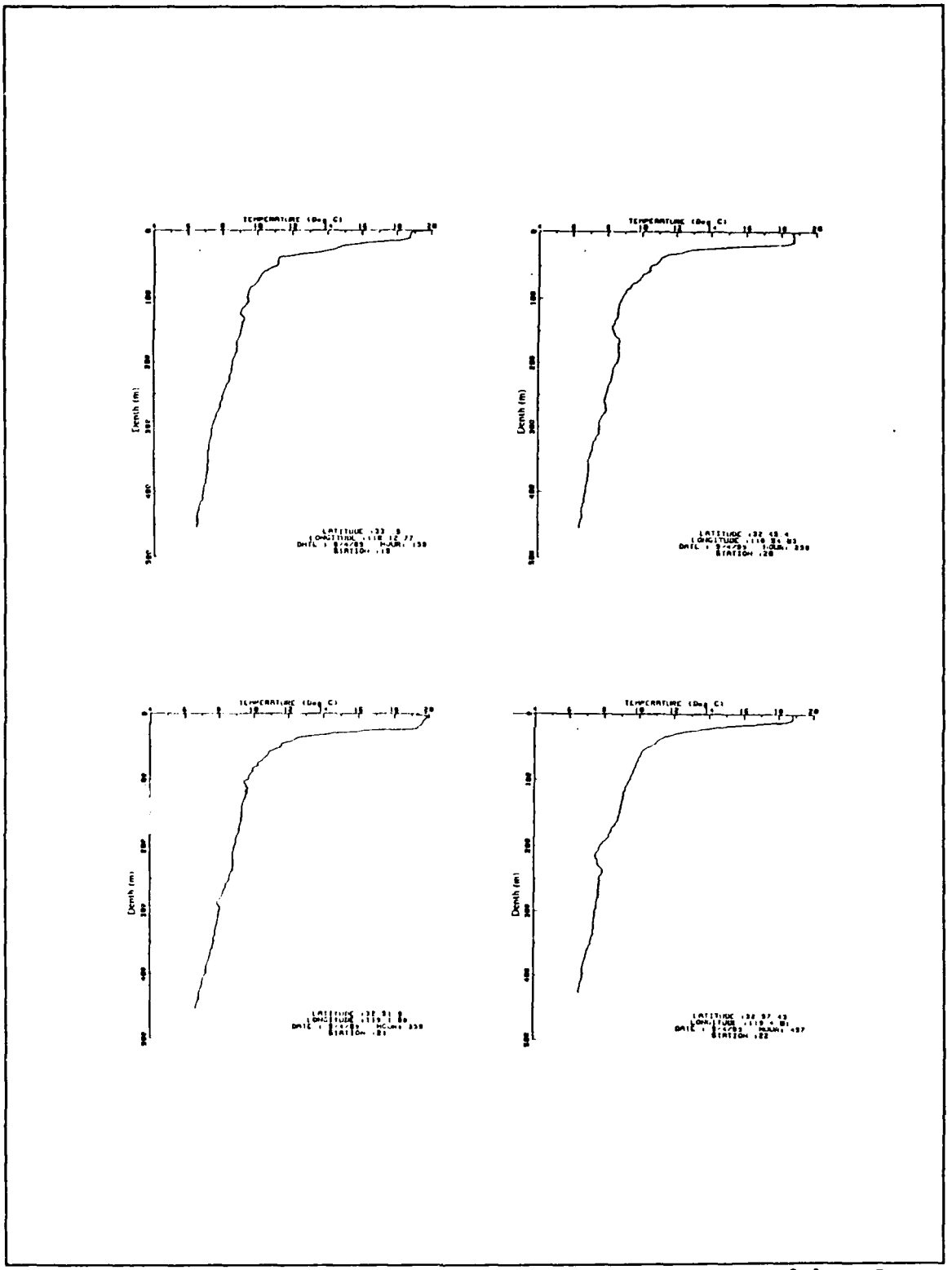

Figure A2. Vertical profile of temperature measured by XBT at station No. 19, No. 20, No. 21, No. 22 in figure 2

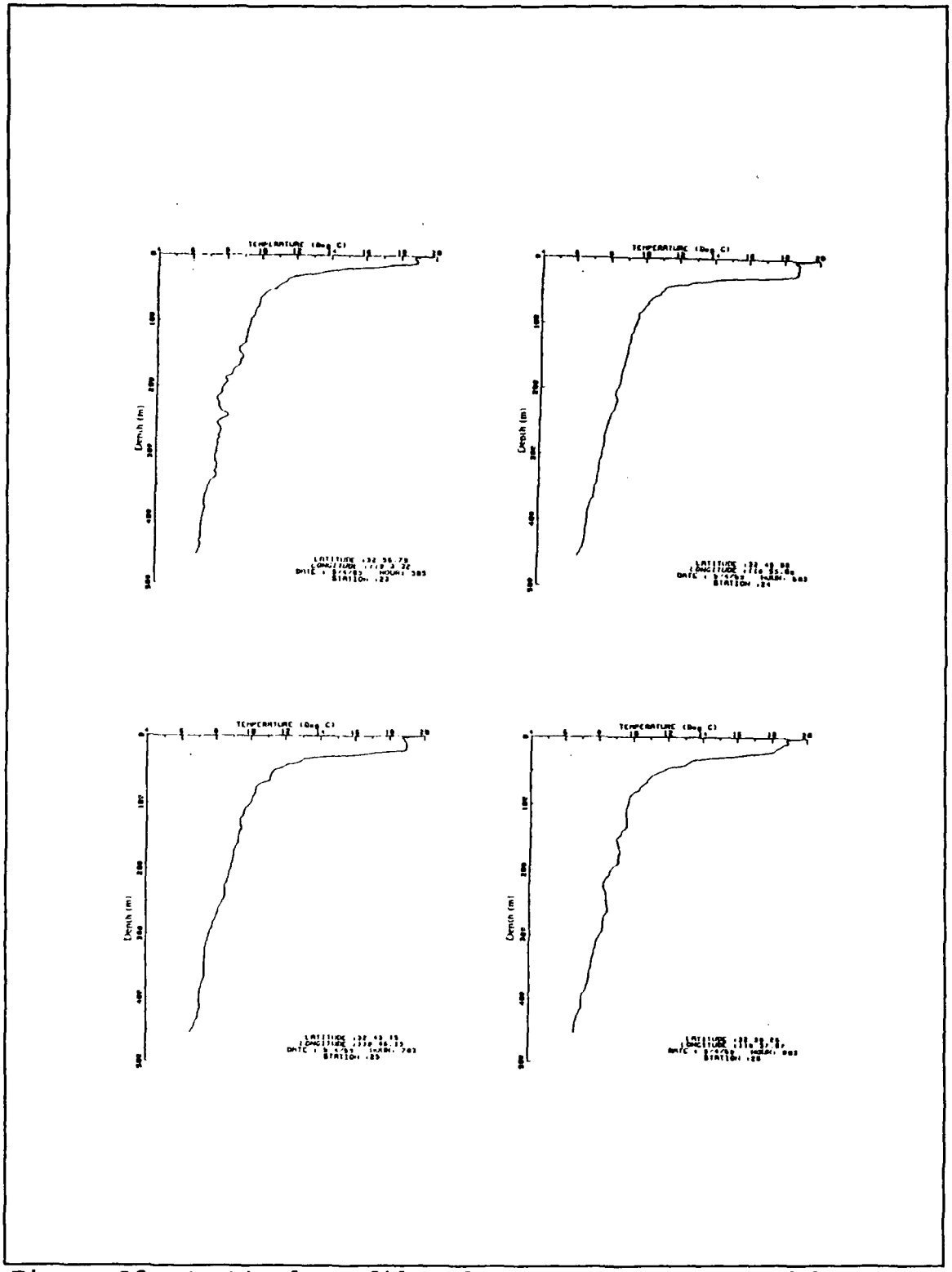

Figure A3. Vertical profile of temperature measured by XBT at station No. 23, No. 24, No. 25, No. 26 in figure 2

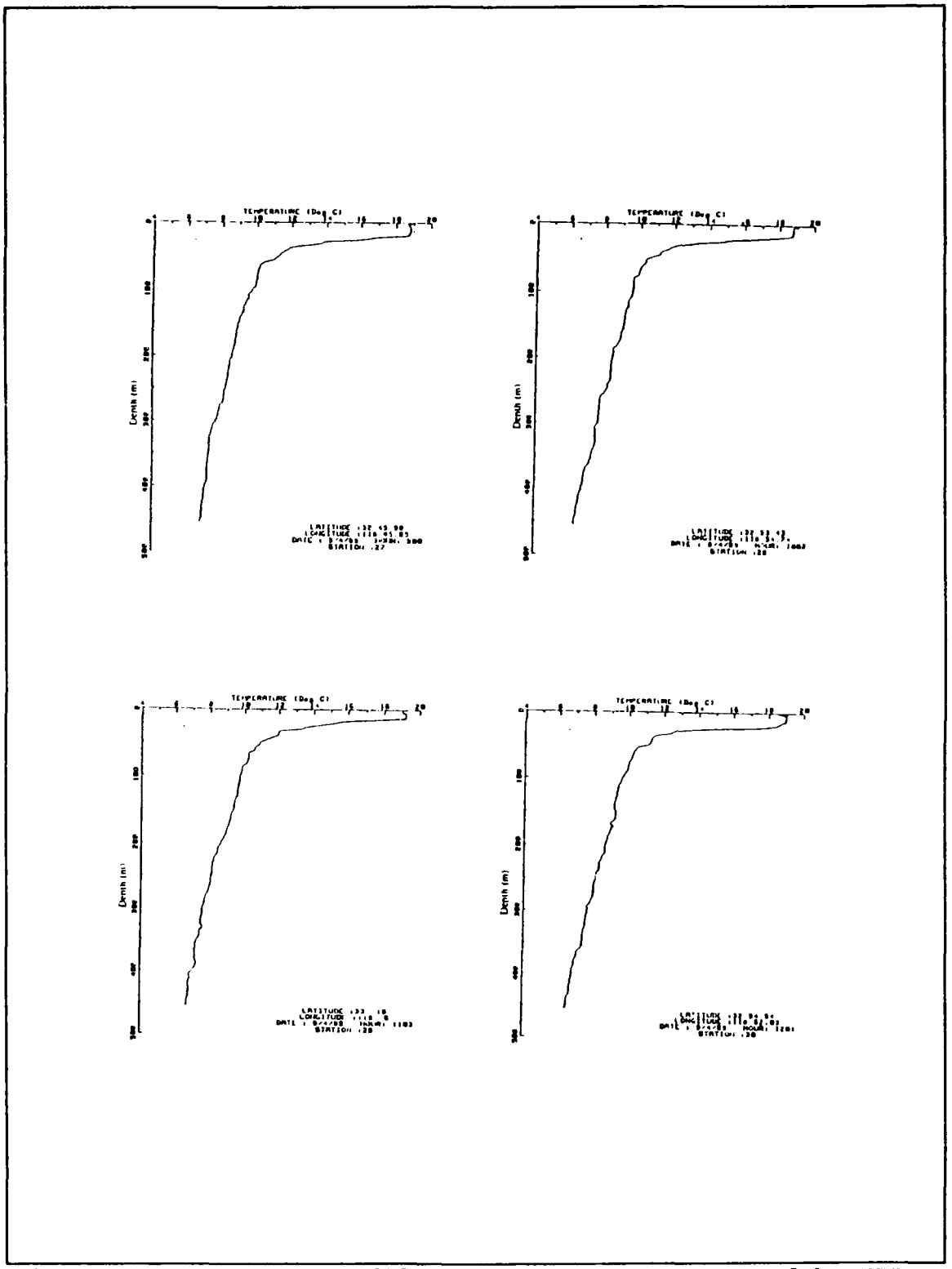

Figure A4. Vertical profile of temperature measured by XBT at station No. 27, No. 28, No. 29, No. 30 in figure 2

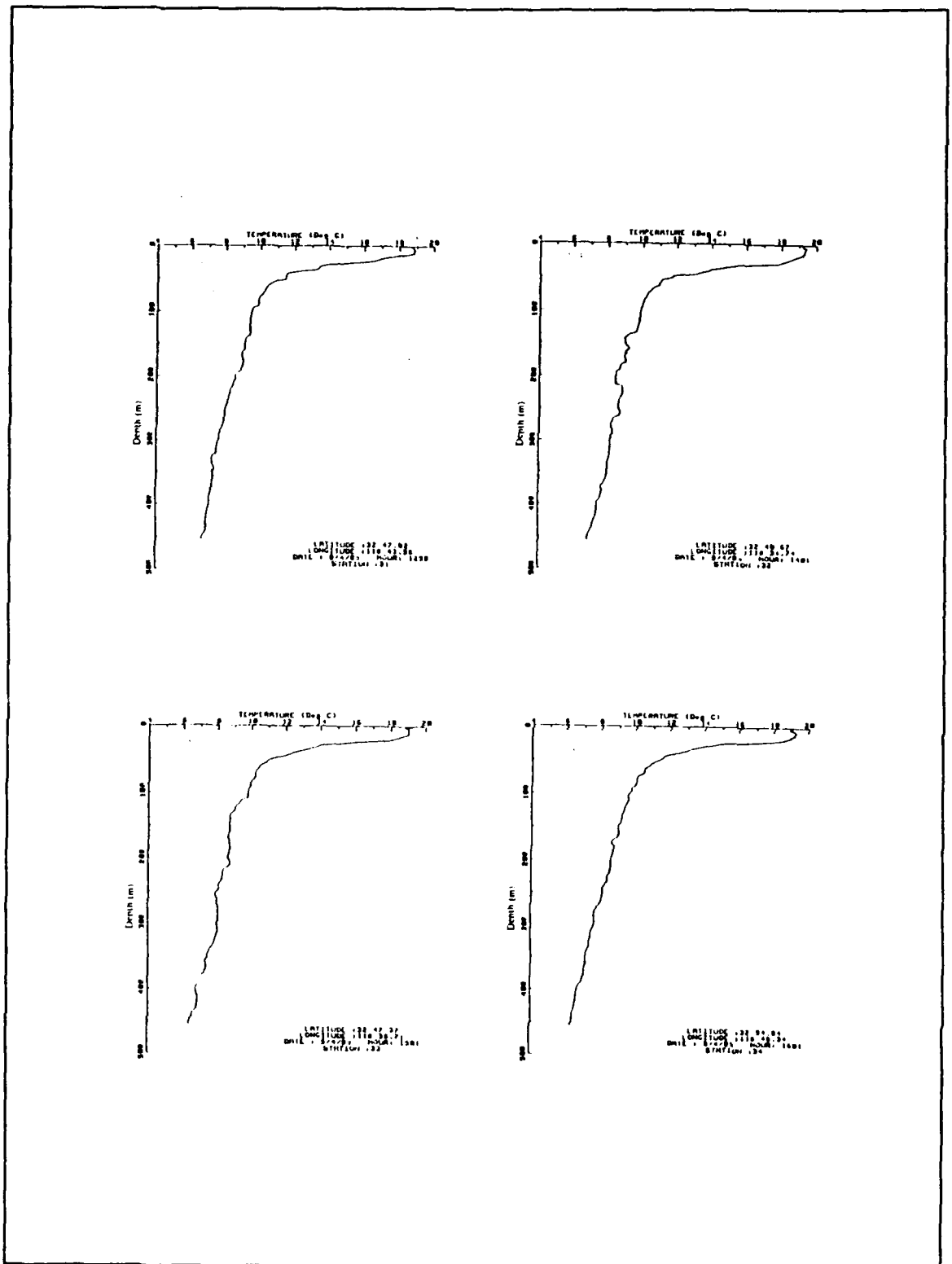

Figure A5. Vertical profile of temperature measured by XBT at station No. 31, No. 32, No. 33, No. 34 in figure 2

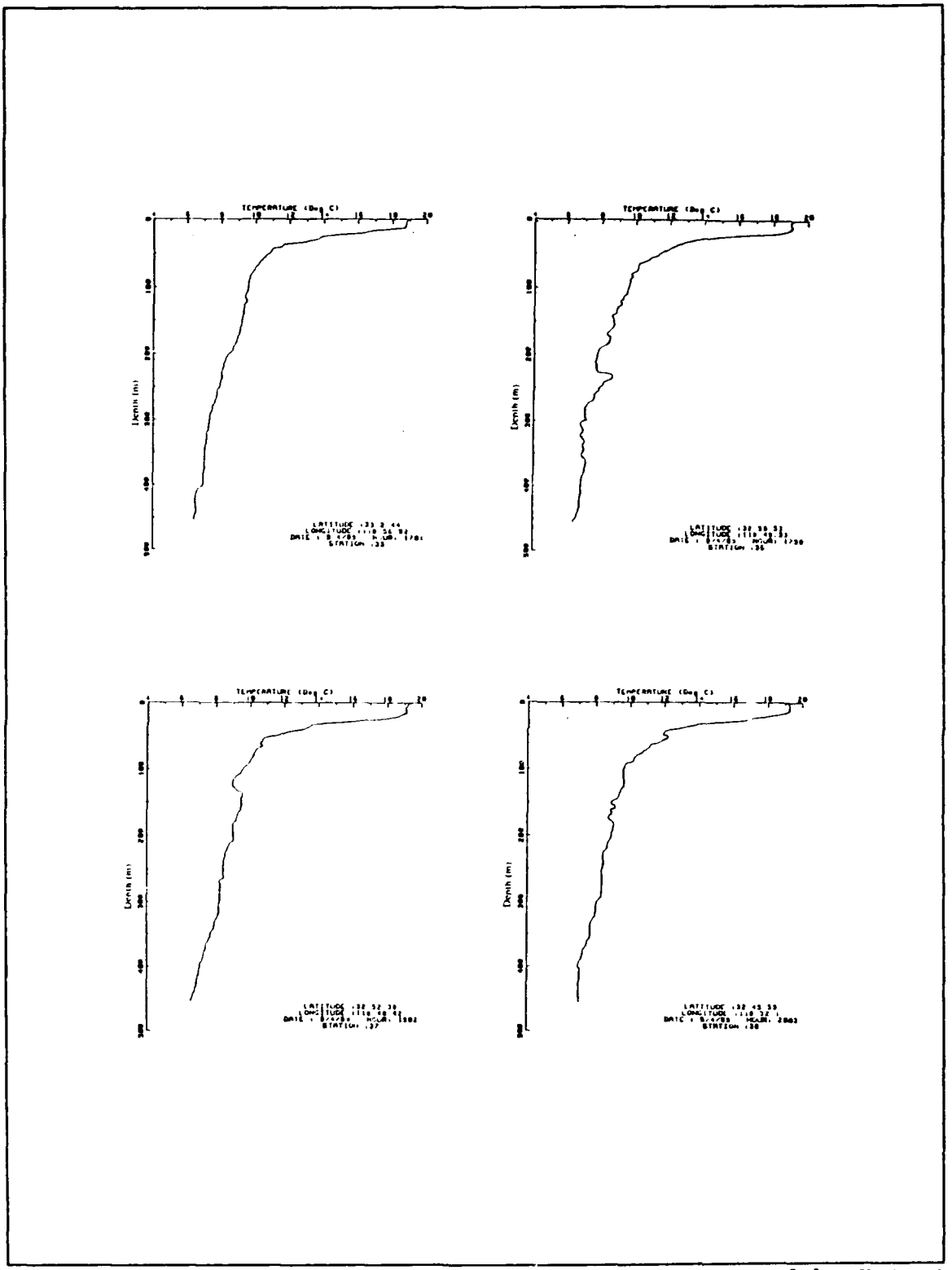

Figure A6. Vertical profile of temperature measured by XBT at station No. 35, No. 36, No. 37, No. 38 in figure 2

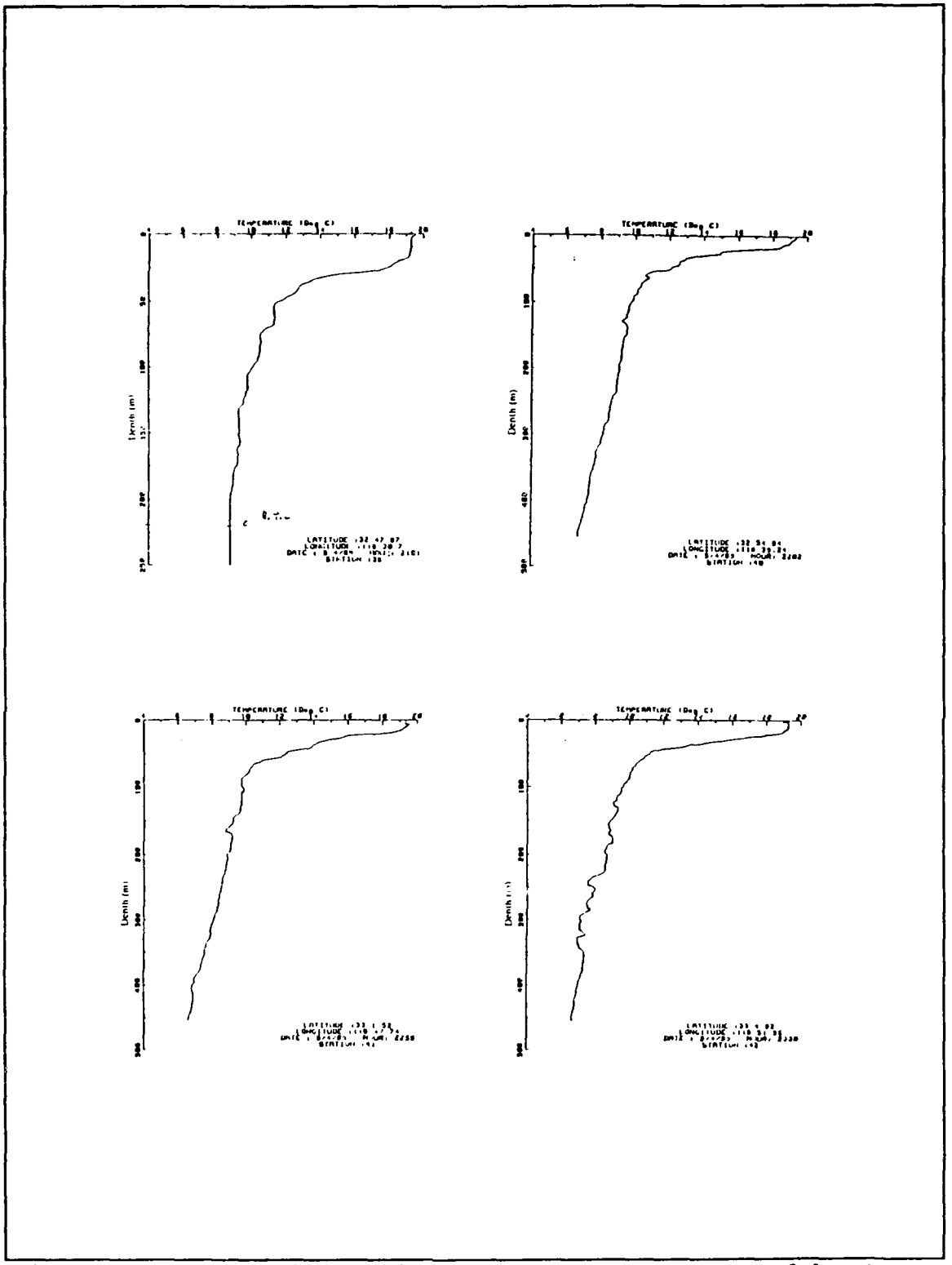

Figure A7. Vertical profile of temperature measured by XBT at station No. 39, No. 40, No. 41, No. 42 in figure 2

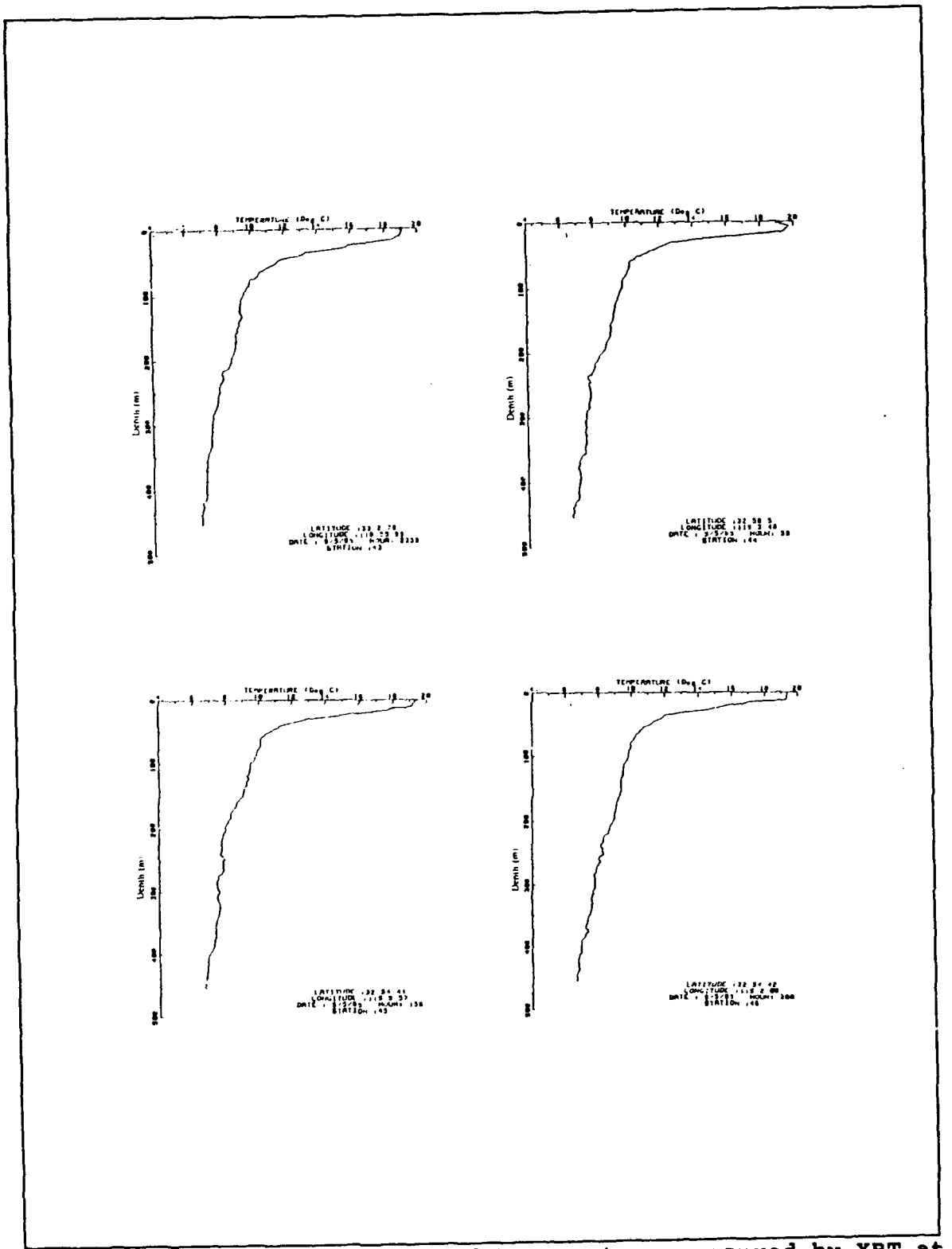

Figure A8. Vertical profile of temperature measured by XBT at station No. 43, No. 44, No. 45, No. 46 in figure 3

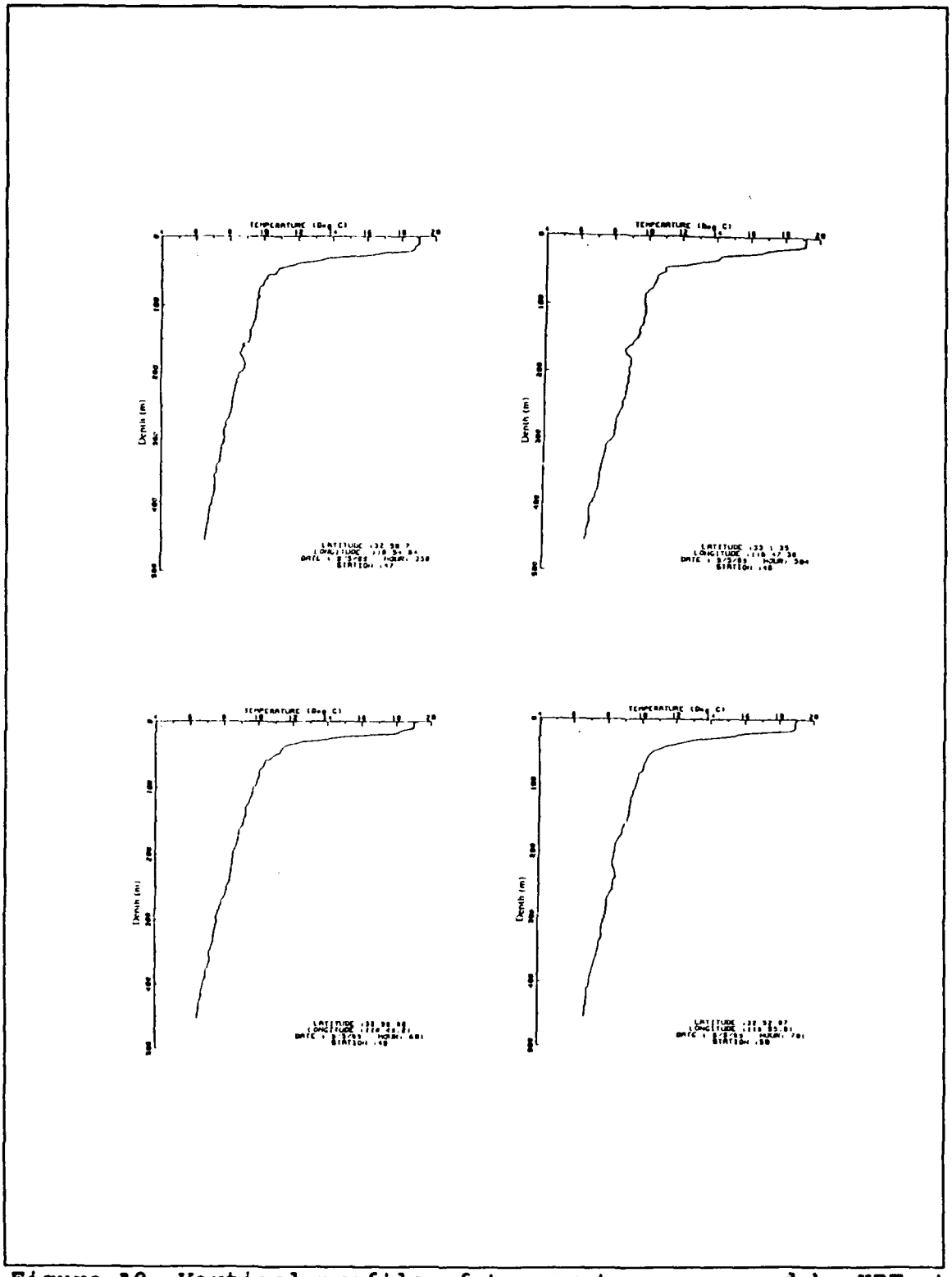

Figure A9. Vertical profile of temperature measured by XBT at station No. 47, No. 48, No. 49, No. 50 in figure 3

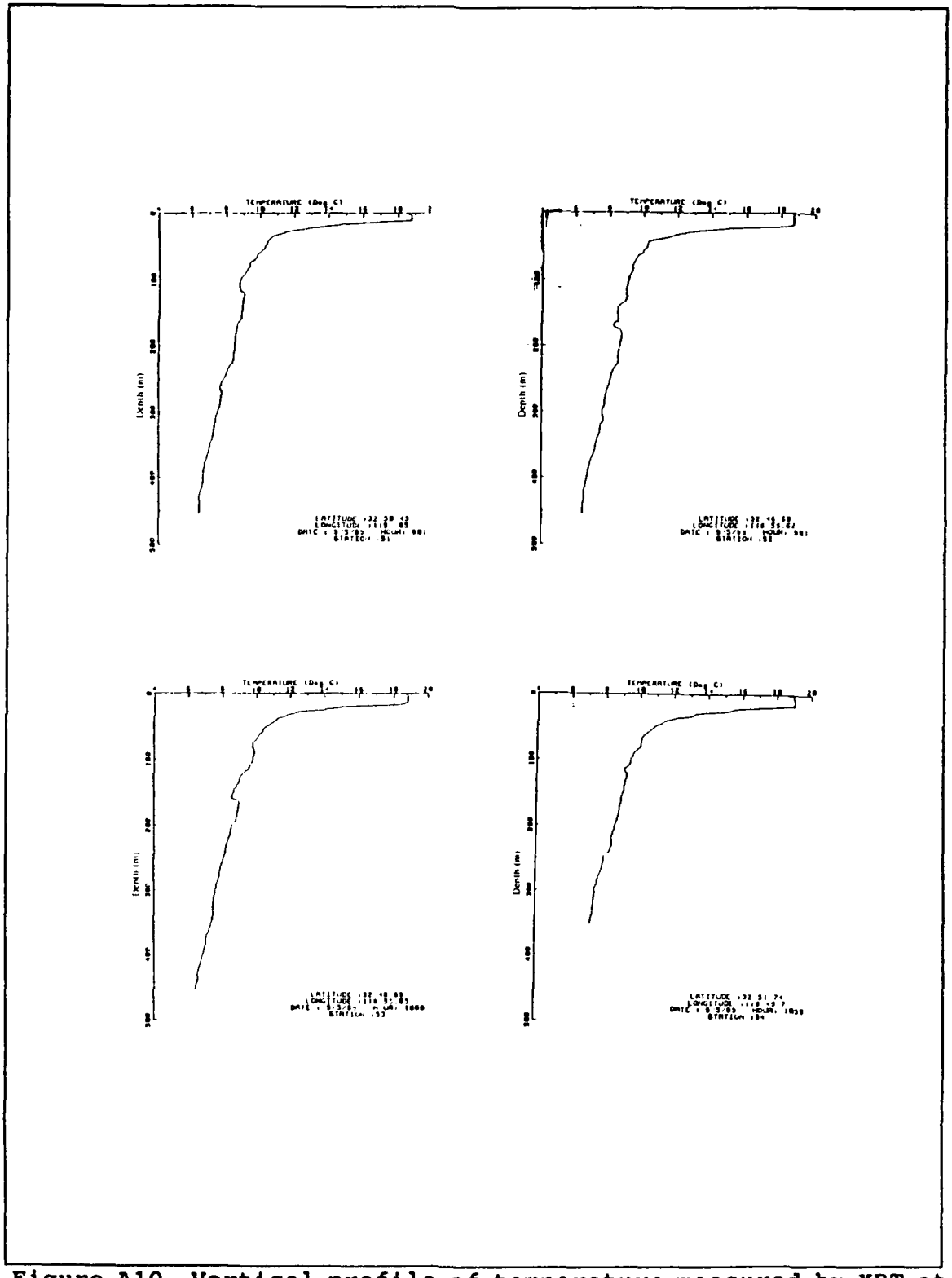

Figure A10. Vertical profile of temperature measured by XBT at station No. 51, No. 52, No. 53, No. 54 in figure 3

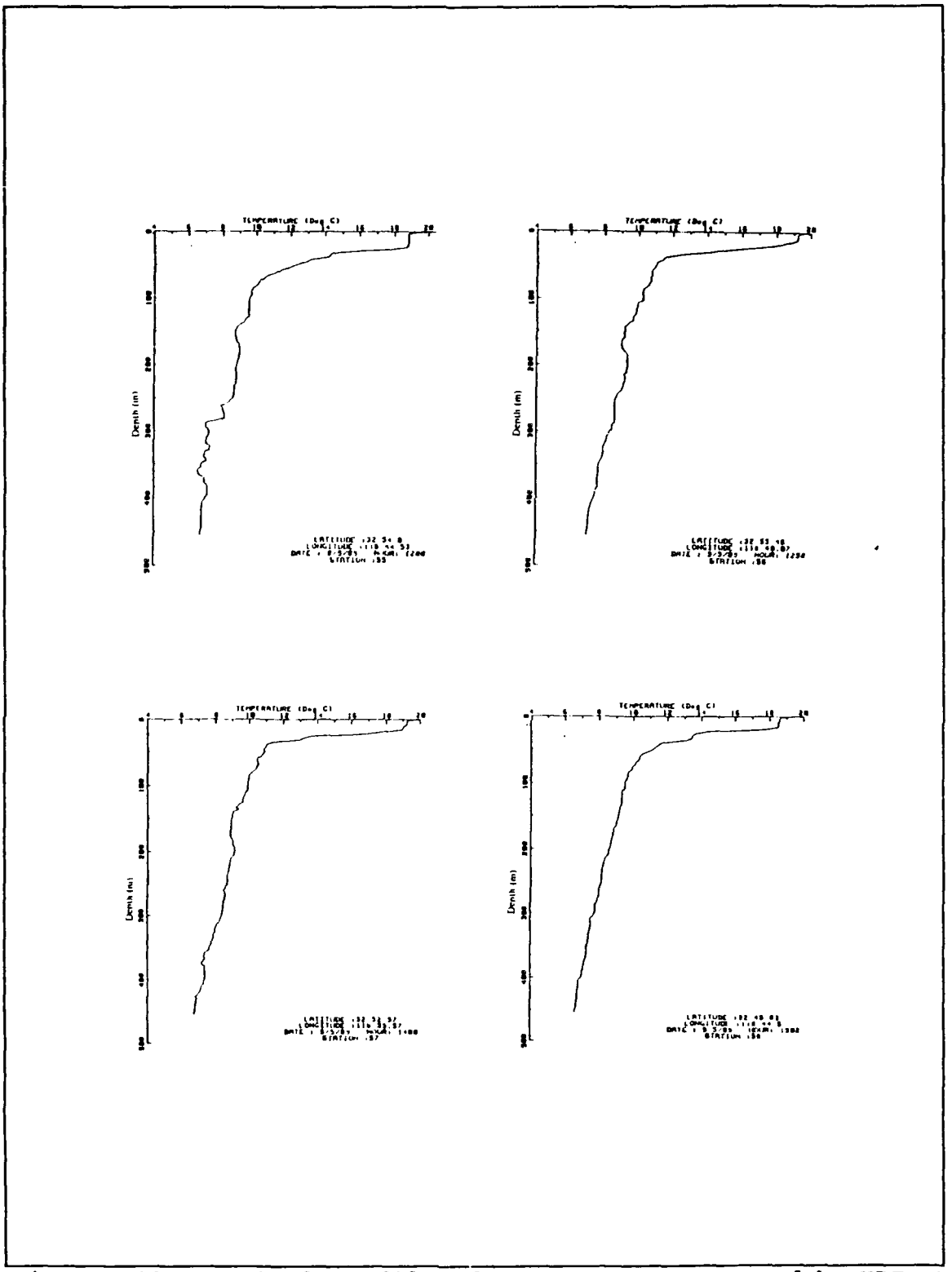

Figure A11. Vertical profile of temperature measured by XBT at station No. 55, No. 56, No. 57, No. 58 in figure 3

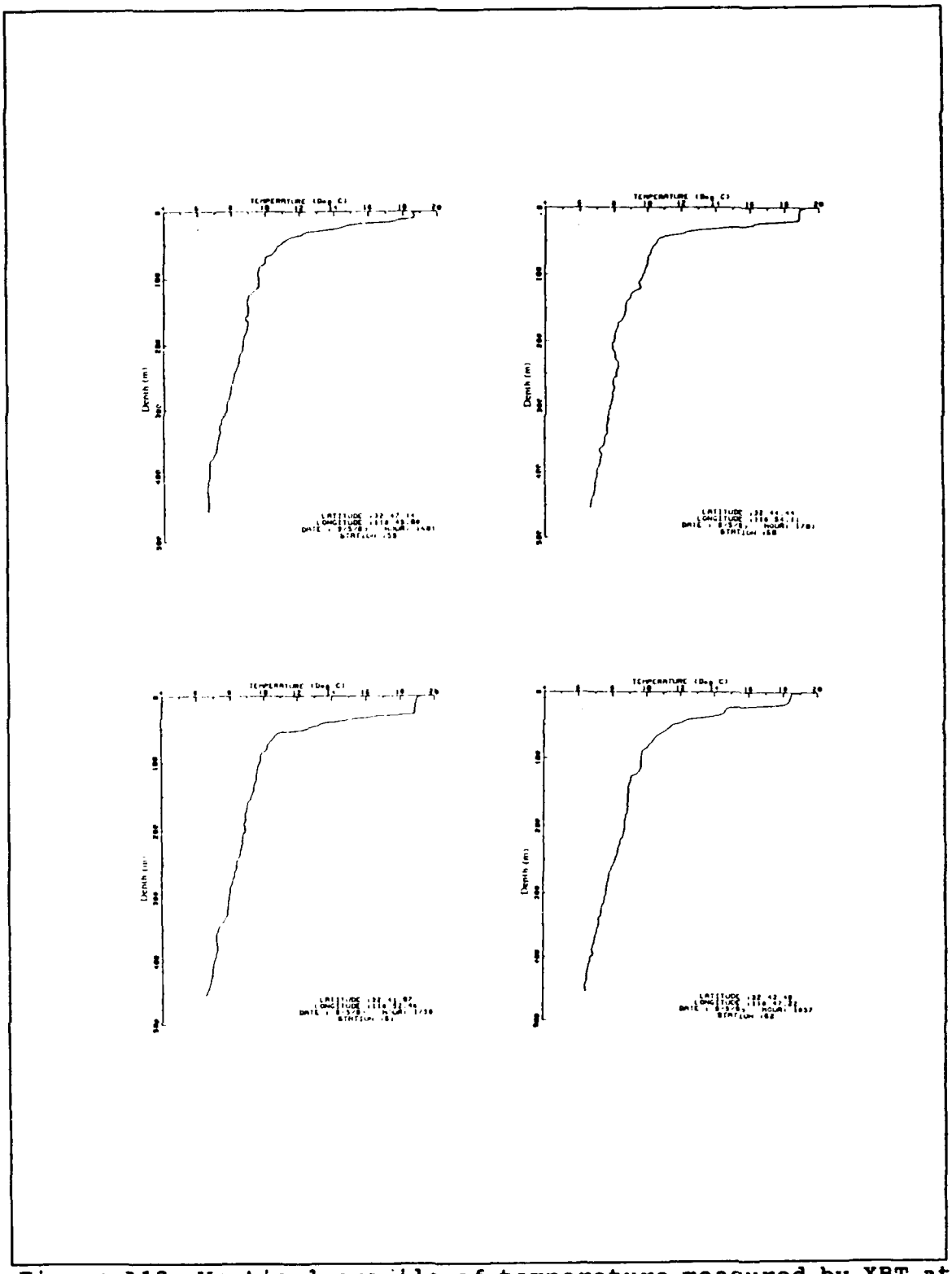

Figure A12. Vertical prorile of temperature measured by XBT at station No. 59, No. 60, No. 61, No. 62 in figure 3

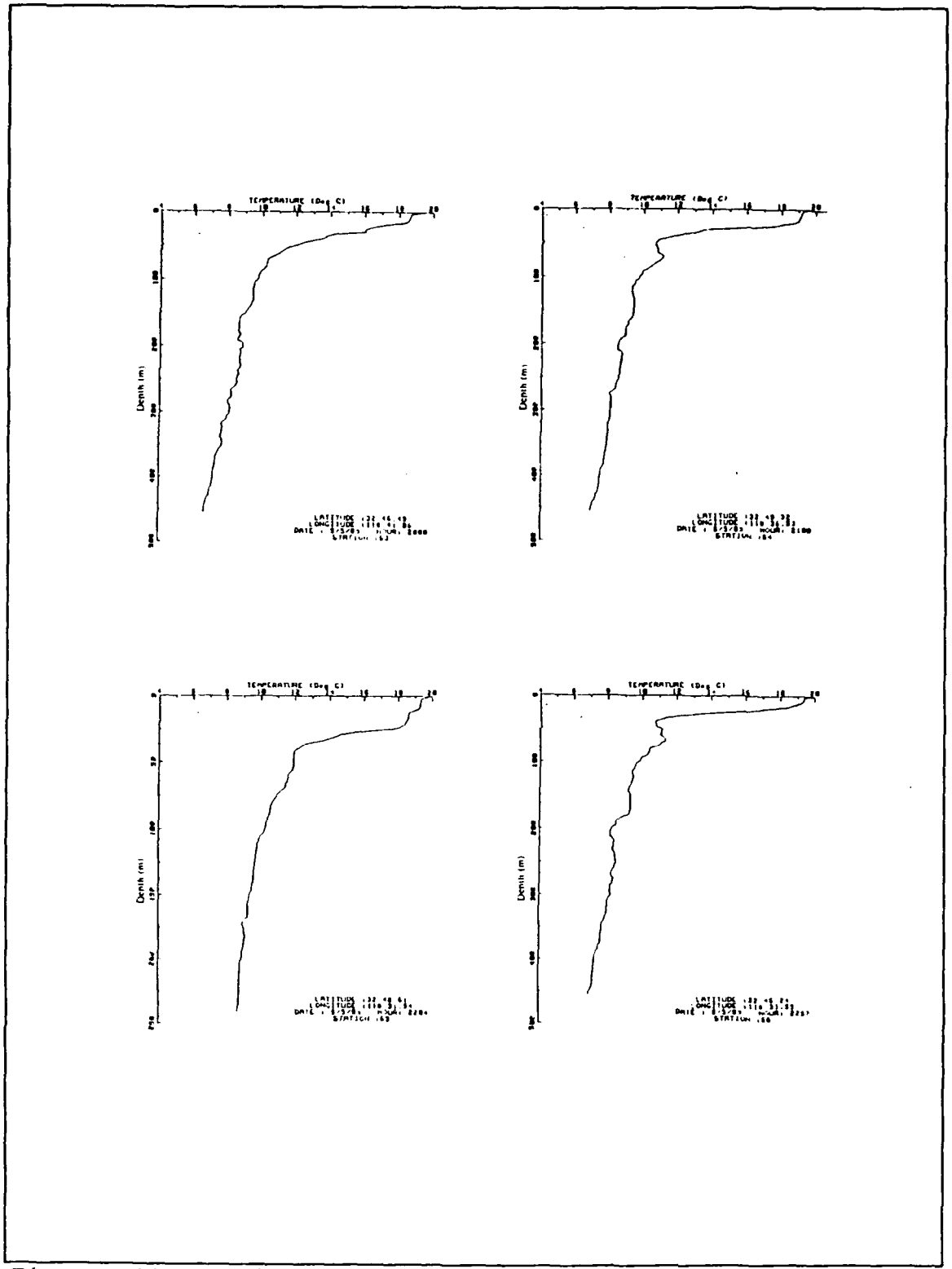

Figure A13. Vertical profile of temperature measured by XBT at station No. 63, No. 64, No. 65, No. 66 in figure 3

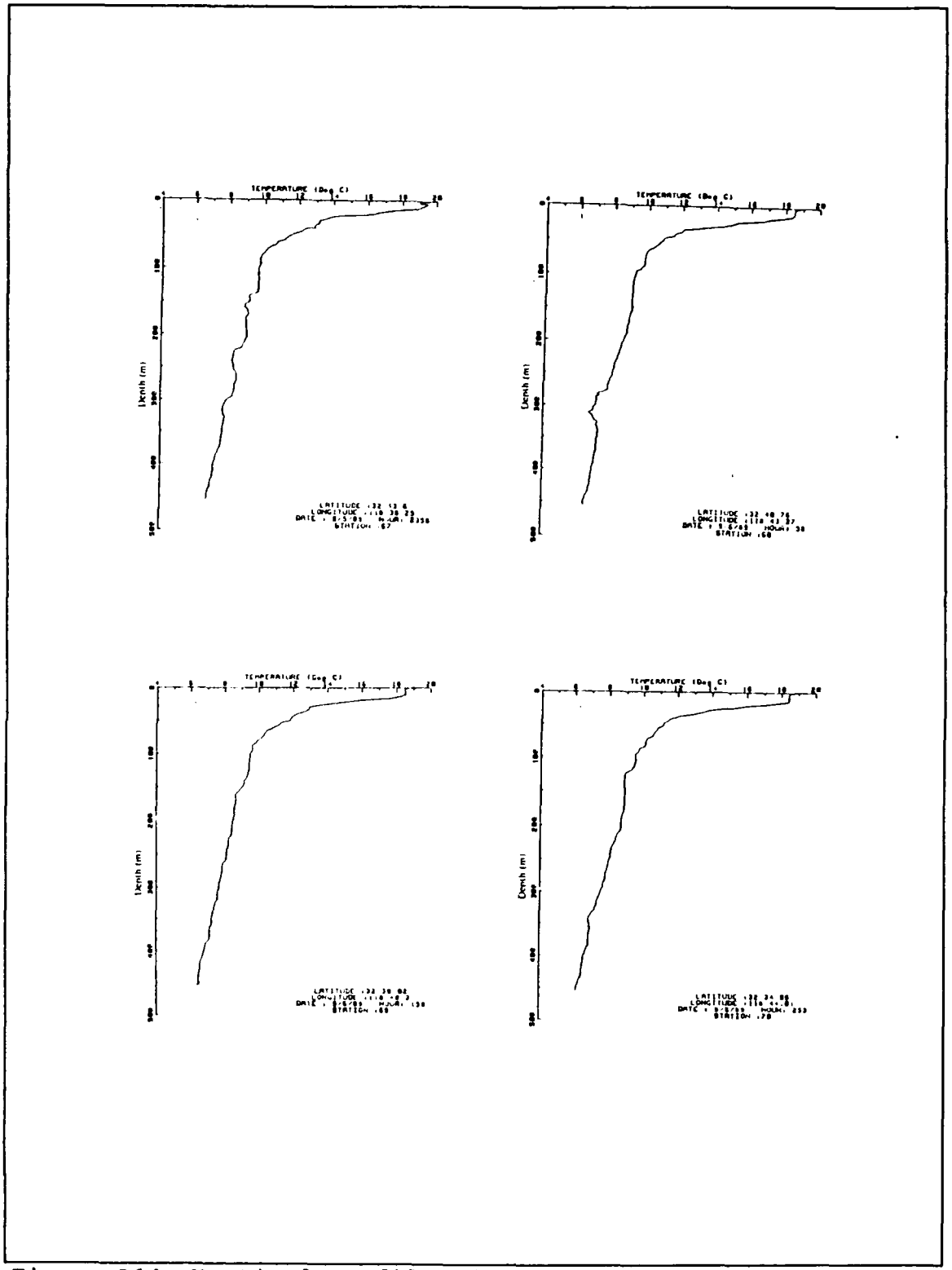

Figure A14. Vertical profile of temperature measured by XBT at station No. 67, No. 68, No. 69, No. 70 in figure 3

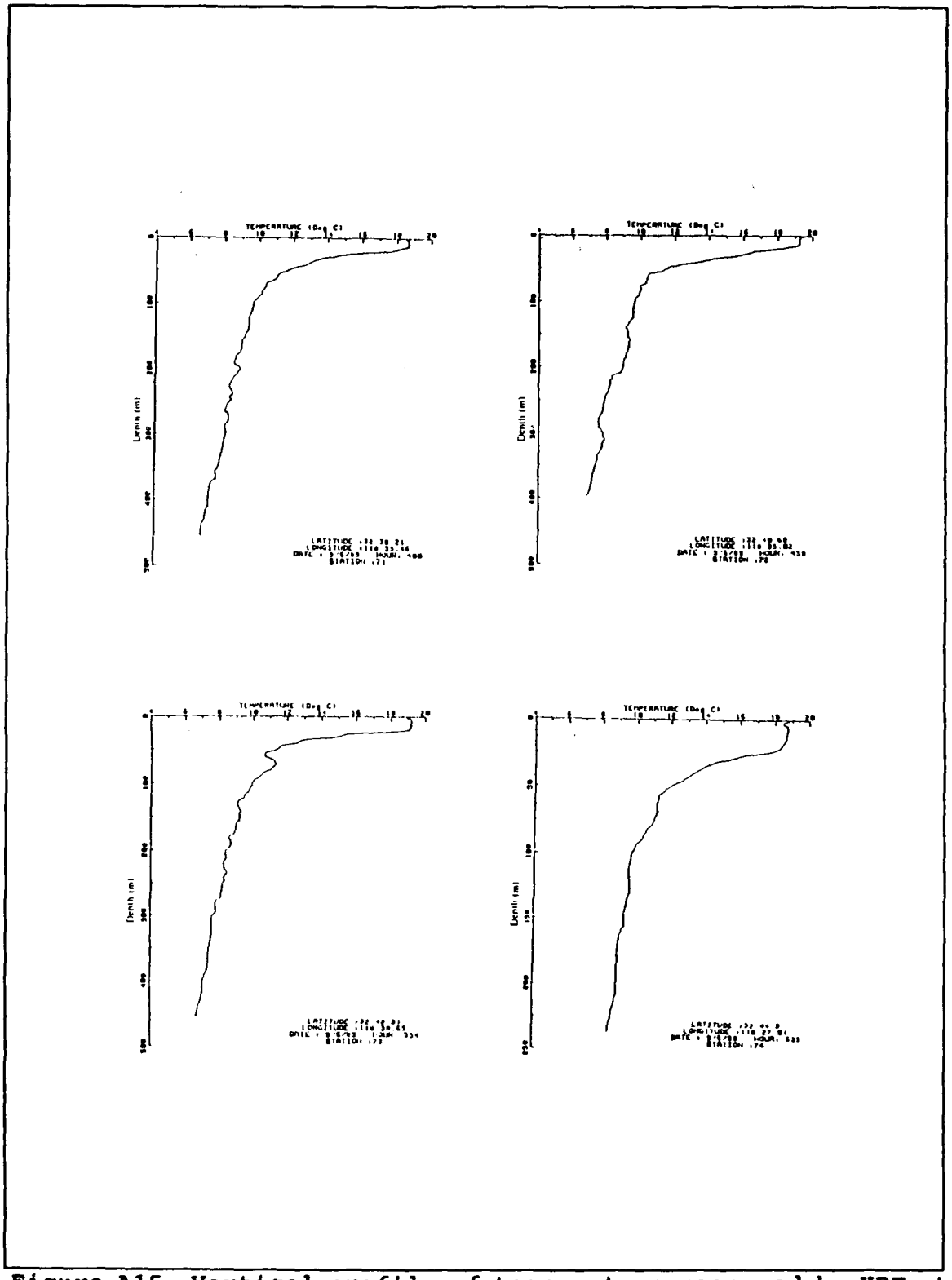

Figure A15. Vertical profile of temperature measured by XBT at station No. 71, No. 72, No. 73, No. 74 in figure 3

APPENDIX B. THE TEMPERATURE AND CURRENT CROSS SECTIONS

This appendix describes the temperature and current profiles during the transit between Moss Landing and San Clemente Island. XBTs were employed every two hours at a ship speed of 10 knots.

The ship route is shown in figure B1. The solid circles denote the locations of XBT sounding. The numbers ranging from 1-14 are the XBT stations (from 1 near Monterey Bay to 14 near the NW corner of the study area).

A. VELOCITY SECTION

1. First Cruise (SCBE-I)

Figures B2 and B3 show the cross shore and alongshore currents made during the steam from Moss Landing to the study area during the first cruise, with a mean heading of approximately 133°. Figure B2 shows onshore currents between Point Sur and Santa Cruz Island. The other onshore current was shown near San Nicolas Island. The maximum onshore current (20 cm/s) was located near the Point Piedras Blancas.

Figure B2 shows weak offshore currents located at the southern and northern parts of San Nicolas Island. Figure B3 shows poleward flow between Point Sur and Point Conception, and equatorial flow between Point Conception and the study

area. The maximum equatorward flow (25 cm/s) was located at the south of Point Piedras Blancas.

Figures B4 and B5 show the cross shore and alongshore currents made during the way back from the study area to Moss Landing.

2. Second Cruise (SCBE-II)

Figures B6 and B7 show the cross shore and alongshore currents during the second cruise, with a mean heading of approximately 133°. Figure B6 shows the offshore velocity from the surface to 400 m depth. The numbers on the top are XBT casting stations; the number on the contours are velocity (cm/s). The solid line (positive value) denotes an offshore current; the dash line (negative value) denotes an onshore current. The offshore current occured between station 11 (Santa Cruz island) and 14, where the depth is over 400 m. The maximum offshore velocity (15 cm/s) was located between stations 12 and 13 (near San Nicolas Island) from the surface to a depth of 50 m. The onshore currents were found between stations 1 and 11 (between Point Sur and Santa Cruz Island) from the surface to the bottom. The maximum onshore velocity (20 cm/s) was located on the surface between stations 9 and 10 (between Point Conception and Santa Cruz island).

Figure B7 shows the alongshore velocity from the surface to a depth of 400 meters. Again, a solid line (positive value) denotes an equatorial current; a dash line (negative value) denote a poleward current. The equatorward currents were found

from station 9 to station 14 (between Santa Cruz Island and study area). The maximum equatorward velocity (20 cm/s) was located between station 11 and 12 near the bottom. The poleward flow was found between station 1 and 9 (between Point Sur and Point Conception). The maximum poleward flow velocity (25 cm/s) was located around Point Piedras Blancas and station 2 from the surface to 50 m depth.

B. TEMPERATURE SECTION

Figure B8 shows the vertical section of temperature seen during the steam from Moss Landing to the study area 2-3 September 1989. Surface temperature varied along the cruise track from 14°C (betweem Point Sur and Point Piedras Blancas) to 19°C (around San Nicolas Island where the water is deeper than 400 m). The temperature on the bottom was between 7°C and 10°C depending to the water depth (10°C at 100m; 9°C at 200 m; 8°C at 300 m).

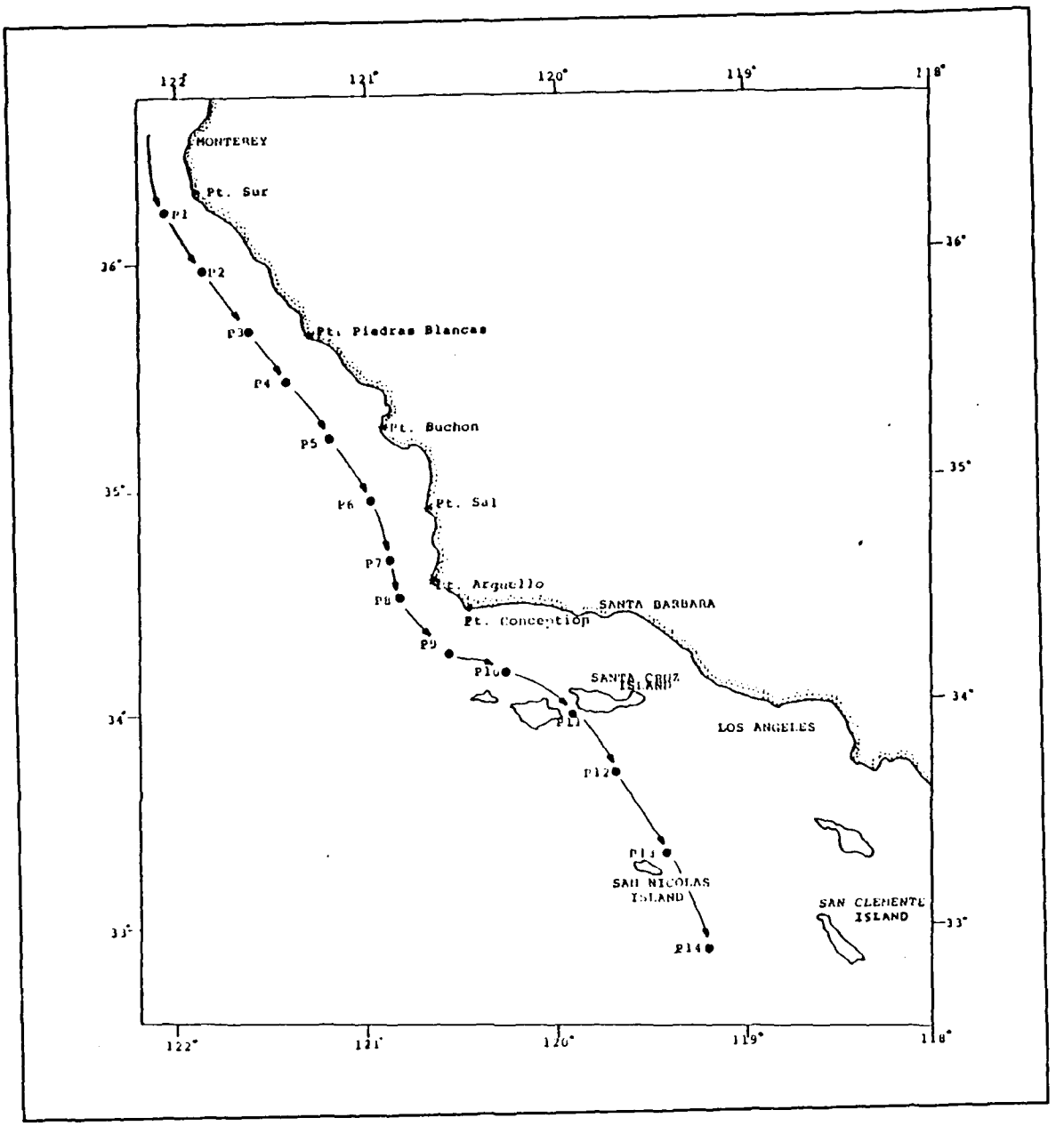

Figure B1. Cruise track followed during the steam from the Moss Landing to San Clemente Island during the cruise SCBE-II, 2-6 September, 1989. The solid circle denotes the location of XBT sounding.

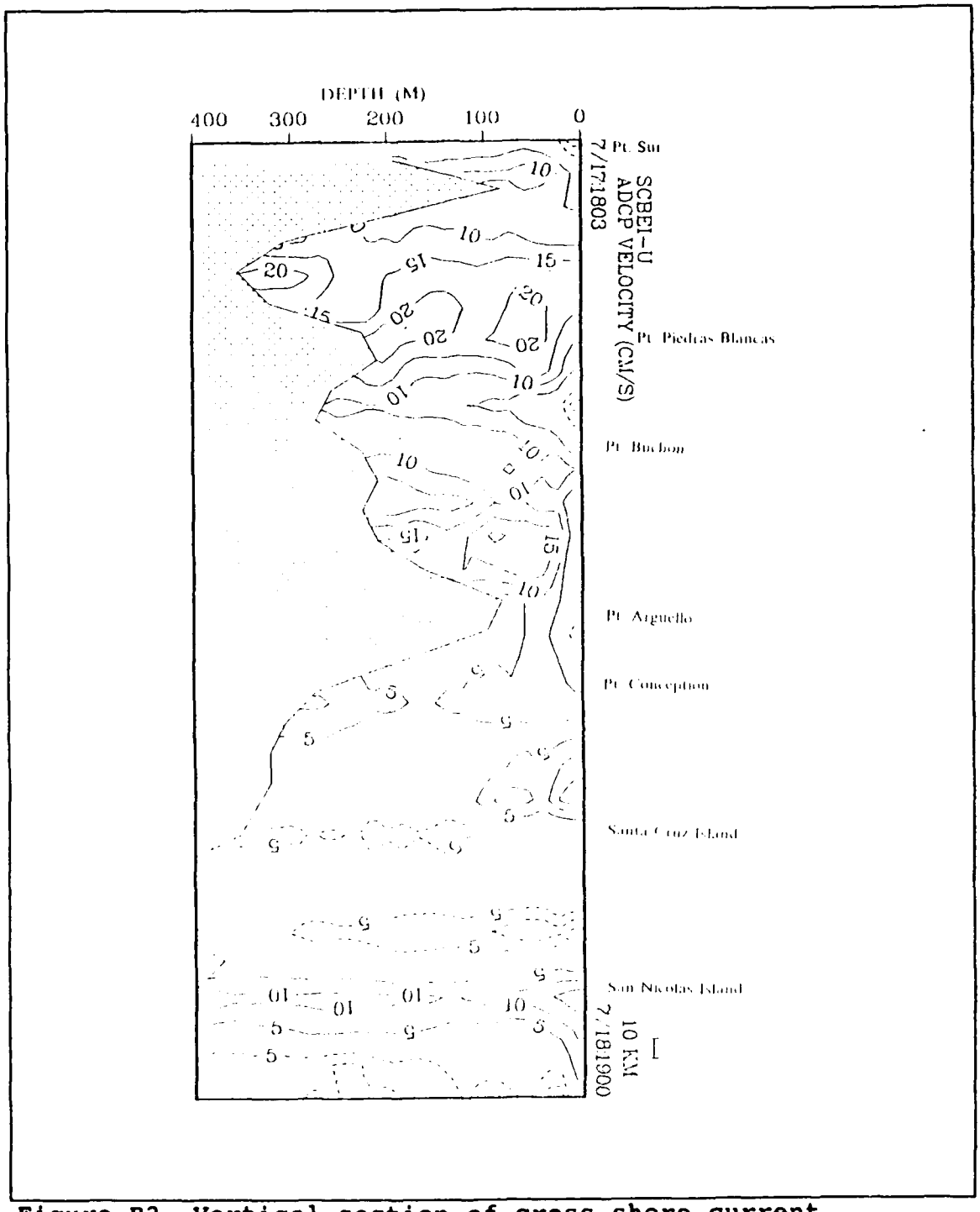

Figure B2. Vertical section of cross shore current (u-component) made during the steam from Moss Landing to the study area during 17-18 July, 1989, (SCBE-I)

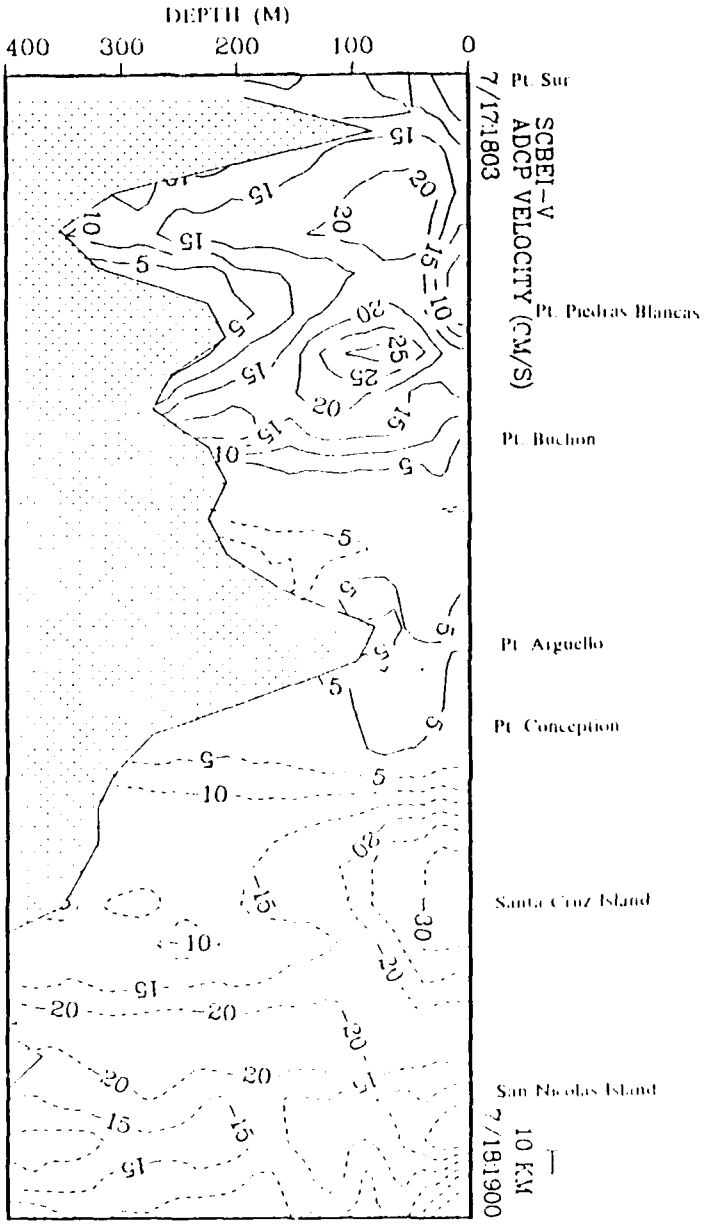

Figure B3. Vertical section of alongshore current (v-component) made during the steam from Moss Landing to the study area during 17-18 July, 1989 (SCBE-I)

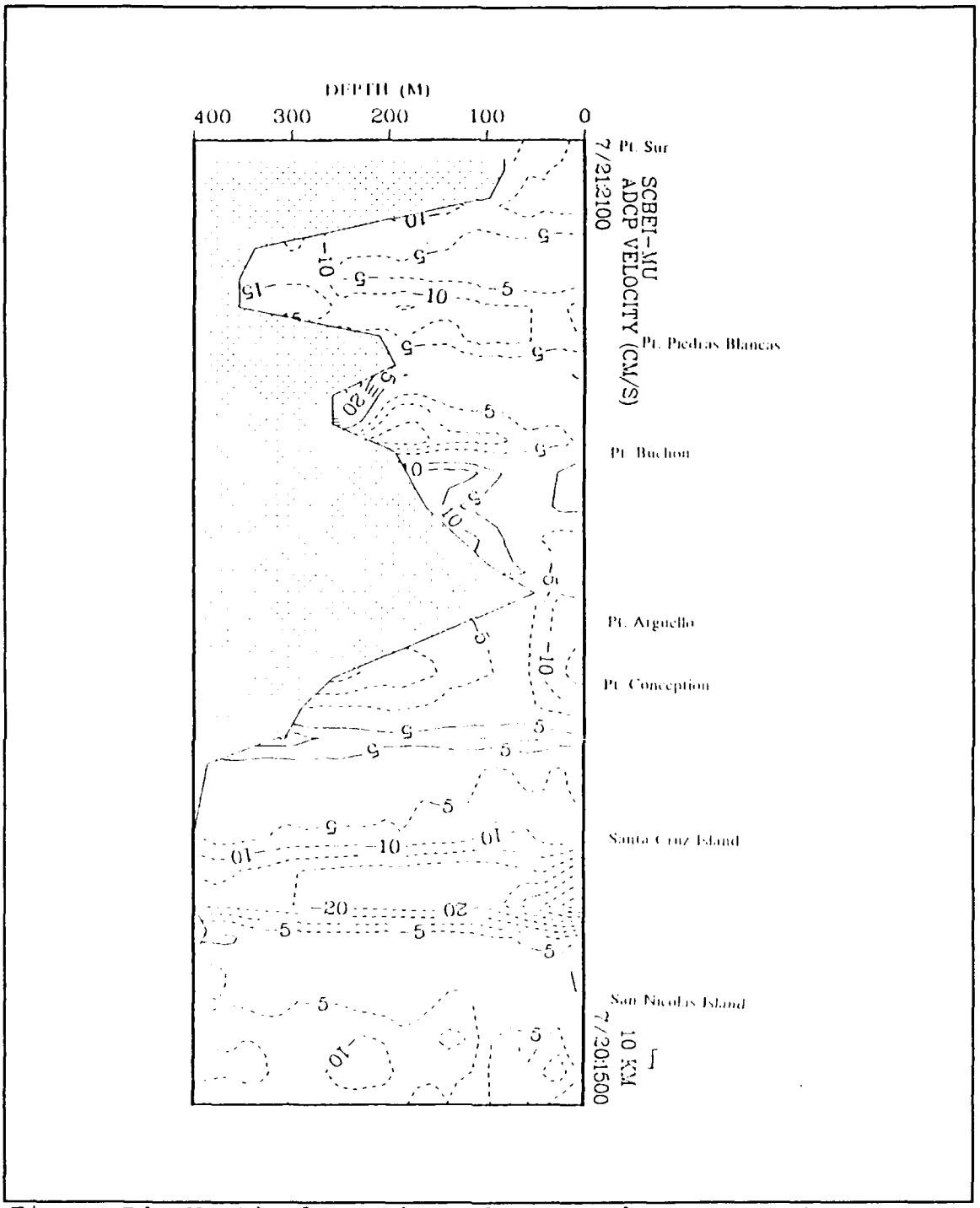

Figure B4. Vertical section of cross shore current (u-component) made during the steam back from study area to Moss Landing during 20-21 July, 1989 (SCBE-I)

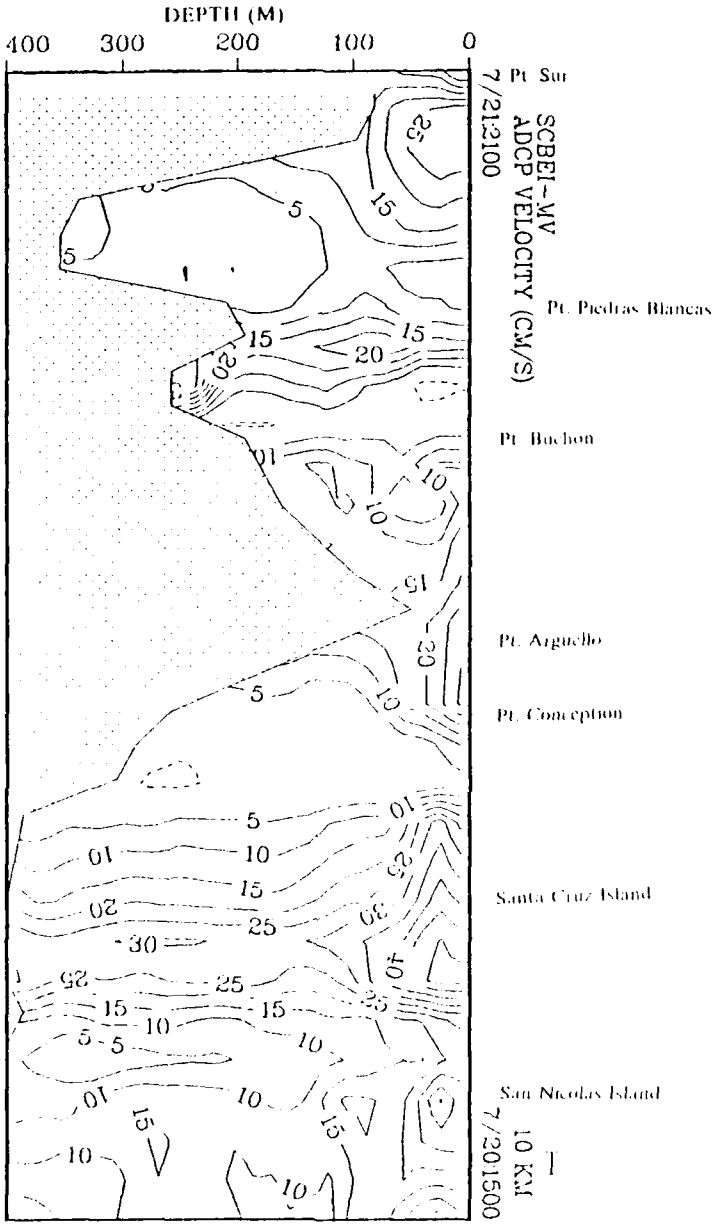

Figure B5. Vertical section of alongshore current (v-component) made during the steam back from study area to Moss Landing during 20-21 July, 1989 (SCBE-I)

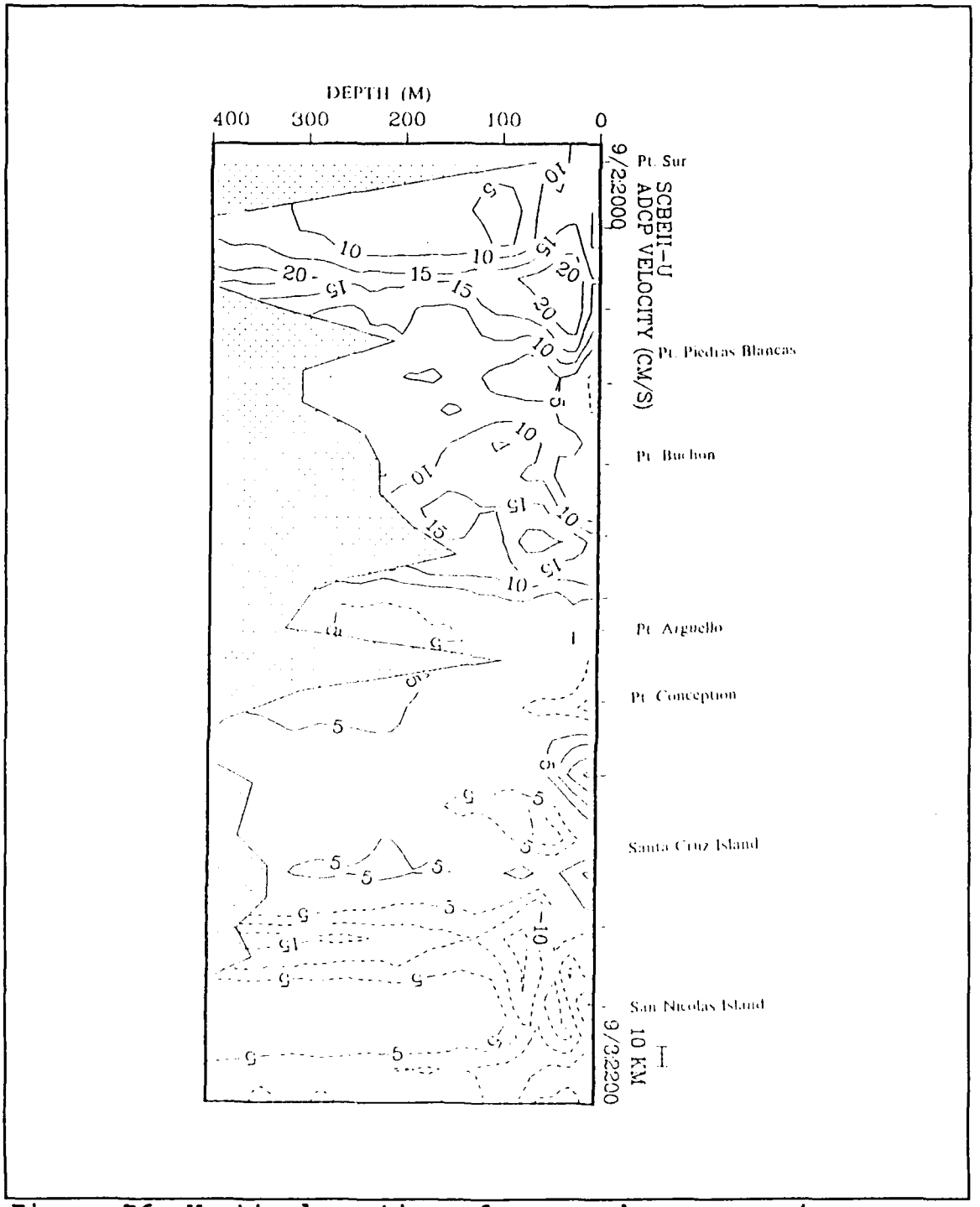

Figure B6. Vertical section of cross shore current (u-component) made during the steam from Moss Landing to the study area during 2-6 September, 1989 (SCBE-II).

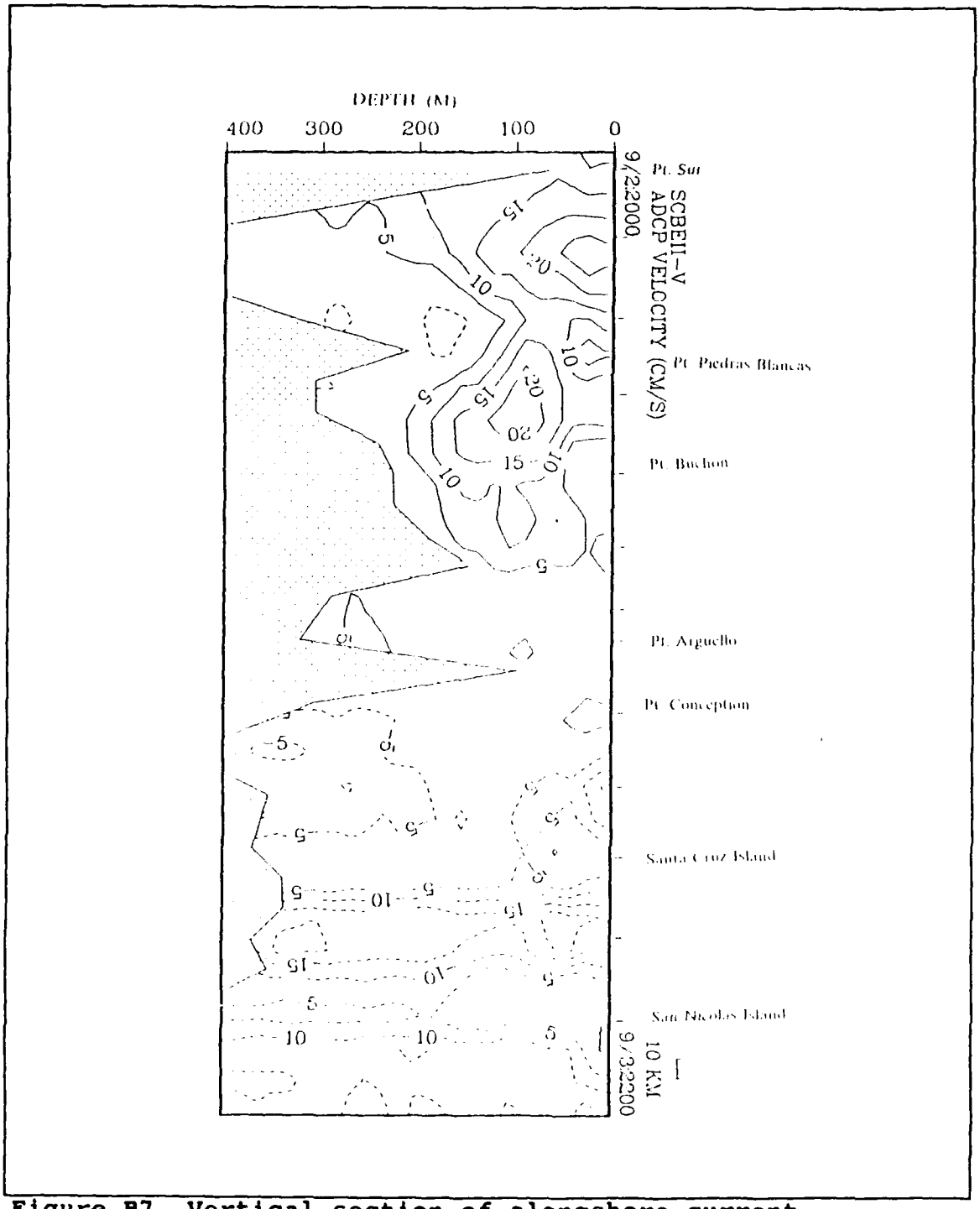

Figure B7. Vertical section of alongshore current (V-component) made during the steam from Moss Landing to the study area during 2-6 September, 1989 (SCBE-II).

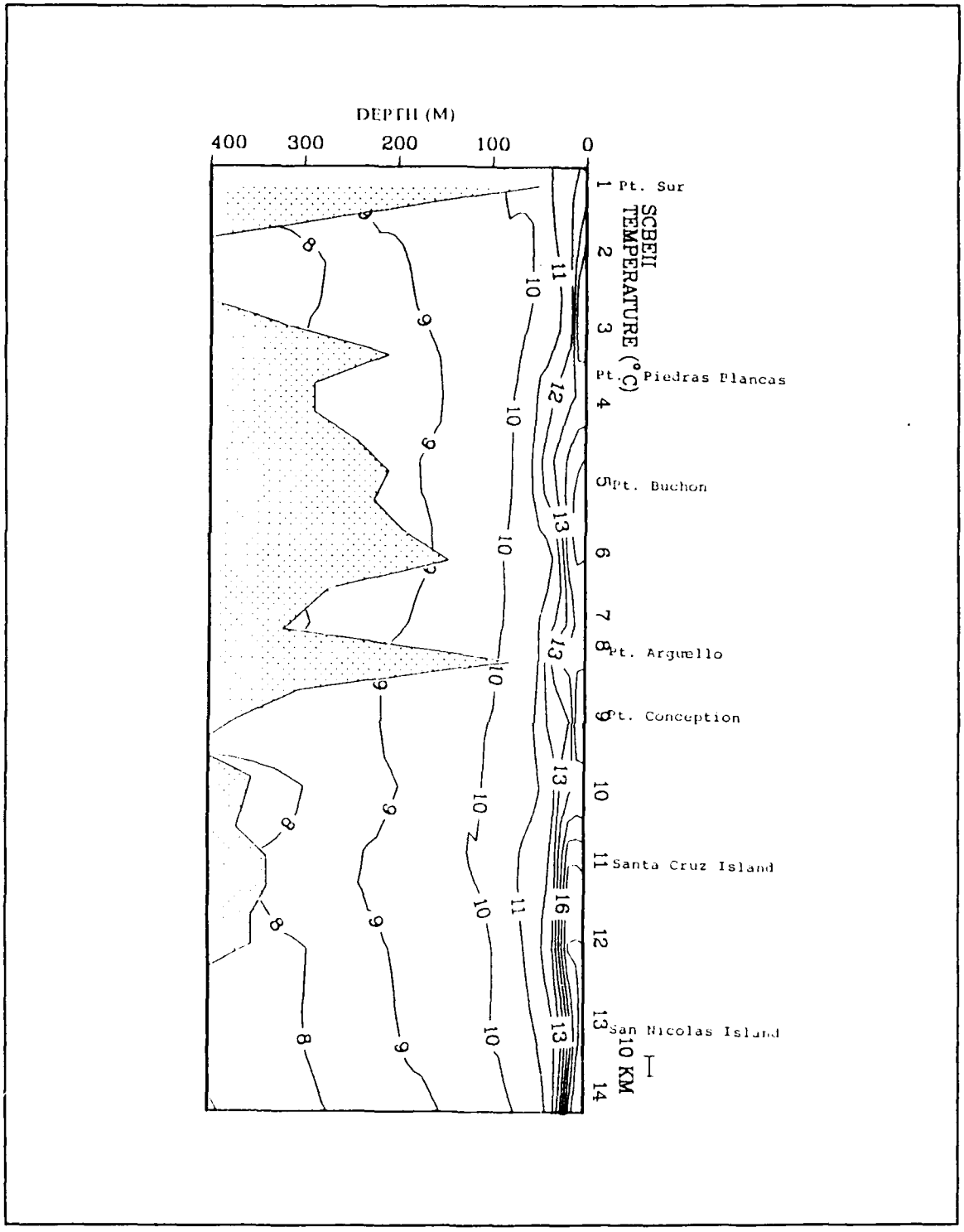

Figure B8. Vertical section of temperature made during the steam from Moss Landing to the study area during 2-6 September, 1989 (SCBE-II).

LIST OF REFERENCES

1. Kosro, P.M., Shipboard Acoustic Doppler Current Profiling During the Coastal Ocean Dynamics, Ph.D. Dissertation, SIO Ref. 85-8, Script Institution of Oceanography, 1985.

2. Kosro, P.M., Structure of the Coastal Current Field off Northern California During the Coastal Ocean Dynamics Experiment, *J. Geophs. Res.*, Vol. 92, pp.1637-1654, 1987.

3. King, Charles H., A Comparison of Pegasus and Combined CTD/ADCP Current Profiles off the California Coast in March 1989, NPS Thesis.

4. Smith, Orson P. and John M. Morrison, Shipboard Acoustic Doppler Current Profile in the Eastern Caribbean Sea, 1985-1986. *J. Geophs. Res.*, Vol. 94, pp. 9713-9719, 1989.

5. Joyce, Terrence M., On In Situ "Calibration" of Shipboard ADCP, *J. Atmos. Oceanic Technol.*, Vol. 6, pp. 169-172, 1989.

6. Winant, C. D. and M. A. Bray, Velocity and Temperature Structure along the 90 m isobath from Pt. Reyes to Cape Blanco, Wecoma Transit Cruise report, 1989.

7. Huyer, Adriana and P. Michael Kosro, Mesoscale Surveys over the Shelf and Slope in the Upwelling Region Near Point Arena, California, *J. Geophs. Res.*, Vol. 92, pp. 1655-1681, 1987.

8. Brown, Wendell S. and James D. Irish, A Description of Subtidal Pressure Field Observations on the Northern California Continental Shelf During the Coastal Ocean Dynamics Experiment, *J. Geophs. Res.*, Vol. 92, pp. 1605-1635, 1987.

9. Lynn, Ronald J. and James J. Simpson, The Influence of Bathymetry upon the Flow of the Undercurrent Off, *J. Geophs. Res.*, 1990, in press.

10. Barth, J. A. and K. H. Brink, Shipboard Acoustic Doppler Profiler Velocity Observations near Point Conception: Spring 1983, *J. Geophs. Res.*, Vol. 92, pp. 3925-3943, 1987.

11. Reid, Joseph L. and Arnold W. Mantyla, The Effect of the Geostrophic Flow Upon Coastal Sea Elevations in the Northern North Pacific Ocean, *J. Geophs. Res.*, Vol. 81, pp. 3100-3110, 1976.

12. Heinmiller, Robert H., Ebbesmeyer, Curtis C., Taft, Bruce A., Olson, Donald B. and Nikitin, Oleg P., Systematic Errors in Expendable Bathythermography (XBT) Profiles, *Deep-Sea Res.*, vol. 30, pp. 1185-1197, 1983.

13. Chelton, Dudley B., Seasonal Variability of Alongshore Geostrophic Velocity Off Central California, *J. Geophs. Res.*, Vol. 89, pp. 3473-3486, 1984.

14. Koehler, Kim and Negron, Anthony, Evaluation of Currents Along the Point Sur Transect in November 1989, NPS Student Cruise Report, unpublished ms.

15. Pickard, George L. and Emery, William J., *Descriptive Physical Oceanography,* pp. 89-93.

INITIAL DISTRIBUTION LIST

		No. Copies
1.	Defense Technical Information Center Cameron Station Alexandria, VA 22304-6145	2
2.	Library, Code 0142 Naval Postgraduate School Monterey, CA 93943-5002	2
3.	CDR Ching-Mao Tsai 8, Alley 12, Lane 61, Tian-Shyang 2nd Rd. Kaohsiung, Taiwan, R. O. C.	5
4.	Naval Facilities Engineering Command Chesapeake Division (CFO-1) Washington Naval Yard Washington D.C. 20374	2
5.	Department of Oceanography Naval Postgraduate School	
	Attn: Chairman (Code 68Co)	2
	Dr. Pe-Cheng Chu (Code 68Cu)	2
	Dr. Steve Ramp	1
	Paul Jessen	1
	Toby Garfield	1
	Leslie Rosenfeld	1
	Monterey CA 93943-5000	
6.	Chairman (Code 63Rd) Department of Meteorology Naval Postgraduate School Monterey, CA 93943-5000	1
7.	Department of Oceanography Naval Postgraduate School	
	Attn: CDR F.K. Kuo (SMC 2303)	1
	LCRD B.K. Wu (SMC 1427)	1
	LCDR C. L. Tan (SMC 1135)	1
	LCDR Cheng Liu (SMC 2138)	1
	LCDRT. C. Yin (SMC 2408)	1
	Monterey CA 93943	

8. Commanding Officer 1
Navy Headquarters
Taipei, Taiwan, R.O.C.

9. Commanding Officer 1
Naval Hydrographic & Oceanographic Office
Tso-Ying, Kaohsiung, Taiwan, R.O.C.

10. Department of Oceanography 1
National Taiwan University
Taipei, Taiwan, R.O.C.

11. Department of Oceanography 1
National Chung Shung University
Kaohsiung, Taiwan, R.O.C.

12. Department of Oceanography 1
National College of Marine & Oceanic Technology
Keelung, Taiwan, R.O.C.

13. Department of Oceanography 1
College of Chinese Culture
Taipei, Taiwan, R.O.C.

14. Director, Naval Oceanography Division 1
Naval Observatory
34th and Massachusetts Avenue NW
Washington, D.C. 20390

15. Commander 1
Naval Oceanogrphy Command
Stennis Space Center, MS 39529-5000

16. Commanding Officer 1
Naval Oceanogrphic Office
Stennis Space Center, MS 39522-5001

17. Commanding Officer 1
Fleet Numerical Oceanography Center
Monterey, CA 93943

18. Commanding Officer 1
Naval Ocean & Atmosphere Research Laboratory
Stennis Space Center, MS 39522-5001

19. Commanding Officer 1
Naval Ocean & Atmosphere Research Laboratory (west)
Stennis Space Center, MS 93943-5006

20. Chairman, Oceanography Department 1
U.S. Naval Academy
Annapolis, MD 21402

21. Chief of Naval Research 1
800 North Quincy Street
Arlinton, VA 22217

22. Dr. David L. Evans 1
Dr. Thomas H. Kinder 1
Office of Naval Research
Physical Oceanogrphy Program
Code 1122 PO
800 North Quincy Street
Arlington, VA 22217

23. Dr. Jeff Smart 1
Applied Physics Laboratory
The Johns Hopkins University
Johns Hopkins Road
Laurel, MD 20707

24. Scripps Institution of Oceanography
Attn: Library 1
Dr. Jim Simpson 1
Dr. Joe Reid 1
P.O. Box 2367
La Jolla, CA 92037

25. School of Oceanography
University of Washington
Attn: Library 1
Dr. M. Gregg 1
Dr. Barbara Hickey 1
Dr. C. Eriksen 1
Seattle, WA 98195

26. School of Oceanography
Oregon State University
Attn: Library 1
Dr. Mike Kosro 1
Corvallis, OR 97331

27. Dr. Eric Firing 1
Department of Oceanography
University of Hawaii
Honolulu, HI 96822